UNIVERSIDADE DE LISBOA
FACULDADE DE CIÊNCIAS
DEPARTAMENTO DE FÍSICA

Extraction and quantification of perivascular spaces based on vesselness filtering: A potential biomarker for Fabry disease

Tiago Emanuel Nogueira da Silva

Mestrado Integrado em Engenharia Biomédica e Biofísica
Perfil em Engenharia Clínica e Instrumentação Médica

Dissertação orientada por:
Rita Homem de Gouveia Costanzo Nunes
Nuno Miguel de Pinto Lobo e Matela

2020

” ... 100 billion neurons, each neuron is connected to 10 thousand other...sitting on your shoulders, the brain is the most complicated object in the known universe...”

Michio Kaku

Acknowledgments

Firstly, I would like to thank my supervisor, Prof.Rita Nunes, for the opportunity given to me to develop my project and study a area of my interest in the Institute for Systems and Robotics (LaSEEB), at Instituto Superior Técnico (IST). Also, for being always available to help me by guiding me in the right directions, and for giving me additional strength and encouragement in this difficult final phase. Also, a special thanks to my internal supervisor Prof. Nuno Matela for all support and motivation during this project, as well as for the experience, knowledge and advice transmitted during my Master in Biomedical and Biophysics Engineering.

Moreover, this work would never been possible without all the help and data acquired from the Centro Hospitalar Universitário Lisboa Norte, EPE (CHLN) - Hospital Santa Maria (HSM), therefore, a special thanks to Professor Sofia Reimão, MD, PhD and João Madureira, MD. both neurologists of the referred hospital.

So, for the people mentioned above, a special thanks, your help was crucial throughout the development of this thesis.

Also, thanks to Joana Moreira, Joana Vaz Sousa and Ricardo Leitão for welcoming me so well at LaSEEB and helping me to achieve the first steps in some methodologies.

A special thanks to my girlfriend Ana Sofia Castro Verde, for all the time spent together during this journey, as well for all the love, motivation and knowledge, her company made even the most stressful moments better. I would also like to mention João Campagnolo, João Figueiredo, Nuno Mendes and Beatriz Alves Martins for all faithful friendship and good moments spent together these two years at FCUL.

Finally, I must express my very profound gratitude to my Family, especially my parents for providing me the best conditions during university with unfailing support and continuous encouragement throughout my years of study and development of this work. This achievement would not be possible without their support, so this work is primarily and especially dedicated to them.

Thank you.

Resumo

Os Espaços perivasculares (EPV) estão compreendidos entre as paredes das artérias perfurantes do encéfalo e meninges, estando preenchidos por líquido céfalorraquidiano (LCR) e líquido intersticial. Por vezes ficam dilatados, tornando-se visíveis em imagens de ressonância magnética (IRM), apesar das suas dimensões próximas da resolução espacial dos equipamentos de ressonância magnética (RM) atuais. Ao longo dos anos tem sido colocada a hipótese de o número dessas estruturas dilatadas se correlacionar com algumas doenças, por exemplo acidentes vasculares cerebrais ou demência. No entanto, estes estudos baseiam-se em contagens e escalas semi-quantitativas em algumas regiões cerebrais de interesse, por visualização das imagens.

A marcação manual destas estruturas consumiria muito tempo, pois os médicos necessitariam de verificar vários planos de modo a obter uma segmentação precisa. Assim, este estudo tem por base a implementação de um sistema semi-automático que, utilizando imagens de ressonância magnética, seja capaz de extrair estas estruturas, proporcionando informação relativa à sua quantificação e orientação espacial no cérebro. A realização deste método possibilitaria também, do ponto de vista clínico, uma ferramenta rápida de triagem e contínua monitorização da condição patológica de cada paciente, ao invés da marcação manual de cada estrutura, corte a corte.

Esta tese pretende descrever as atividades realizadas na dissertação do Mestrado Integrado em Engenharia Biomédica e Biofísica, pela Faculdade de Ciências da Universidade de Lisboa, no perfil de Engenharia Clínica e Instrumentação Médica. Este projecto experimental realizou-se no no Instituto de Sistemas e Robótica (ISR), mais propriamente no Laboratório de Sistemas Evolutivos e Engenharia Biomédica (LaSEEB), associado ao Instituto Superior Técnico (IST), sobre a orientação da Professora Doutora Rita Nunes e do Professor Doutor Nuno Matela.

Nesse sentido, este trabalho focou-se na implementação de um filtro de vasos (filtro de Frangi), que tem a capacidade de delinear e detetar estruturas com características semelhantes a um vaso sanguíneo.

Para obtenção de uma máscara de EPV, neste trabalho, foram definidos três passos distintos: pré processamento, aplicação do filtro, e melhoria da máscara obtida após aplicação do filtro.

Tanto o pré-processamento como a melhoria da máscara de vasos obtida pela aplicação do filtro foram realizados com recurso ao FSL. Mais especificamente, o input usado para aplicação do filtro correspondeu à criação de uma região de interesse (RI) otimizada , que no contexto deste trabalho foi estabelecido como a substância branca. A criação desta Região de Interesse (RI) foi criada com base no uso das funções BET (remoção do escalpe e outras heterogeneidades do cérebro), FAST (cálculo de um atlas de probabilidades, considerando que as intensidades de cada região seguem uma distribuição gaussiana é realizado uma segmentação ao nível da substância branca (SB), substância cinzenta (SC) e LCR. Foi usado também a função do FSL FLIRT registo linear.

Para a implementação do filtro recorreu-se ao uso do Matlab R2016(b). De forma a obter uma maior fiabilidade clínica relativamente à máscara gerada pelo filtro, foi necessária uma otimização ao nível dos parâmetros usados. É importante referir que este filtro usa como grande referência para a identificação de estruturas tubulares, assim como a sua extração, os sinais e magnitudes dos valores próprios da matriz hessiana, com base na forma, orientação e diferenças de contraste comparativamente ao plano de fundo. Em IRM, na sequência T1 os EPV surgem como estruturas hipointensas na substância branca, pelo que na sequência T2 surgem como estruturas hiperintensas. Com base nestas diferenças de contraste entre a intensidade do LCR e SB é possível ajustar e realizar uma otimização

ao nível dos parâmetros usados.

Ao longo da implementação verificou-se que os parâmetros que revelaram uma maior efeito no output foram α e σ. Sigma σ controla a escala em que uma determinada estrutura pode ser encontrada, aumentando consideravelmente a sensibilidade na resposta do filtro. Por outro lado, Alfa α controla a sensibilidade em que uma estrutura hiper ou hipointensa comparativamente ao seu respetivo *background* é extraída e delineada. O comportamento e a sensibilidade demonstrados por ambos os parâmetros foram muito semelhantes em T1 e T2. Por outro lado, usando a sequência otimizada de parâmetros para T1 e T2 verificou-se que em imagens T2 o desempenho do filtro foi superior, conseguindo numa mesma RI delinear e extrair um maior número de EPV com a orientação e estrutura esperada, mostrando robustez relativamente à presença de artefactos de movimento e lesões de SB, compativamente a T1. Foi notado que o desempenho do filtro revelou ser extremamente sensível a diferenças de contraste, e por isso, quando a máscara que continha a RI continha rebordos com hiperintensidades, resultante de uma má segmentação obtida pelo FSL, estruturas não pertencendo a EPV eram delineadas, diminuindo a fiabilidade. Também foi testado o uso do filtro de Frangi em imagens T2-FLAIR, mas nenhum EPV foi extraído com sucesso. Porém, a análise do *output* neste tipo de imagens revelou-se promissor na deteção de lesões de SB. Consequentemente, toda a análise de quantificação e segmentação teve por base o uso de imagens T2.

Depois de se terem estabelecido todas as condições necessárias para a aplicação deste método na identificação e extração de EPV, prosseguiu-se com a quantificação de EPV por lobo cerebral recorrendo a um atlas, permitindo a segmentação apenas nas regiões desejadas. Uma vez otimizado o filtro, o principal objetivo foi verificar se existiam diferenças significativas ao nível da distribuição de EPV por região do cérebro em imagens de pacientes com Atrofia Múltipla Sistémica (MSA), Paralisia supranuclear progressiva (PSP) e doença de Fabry (FD). Cada volume de EPV por paciente foi normalizado. A normalização teve por base o volume total de EPV obtido pelo filtro, nas regiões segmentadas, dividido pelo volume correspondente de SB.

Uma vez que o pressuposto de normalidade não foi verificado, com base no resultado estatístico de *kolmogorov-Smirnov* ($p<0.05$) a um intervalo de confiança de 95%, procedeu-se à utilização de testes não-paramétricos. Todos os cálculos estatísticos foram realizados com recurso ao R-Studio.

Relativamente aos volumes normalizados de EPV observados em indivíduos pertencentes a um grupo de Atrofia Múltipla Sistémica (MSA), foi notada uma tendência para significância estatística de maior densidade de EPV no lobo frontal ($p = 0.05351$), resultado estatístico obtido através de comparações múltiplas, calculado usando o teste de *TukeyHSD*.

Numa outra análise, tentou-se verificar se existiam diferenças significativas entre controlos e indivíduos patológicos. Deste modo, aglomerou-se individuos associados a MSA, PSP e FD, comparando estes com indivíduos controlos. Foi encontrado significância estatística, a num intervalo de confiança de 95% quando se compararam estes dois grupos ($p = 0.0382$).

Numa fase final do estudo comparou-se a avaliação quantitativa realizada com valores atribuídos com base na escala visual de Wardlaw e Patankar. Esta escala permite atribuir a cada paciente um certo nível de severidade, tendo em conta a distribuição e densidade de EPV presentes no cérebro.

Também, no contexto deste trabalho, a comparação entre os *scores* visuais, obtidas pela escala de Wardlaw, e os resultados quantitativos fornecidos pela segmentação do filtro de Frangi, permitiu uma maior validação ao nível da fiabilidade deste método.

Os respetivos resultados revelaram uma correlação significativa entre a métrica estudada quando comparada com os *scores* atribuidos ($p = 0.0243$).

Por outras palavras, estes resultados indicam que um indivíduo a quem seja atribuído um *score* mais elevado de severidade, ao nível da distribuição destas estruturas, será mais susceptível a um maior volume de EPV.

Concluindo, a segmentação de EPV com este método permitiu a análise da distribuição e orientação espacial ao nível do cérebro, apresentando-se como uma possível ferramenta de monitorização e de apoio clínico, podendo no futuro ser utilizado como um biomarcador para a doença dos pequenos vasos.

Palavras-chave: Espaços perivasculares, doença dos pequenos vasos, Imagem por ressonância magnética, filro de Frangi, segmentação e quantificação.

Abstract

Perivascular Spaces (PVS) allow interstitial solutes to be cleared from the brain contributing to the brain‘s homeostasis. Dysfunction of these pathways can occur if there is deposition of substances causing stagnation of fluid (CSF). Quantitative analysis of PVS on Magnetic Resonance Images (MRI) is important for understanding their relationship with dementia, stroke and vascular diseases.

Manual delineation of PVS is very time consuming, and clinicians have to check multiple views in order to obtain a very accurate segmentation. Therefore, finding a method that would provide a reliable visual and quantitative information of a patient with PVS would enable a continuous monitoring giving clinical support throughout the development of each disease. Moreover, it would allow to understand and characterize PVS, provide useful insights into their role in normal brain physiology and small vessel disease (SVD). This work focused on the segmentation and further quantification of PVS in the brain using a vesselness filter (Frangi filter) . The Frangi filter, typically used to detect vessel-like or tube-like structures and fibers in volumetric image data, was capable to delineate, map and extract elongated and dot like features of PVS that were not easily seen when comparing with the non filtered images. However, this method requires a careful parameter optimization and further validation, since it presented different output behaviour in each MRI acquisition (T1-Weighted, T2-Weighted and T2-FLAIR).

Also, quantitative analysis regarding the Frangi segmentation indicate that PVS visual rating scores may have a positive association with PVS volume. Statistical significance was found by clustering patients diagnosed with Multiple System atrophy (MSA), Progressive Supranuclear Palsy (PSP) and Fabry disease (FD) when compared with control patients.

Keywords: Perivascular spaces, small vessel disease, Magnetic ressonance imaging, segmentation, Frangi filter, quantification.

Contents

List of Tables

List of Figures

Nomenclature

AD Alzheimer‘s Disease.

AHT Systemic arterial hypertension.

BET FSL‘s Brain Extraction Tool.

CAA Cerebral amyloid angiopathy.

CADASIL Cerebral autossomal dominant arteriopathy with subcortical ischemic strokes and leukoencephalopathy.

CBD Corticobasal degeneration.

CMB Cerebral microbleeds.

CSF Cerebrospinal fluid.

DM2 Type 2 Diabetes mellitus.

EPVS Enlarged perivascular space.

FAST FSL‘s Automated Segmentation Toolbox.

FD Fabry disease.

FLAIR Fluid attenuated inversion recovery.

FLIRT FMRIB’s Linear Image Registration Tool.

GM Grey matter.

HLT Healthy (Control group).

MFS Magnetic field strength.

MRI Magnetic Resonance Image.

MSA-C Cerebellar MSA.

MSA-P Parkinsonian MSA.

MSA Multiple System Atrophy.

PD Parkinson‘s disease.

PSP Progressive supranuclear palsy.

PVS Perivascular spaces.

ROI Region of interest.

SVD Small vessel disease.

T1W T1-Weighted-image.

T2W T2-Weighted image.

TE Echo time.

TR Repetition time.

T Transpose.

VRS Virchow-Robin space.

WMH White matter hyperintensities.

WML White matter lesions.

WM White matter.

α Frangi filter parameter.

β Frangi filter parameter.

λ orthonormal directions of curvature.

σ Frangi filter parameter.

C Frangi filter parameter.

df degrees of freedom

i, j, k Computational indexes.

x, y, z Cartesian components.

n Normal component.

p p-value.

ref Reference condition.

Chapter 1

Introduction

1.1 Motivation

Cerebrovascular diseases remain a leading cause of death and functional disability worldwide. Vascular disorders of the brain, including stroke are a major cause of death in addition to physical and cognitive disability [1]. In a 2013 study, the American Heart Association identified greater stroke burden in men than women with 133/100,000 males-years and 99/100,000 females-years incidence of ischemic stroke [2]. Vascular disorders of the brain, including Cerebral small vessel disease (SVD) are commonly observed on neuroimaging among elderly individuals and recognized as a major vascular contributor to dementia, cognitive decline, gait impairment, mood disturbance and stroke. Vascular cognitive impairment can be caused by various types of cerebrovascular disease, including cortical and subcortical infarcts, resulting in white matter injury causing neurodegeneration [1, 3]. With an ageing population the number of people affected is expected to double over the next two decades [2].

Recently, several studies evidence that Perivascular spaces contribute to the brain‘s homeostasis, were solutes presented in interstitial fluid are cleared from the brain, resulting in a drainage system [4]. Dysfunction of PVS pathways can occur if there is deposition of substances causing stagnation of this fluid, and thus may lead to the dilation of these cavity forming an enlarged Perivascular space. Subsequent neuronal dysfunction and myelin loss are related with this process, which clearly have profound implications in small vessel disease [5]. Type 3 of small vessel disease is Fabry disease, which can be characterized as lysossomal storage disorder resulting in a cascade of several cellular events including cellular dysfunction and microvascular pathology [6].

The main goal of my Master Thesis was the Quantification of Perivascular spaces (PVS) on Magnetic Resonance Image in patients diagnosed with neurological diseases, with our main focus in patients diagnosed with Fabry disease, Multiple System Atrophy and Progressive supranuclear palsy.

There are no publications that claim that the enlargement of PVS is directly connected with any of these neurological conditions. This analysis will give us a better understanding of the relationship between the enlargement of PVS within the referred neurological diseases.

Manual delineation of tubular structures such as PVS in a three-dimentional image can be very time consuming, and clinicians have to check multiple views to obtain a very accurate delineation. Recent studies show it is possible to capture the 3D geometrical shape of PVS using a certain type of vesselness filtering, thus this method shows

promise for identifying and quantifying these structures [7, 8].

During the past decades, imaging has become an indispensable tool in the diagnosis and treatment planning for these diseases. However, it is extremely necessary to find new methods in order to increase the specificity and sensitivity of neuroimaging. Quantitative measurements will also better characterize the severity of Perivascular spaces in ageing people and their associations with cerebrovascular diseases.

This first chapter presents a literature review of the methods for quantification and segmentation of PVS in patients diagnosed with Fabry disease (FD), Multiple System Atrophy (MSA) and Progressive supranuclear palsy (PSP) . PVS are an important part of the brain circulation and glymphatic drainage system. Dilated PVS found to be associated with many conditions including ageing, dementia, SVD, and their quantitative analysis is important for a better understanding of their role and relationship with neurological diseases, in particular SVD. This literature search was performed using PubMed, Web of Science. For this search a combination of the following terms was used: segmentation, perivascular space(s),Virchow-Robin, VRS, methods, quantification, MRI, SVD.

1.2 Background

1.2.1 Perivascular Spaces

PVS also referred as the Virchow-Robin spaces (VRS), are fluid filled compartments or cavities containing CSF-like fluid [4], surrounding small arteries and arterioles as they perforate from the subarachnoid space through the brain parenchyma, represented in Figure 1.1, working as a major conduct for drainage of interstitial fluid (ISF) and CSF from the brain and clearance of waste products from the brain [9, 10], playing an important role in normal brain homeostasis. In this drainage system, the efflux of ISF occurs to facilitate the waste clearance while the influx of CSF from the subarachnoid spaces into the periarteriolar spaces acts in the delivering of metabolic factors and signalling molecules, required for brain function[5]. Normal PVS are not typically seen on conventional structural brain MRI [10], but when these spaces start to become dilated, due to the stagnation of fluid drainage by the accumulation of protein and cell debris, they cause an edema in the White matter (WM) becoming visible [9], resulting in Enlarge Perivascular Spaces (EPVS). EPVS are an important marker of various neurological conditions, including aging, dementia [4, 10], Alzheimers disease(AD) [5], traumatic brain injury, stroke, and other white-matter lesions[9, 10]. Some studies also refer that these dilation may due to neuroinflammation, neurodegeneration, demyelination, being a sign of a lymphatic dysfunction [10, 11, 12], contributing for the pathogenesis of several SVD, but not being the result of the disease [9].

These cavities can be found in various regions, and its anatomy varies by location. They appear only in white matter regions being commonly found in the basal ganglia, centrum semiovale and pontomesencephalic junction [5, 10-12]. In the arteries of the basal ganglia is where the largest CSF influxes occur contributing to a common site for EPVS formation in SVD. Also, the size and shape of EPVS can vary in these locations, and can be commonly mistaken with Lacunes , Lacunar infarcts and punctuate white matter hyperintensities[5,6] since its diameter is very similar, ranging 3-20 mm. Only looking at the shape and intensity on a MRI scan it is possible to differentiate EPVS from these spaces. EPVS when seen on MRI scans tend to be round or oval if viewed transversally and tubular or elongated if longitudinally, with a well-defined smooth boundary, while lacunes and Lacunar infarctions usually present wedge shaped or ovoid, with well and non-well smooth boundary, respectively [6]. According to

intensity on MRI scans, EPVS present hypointensities on fluid attenuated inversion recovery sequences (FLAIR) on T1-Weighted images, and appear as Hyperintensities on T2-weighted image sequences[5-6, 10-12]. Moreover, these cavities tend to form a network of spaces around cerebral microvessels. These structures lie between the basement membrane around pericytes and the basement membrane at the surface of the glia limitans of the brain vessels. Although, there are no PVS around arteries in the cortex, there is a potential for dilatation of PVS related to arteries in the cerebral white matter [13]. Dilated PVS are seen only in the white matter, basal ganglia, and brainstem [14].

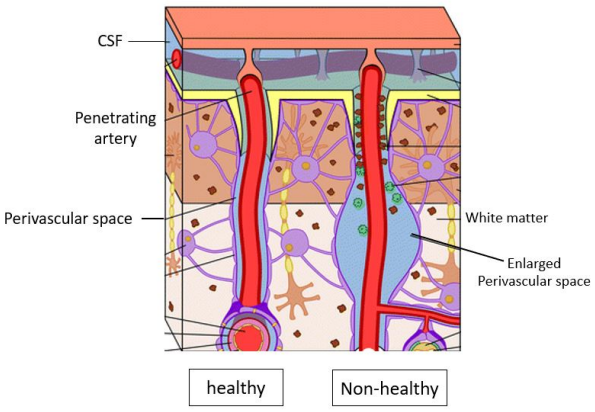

Figure 1.1: Healthy perivascular space (in the left) and a dilated or enlarged perivascular space (in the right)(adapted from [15]).

1.2.2 Role of PVS in cerebral small vessel disease

Small vessel disease (SVD) is a group of age-related neuropathological processes affecting the small perforating arteries, arterioles, capillaries, and venules resulting in damage to the cerebral white and deep grey matter [9]. SVD is responsible for a large proportion of cases like stroke and dementia worldwide [2], and it can manifest in several different ways. The most common subtypes of SVD are the types 1-3. Type 1 consists of sporadic arteriolosclerosis secondary to aging and other vascular risk factors including systemic arterial hypertension (AHT) and type 2 diabetes mellitus (DM2) [2,6]. Type 2 is a sporadic or hereditary cerebral amyloid angiopathy (CAA). Type 3 includes all inherited or genetic SVD subtypes excluding CAA, the most common[18] being cerebral autossomal dominant arteriopathy with subcortical ischemic strokes and leukoencephalopathy (CADASIL). Fabry Disease (FD) can be characterized as a type 3 genetic SVD, where there is a deficiency in the lysossomal enzyme, resulting in a disorder of the glycosphingolipid metabolism [16, 17].

Neuroimaging in SVD contributes to the pathological findings of increased exposure to vascular risk factors in adulthood (particularly hypertension and smoking), cognitive decline [9, 17], increased risk of stroke, and other neurological and psychiatric disorders [16]. In particular MRI images from patients with SVD show white matter hyperintensities (WMH), associated with White matter lesions (WML) comprised of myelin loss, and other characteristic abnormalities, such as enlarged perivascular spaces (EPVS), lacunes and cerebral microbleeds (CMB) [14]. All of these individual imaging features are inter-related contributing to the SVD burden [18].

EPVS are widespread and present in almost all SVD types in both sporadic forms of SVD type 1 and 2 and hereditary type 2 and 3 [16], and are routinely seen together in the Basal ganglia and centrum semiovale, implying a common cause [6]. However, there are no confirmations yet of EPVS in CADASIL patients [18]. These events indicate that EPVS may be a sign of lymphatic fluid stasis and play a role in the pathogenesis of SVD.

PVS are considered to play a role in normal brain homeostasis [10-12].

Glymphatic system

The glymphatic system is a brain-wide pathway along a system of connecting perivascular spaces (PVS) over which cerebroespinal fluid (CSF) surrounding the brain exchanges with the interstitial fluid (ISF) within the parenchima [6,18]. Bulk flow entry of CSF into the periarterial spaces (lymphatic influx) is important for the brain delivery of glucose in energy metabolism, transport of lipids and signaling molecules [18], and apolipoprotein E (apoE)-delivered from the choroid plexus, while the efflux of ISF play a role in the clearance of several metabolic waste products. This lymphatic system requires an adequate CSF production by the choroid plexus to provide a pressure gradient of fluid, moving from ventricles to the subarachnoid space (SAS) and PVS.

1.2.3 Small Vessel Disease

Cerebral SVD refers to a variety of pathological processes that affect the small arteries, arterioles, venules, and capillaries of the brain [2], along with the subsequent damage caused in the white and deep grey matter, which are crucial to the normal brain function [1]. SVD term covers a variety of abnormalities related to small blood vessels in the brain, being the lead cause of cognitive decline and functional loss in the elderly. Its repercussions include disabilities at a cognitive, psychiatric and physical level, adding to the increased risk of stroke and dementia [1]. With the ageing of the population, the prevalence of SVD is increasing and so are the costs associated with its consequences [4]. It is thus essential to improve the assessment of this disease by investigating its clinical manifestations in the brain, which can be achieved through imaging techniques. This pathology affects the small vessels in the brain and its clinical manifestations vary from physical disabilities that in more advanced stages of disease can lead to loss of autonomy, to neuropsychological impairments causing progressive cognitive deterioration and eventually dementia [2]. Therefore, it is of major importance to identify early physiological alterations that might precede vascular damage. Progress in neuroimaging has led to a better understanding of the pathophysiology of SVD, contributing to the development of biomarkers that can provide an evaluation of the disease's progression.

SVD has been subdivided into six different subtypes, based on an aetiopathogenic classification [2]:

(i) arteriolosclerosis: related to ageing and vascular risk factors. Small vessels are affected by the reduction of the number of smooth muscle cells in the tunica media, thickening of the wall and narrowing of the lumen;

(ii) cerebral amyloid angiopathy (both sporadic and hereditary): amyloid -peptide accumulates in small vessels' walls, particularly in small arteries and arterioles. As a consequence, vessels can dilate and even rupture, leading to hemorrhages;

(iii) genetic/inherited SVD: the most common pathologies within this subtype of SVD are CADASIL and Fabry's disease - both of them are associated with genetic mutations;

(iv) inflammatory/immunologically mediated: as the name suggests, these pathologies derive from the presence of inflammatory cells in small vessels' walls;

(v) venous collagenosis: affects mainly veins and venules located near the lateral ventricles. These vessels' lumen becomes narrower due to increased thickness of the walls, which can lead to occlusion;
(vi) other SVD: this subtype of SVD includes post-radiation angiopathy, which appears as an irradiation therapy's side-effect and affects mainly white matter, causing thickening of the vessels' walls.

1.2.4 Fabry Disease

Fabry disease (FD) is an X-linked devastating progressive inborn disorder of the glycosphingolipid metabolism due to a deficient or absent lysossomal enzyme resulting in a cascade of several cellular events [19, 20]. It is reported that the annual incidence ranges from 1 in 476,000 to 1 in 117,000 [19] in the general population. In FD, particularly in the early stages, several important roles such as cellular dysfunction and microvascular pathology are induced, mainly occuring in the late fourth through early sixth decades of life [19, 20].

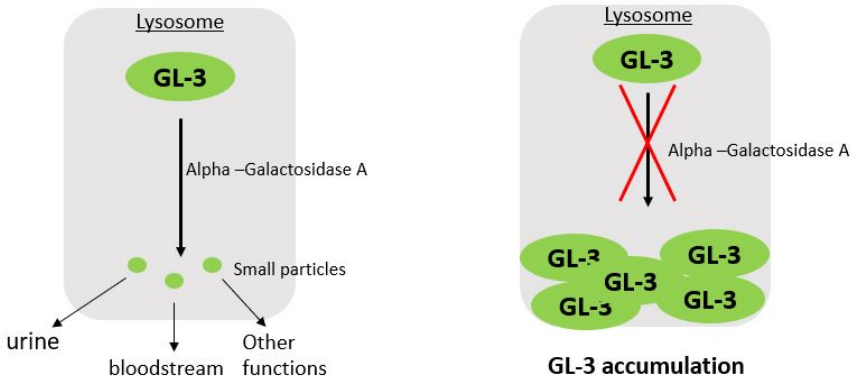

Figure 1.2: Mechanism of Fabry disease. (Left) Healthy pathway, hydrolisation occurs in lysossome. (Right) Deficiency in enzime, resulting in an accumulation of ceramide (Gb3).

FD is transmitted as an X-linked trait and can be mainly characterized by a lysosomal storage disorder, where exists a deficiency or inexistence of the lysosomal hydrolase α - galactosidase A (α-D-galactosidase)[18, 21], coded by an unique gene. GLA consists of seven exons distributed over 12,436 base of pairs[19], leading to a progressive endothelial accumulation of enzyme substrates, mainly globotriaosylceramide (Gb3 or GL-3),also known as ceramide trihexoside(CTH), and related glycosphingolipids (galabiosylceramide) within lysosomes which are ubiquitous subcellular organelles, in several typical locations such as in the vascular endothelium, perithelium, and smooth muscle cells, as well as in parenchymal cells in kidney, heart, dorsal root ganglia, autonomic nervous system, and brain [18-19]. When this progressive accumulation comes to light in these places it is belived that a cascade of several subsequent vascular events emerge including small-vessel injury [17, 13], K(Ca) channel dysfunction in endothelial cells [19], oxidative stress, impaired autophagossome maturation, tissue ischemia, irreversible cardiac and renal tissue fibrosis [20].The primary disease process starts in the early fetal stage of development and the first clinical symptoms arise in childhood, between the ages of 3 and 10 years, commonly diverging according to gender, affecting girls more later comparing to boys, but most of the patients remain clinically asymptomatic. As the years advance symptoms intensity start to increase, becoming more proeminent after the age of 30 [21], and also the clinical condition becomes more delicate, providing progressive damage in several organ systems

including the kidneys, heart and brain,becoming life-threatening, reducing life-expectancy by 20 years compaired with normal population [18].

All these cellular damages can be visualized on both T1-weighted and T2-weighted MR images [21, 22].

1.2.5 Parkinson disease

Parkinson‘s disease (PD) is an idiopathic disease of the nervous system characterized by the inclusions of abnormal intracellular aggregates, Lewy Bodies, containing proteins such as α-synuclein and ubiquitin that impair optimal neuron functioning [23] . These aggregates lead to manifestations in both motor and non-motor system presenting degeneration of dopaminergic neurons (dopamine-producing) in the substantia nigra (SN) of midbrain, resulting in a synaptic dysfunction that interfere with axonal transport and thus neuronal damage [24, 25], causing the core motor features of PD.

Several neurodegenerative disorders like Multiple System Atrophy, Progressive Supranuclear Palsy (PSP) and Corticobasal Degeneration (CBD) can mimic PD. Parkinsonian symptoms may be linked to perivascular spaces. These connection is not clear, but accordingly to some studies, these cavities would have an important role in cortical-subcortical connections and involve the corticostriatal fibres, contributing to a cognitive impairment and parkinsonism [26], respectively. PVS may contribute to an earlier onset of the symptoms of these disorders.

1.2.6 Atypical Parkinsonism

Multiple System Atrophy (MSA)

Multiple System Atrophy (MSA) is an adult-onset, fatal rare sporadic neurodegenerative disease characterized by progressive autonomic failure with neuronal loss, axonal degeneration of multiple neurological systems leading to a myelin loss and microglia activation, resulting in autonomic dysfunction signs [27] and other symptoms such as dysphagia [28], stridor and dysarthria [27, 22], and also non-motor symptoms like anxiety, depression, emotional incontinence, REM sleep behaviour disorder [28].

Genetic and environmental factors may contribute to the initiation of the pathophysiological cascade of MSA. Postmortem examinations reflected olivopontocerebellar atrophy and striatonigral degeneration.

These neurodegenerative conditions lead to cytoplasmic inclusions of the glia that usually occur mainly in the striatonigral system, olivopontocerebellar region, autonomic nuclei of the brainstem and the spinal chord, and as consequence, activated microglia and reactive astrogliosis are a common finding in patients diagnosed with MSA [22]. Glial cytoplasmatic inclusions are constituted by a protein, alpha-synuclein, located in neuronal axons and synapses.

In addition, some authors afirm that a frontal lobe atrophy may also be observed after a long disease duration [24, 22]. Depending on the dominant motor phenotype, MSA can be classified in two subtypes, the Parkinsonian MSA (MSA-P) or Cerebellar MSA (MSA-C).

Moreover, the pathogenesis mechanisms remain unclear. Taking evidences from preclinical models and post-mortem studies, the α-synuclein aggregation may arise from an overexpression of α relocalisation of an important stabilizer of mielin, p25α into the oligodendroglial soma. These interaction between p25α and α-synuclein promotes a phosphorylation and aggregation of synuclein into insoluble oligomers that later on gives rise to the forma-

tion of a glial cytoplasmatic inclusion. These formation will interfere with neuronal support, activating microglial cells [29]. After this process, a neuronal cytoplasmatic inclusion is formed due to the misfolding α-synuclein into the extracellular space, affecting neighbouring neurons. Reaching this point, neuroinflammation, loss of oligodendroglial neurotrophic support and neuronal dysfunction, neuronal death starts to take place [27, 22].

Progressive supranuclear palsy (PSP)

Progressive supranuclear palsy (PSP) is another type of rare, sporadic and progressive neurodegenerative disorder that causes postural instability, seudobulbar palsy, Parkinsonism unresponsive to Levodopa and cognitive impairment [30, 31]. PSP is defined by the accumulation of tau protein and neuropil threads, mainly in the pallidum, subthalamic nucleus, red nucleus, substantia nigra, pontine tegmentum, striatum, oculomotor nucleus, medulla, and dentate nucleus [32].

The main pathological features of PSP are the presence of star-shaped astrocytic tufts and neurophibrillary tangles that can be seen with light microscopy, supporting the role of tau dysfunction in the pathogenesis as a primary tauopathy [32].

1.2.7 Fundamentals of Magnetic Resonance Imaging (MRI)

Magnetic Resonance Imaging (MRI) is an imaging modality that makes use of the magnetic properties of tissues in order to produce an image. This method has provided huge developments in Medical investigation and diagnosis, particularly with avoidance of exposure to potentially dangerous ionizing radiation. This method makes use of the hydrogen nuclei, abundant in the human body and found in water molecules as well as in fat. For that reason, it will spin around its own axis, creating a magnetic moment that can interact with magnetic fields. When placed in a strong external magnetic field, the proton experiences a turning force, or torque, which tries to align its moment with the main field [33].

T1-Weighted

T1 is a parameter related to the regrowth of longitudinal magnetization characterized of specific tissue. The rate at which this longitudinal magnetization grows back is different for protons associated with different tissues, contributing to the fundamental source of contrast in T1-weighted images. Moreover, assuming a 90^{o} RF Pulse, T1 is the time necessary for the longitudinal magnetization reaches 63% of its final value.
The magnetization of tissues with different values of T1 will grow back in the longitudinal direction (T1 relaxation) at different rates.
White matter (WM), Cerebrospinal fluid (CSF) and Gray matter(GM) have different rates of T1-relaxation. WM has a very short T1 time and relaxes rapidly, contributing to the lighter pixels. CSF relaxes at a slow rate obtaining a long T1, contributing for the darker pixels, same intensity of perivascular spaces. GM has an intermediate T1 relaxation and appear in T1W images as pixels with intermediate shades of gray [33, 34].

T2-Weighted

T2 relaxation process occurs simultaneously with the T1. After a 90^o RF pulse T2 decay occurs causing the dephasing of the transverse magnetization, while the longitudinal magnetization grows back parallel to the main magnetic field. After a few seconds, most of the transverse magnetization is dephased. As a consequence, T2 is characterized as the rate of dephasing for the protons, associated with different tissues and corresponds to the time that it takes for the transverse magnetization to decay 37% of its original value.
WM has a short T2, dephases rapidly and is associated with darker pixels. PVS appear in the same intensity as CSF(associated with lighter pixels) due to a slow dephase and long T2. GM has an intermediate T2, dephases intermediately and is associated with gray-level pixels [33, 34].

Fluid attenuated inversion recovery - FLAIR

The inversion-recovery pulse sequence is useful for suppressing unwanted signals in MR images. This type of sequence will attenuate or suppress fluid and is characterized by having an additional 180^o RF pulse, prior to the regular spin-echo pulse sequence. Moreover, this additional RF pulse causes an initial inversion, towards in the z axis of the longitudinal magnetization, so that it is aligned in the -z direction, and after this RF pulse the magnetization will grow back towards +z direction. Once again, different tissues presents different grow back rates, and since the magnetization passes through the -z to the +z will cross zero axis, where the signal of magnetization is zero. GM appears brighter than WM, while the CSF is dark instead of bright [33, 34].

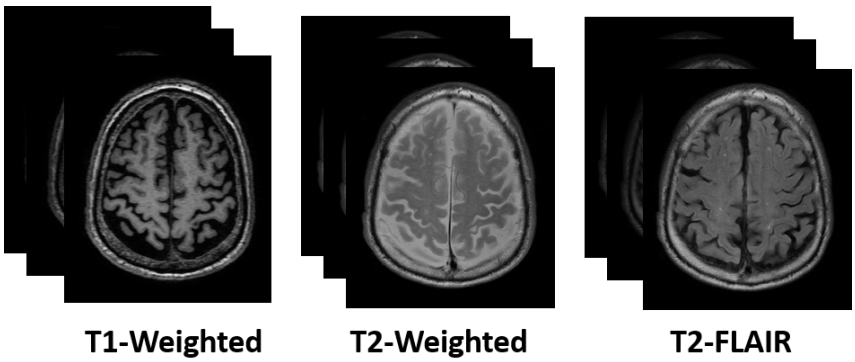

Figure 1.3: MRI sequences used in the study: T1-Weighted (T1W), T2-Weighted (T2W) and T2-Flair.

1.3 State-of-the-art

So far, few studies showed that is possible to capture the 3D shape of a perivascular space using an automatic method, and very few of those showed accuracy, in terms of segmentation, and a correct correlation when compared with neurological assessments performed by clinicians. Most recent works developed in 2018 proposed a segmentation technique based on vesselness filtering, especially using 3D Frangi filter [7, 35, 36, 37], showing promising results in the analysis of the spatial distribution, orientation and density. Descombes et al. in 2004 constructed a model for PVS segmentation using Markov chain Monte Carlo to optimize pre-defined filters [38], becoming the first author who proposed a segmentation method for these features using Markov models for opti-

mization. Moreover, an algorithm enabling automatic detection of lacunar infarcts using intensity thresholding was proposed in 2007 [39] by Yokoyama et al. They evaluated their method to detect lacunar infarct and prevent the ocurrence of cerebral apoplexy in high-risk patients. Thereafter, the sensitivity of the detection of lacunar infarct was 90.1% on 828 MR images from 80 patients. Since 2008, several authors proposed a extraction methods by using intensity thresholding. Wuerfel et al.(2008) investigated PVS distribution in different brain regions [9] in 45 Multiple Sclerosis (MS) patients and 30 healthy controls using different MRI sequence (T2-weighted and T1-weighted). In this study, MS patients had significantly larger PVS volumes comparing with healthy subjects. PVS were visualized as hyperintense regions on T2-weighted and as hypointense regions. A different method in 2011 was proposed by Ramirez et al, using Lesion Explorer, a semi-automatic segmentation method [40].This method allowed to exploit both T1 and T2 images for subcortical hyperintensities segmentation. In this study, subcortical hyperintensities and PVS were extracted by applying thresholds derived from both image sequences. Similar to [15], Zong et al.(2016) developed also a semi-automatic method using Frangi vesselness filter performing a detailed distribution, length and volume of PVS [5]. For this study, T1 and T2 MRI sequences were acquired using a 7 T Siemens scanner, with a 32-channel receive head coil in 17 healthy volunteers between ages (21-37).

In 2018 Ballerini et al. proposed a segmentation technique using Frangi Filter [41], being capable to extract PVS from MRI. They applied this filter in a dementia sample of 20 patients and 48 patients suffering Mild to moderate stroke. Before the filtering application, a mask containing the region of interest was created for each image, where automatic brain, CSF and white-matter extraction were performed on T1-W and T2-W MR images using FMRIB software library (FSL). In this work the parameters of the Frangi filter were optimized using a Log-likelihood function. The results of this study presented a good correlation with the visual rating scores, obtaining a Spearman's ρ= 0.47 and a *p-value*= 0.001. The optimization procedure was applied to both T1W and T2W MRI sequences.

In [42, 5, 37] studies, the authors suggest that the most effective method to extract tubular features from White matter is using Frangi filter. Another learning based PVS segmentation method was proposed [5], where first the region of interest (ROI) was extracted using Brain extraction tool, dividing brain in different regions, creating a ground-thruth for PVS masks.

In another recent study realized in 2018 by Feldman et al. with the main purpose to evaluate and compare PVS density in different brain hemispheres [8], in a group of epilepsy and healthy patients, an ultra-high resolution MRI (7 Tesla). The location and cross-sectional diameter of all structures were manually marked, and their anatomical landmarks in the same coordinate axis were exported from Osirix to a custom built software using Matlab. Using these coordinates, each marked PVS was categorized as being localized in either left or right hemisphere of the brain. Afterwards, the quantitative analysis in this study showed that great overall PVS asymmetry exists in the brains of epilepsy patients when compared to healthy controls (p = 0.016). Moreover, PVS density was found to increase with age and their distribution may be strongly linked to effects of epilepsy and neurological structure and function.

Table 1.1: State-of-the-art (review)- Methods for Perivascular Spaces extraction and similar features

Study	Computational method	Features analyzed	MR sequences used	Sample size	Sample type	Results
Sachdev et al. 1999 [38]	Manual delineation by thresholding using AnalyzeTM software	MR signal hyperintensities (EPVS identified for exclusion)	PD and T2-weighted (T1-weighted used as reference) at 1.5T	98	62 schizophrenic elderly subjects and 36 controls	The correlation between visual and computerized methods was good except for ratings of hyperintensities in subcortical nuclei
Descombes et al. 2004 [38]	Manual delineation using Markov chain Monte Carlo for optimization	PVS	T1-Weighted T2-Weighted 1.5 T	-	-	This method showed promising results with visual rating scores
Ramirez et al. 2011 [40]	Semi-automatic segmentation method (lesion explorer)	Subcortical hyperintensities	T1-weighted T2-weighted 1.5 T	-	-	Subcortical hyperintensities and PVS were extracted
Wuerfel et al. 2008 [9]	Threshold-based semi-automatic method	Lacunar infarcts and PVS (number and volume)	T1-weighted T2-weighted FLAIR - 1.5 Tesla	75	45 subjects with Multiple Sclerosis (MS) 30 healthy subjects	Lacunar infarcts and PVS were extracted with success.
Uchiyama et al. 2008 [35]	Enhanced intensities using White-top-hat transformation taking acount intensity and threshold	lacunar infarcts PVS	T1-Weighted T2-Weighted 1,5 T	109	Information not visible	Area under the ROC curve was 0.945.
Yokohama et al. 2007 [39]	Proposed method using intensity and thresholding for morphological segmentation	lacunar infarcts	T1-Weighted T2-Weighted 3 Tesla	80	cerebral apoplexy sample	sensitivity of detection was 90.1 %

Table 1.2: State-of-the-art Segmentation of perivascular spaces methods(Continue).

Study	Computational method	Features analyzed	MR sequences used	Sample size	Sample type	Results
S. Hyun Park et al. 2016 [11]	Proposed semi-automatic method based in anatomical brain vesselness thresholding Frangi filter Markov random field models	PVS and tubular structures (volume and diameter)	7 Tesla scanner (SIEMENS) T1/T2 acquired with MPRAGE sequence	17	17 healthy individuals (25-37 years old)	Most tubular structures were extracted from WM
Zong et al. 2016 [5]	Semi-automatic method using Frangi vesselness Filter	PVS	7 Tesla scanner (SIEMENS) with head coil receiver	-	-	PVS were well visualized and extracted from WM
Feldman et al. 2018 [8]	Osirix (Pixmeo, Geneva) Matlab (custom made)	PVS	axial (T1- Weighted and T2-weighted turbo spin echo-TSE) 7 Tesla	38	21 subjects with focal epilepsy 33+/- 11 years (13 males , 8 females) 17 healthy - 33 +/- 9 years (11 males,6 females)	PVS distribution found to be more asymmetric in epilepsy patients when compared to healthy control groups. Number of PVS increase with age.
Ballerini et al 2018 [41]	Proposed segmentation using 3D Frangi Filter	PVS	T1-Weighted T2-Weighted FLAIR 7 Tesla Scanner	68	20 (dementia sample) 48(mild to moderate stroke)	Spearman‘s = 0.47 ; p-value= 0.001

1.4 Objectives

The objectives to be achieved in this thesis can be divided in two groups. Firstly, use a filter capable to extract the desired features in T1 and T2-Weighted MR images, the Frangi Filter, in order to enhance perivascular spaces, and then perform a clinical validation accordingly with the output given by the filter, by comparing it with samples previously marked by physicians. During this stage, image processing will be performed by using a MRI software tool (FSL) in order to create a region of interest (ROI), giving the filter the best conditions to achieve a reliable output. After performing image processing, the implementation of the filter advances using matlab, and is important to verify which sequence possesses an higher level of clinical reliability by comparing the respectively output. During this process several parameters of the filter will be tested, and reported, in order to test the sensitivity of the filter, optimising that values accordingly to the visual output expected, finding the most adequate and reliable interval values of parameters, capable of extracting only perivascular spaces.

Secondly, after finding the best parameter values, the second main goal of my thesis is performing a quantification based on the density of perivascular spaces accordingly to each type of disease. It is also interesting to perform a quantification in each brain region, using an atlas, and check for statistical significance in both analysis.

This analysis would give a better understanding of the major role and connection that these structures have in neurological diseases.

1.5 Thesis Outline

This dissertation is composed by six chapters, which are organised as follows: the present chapter introduces a motivation for the following study, also the respective background regarding concepts that are addressed throughout the dissertation, and a literature review on previous studies containing possible methods that allow vessel feature enhancement regarding the features of a perivascular space, and their results. Chapter 2 presents a full description of the data and the methodology applied, including the pipelines used from the pre-processing of MR images to the application of the filter, including parameter optimization in order to obtain a more reliable output regarding the ground-truth. In other words, this trials will allow to verify the behaviour and sensitivity of each parameter present in the segmentation of structures. Chapter 3 displays the results of the application of the filter with parameter optimization, and also a verification and validation of the output. Chapter 4 includes statistical analysis in the context of the work. The last two chapters, Chapter 5 and 6, provide the principal discussion and conclusions of this study. Moreover, some limitations are presented in the last chapter, and how they could be addressed in future works.

Chapter 2

Methods

The segmentation and quantification of PVS has been a true challenge, especially, the differentiation between lacunes and other tubular structures from PVS. The present chapter focuses on the description of all methodology used in this study in order to respond to the defined objectives. Therefore, in this section is included a full description of the data used regarding MRI acquisition and the proposed pipelines regarding the optimization and selection of regions of interest (ROI), used as input to the filter. Also, the methodology used to perform an improvement of the mask given by the filter, and finally, the pipeline used for PVS quantification.

2.1 Data Description

2.1.1 Imaging data

All the data used in this study were provided by Hospital Santa Maria - CHLN (Centro Hospitalar Lisboa Norte), especially gathered by Professor Sofia Reimão, MD, PhD. and João Madureira, MD, both physicians working in the neuroimaging department of the mentioned Hospital. Moreover, the collected data for the following study were comprised of 4 groups: 3 control patients, 2 patients diagnosed with Fabry disease (FD), 7 patients diagnosed with MSA and 3 PSP patients, making a total of 15 individuals.

The MRI data, acquired on a 3T Philips MRI system, were composed by a set of structural images, whereby the ones analysed in this study were T1-Weighted (T1W) images obtained using an MPRAGE sequence, T2-Weighted (T2W) and T2-FLAIR images obtained using a fluid attenuation inversion recovery sequence. The MRI acquisition parameters used in this study for the sequences T1W, T2W and T2-FLAIR are displayed in table 2.1.

Table 2.1: MRI acquisition Parameters used in the study.

	T1-Weighted MPRAGE	**T2-Weighted**	**T2-FLAIR**
Magnetic Field Strength	3 Tesla	3 Tesla	3 Tesla
TE (ms)	4.6	80	136
TR (ms)	2250	8500	6200
TI (ms)	-	-	1882
Voxel size (x,y,z) [mm]	1x0.4883x0.4883	0.4688x0.4688x5	0.4688x0.4688x6.2
Matrix size (x,y,z)	512x512x150	512x512x28	512x512x24
Flip Angle (degrees)	90	90	variable

2.2 Segmentation

Segmentation is very important for the assessment of PVS, distinguishing it from confounding tissue boundaries or similar regions like lacunar infarcts, and in other cases to reduce errors from minor imaging artifacts. An accurate segmentation of PVS will allow the analysis of their spatial distribution, orientation and density.

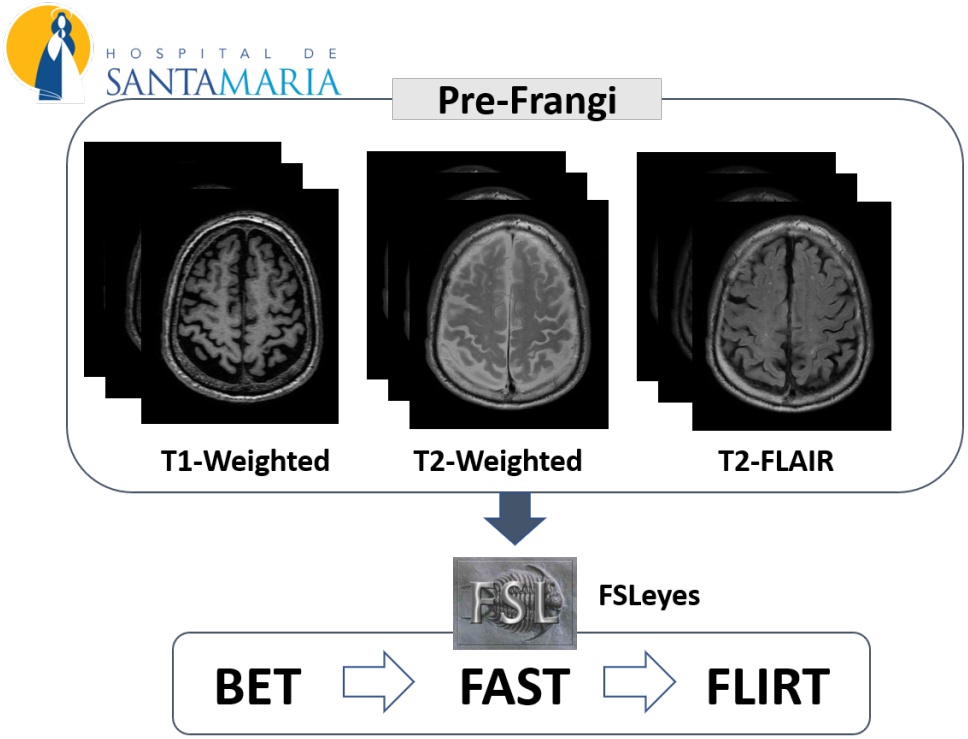

Figure 2.1: Brief review of the methodology used to extract the region-of-interest, used as input to the filter.

To segment an extremely narrow structure as the PVS some techniques are not capable of capturing the discriminative features and characteristics of PVS. Image processing algorithms such as segmentation, texture analysis or classification that use the gray level values of image pixels will not produce satisfactory results due to the existence of bias field. Bias field signal is a low-frequency that blurs images reducing the high frequency of the image such as edges and contours, changing the intensity values of image pixels so that the same tissue has different gray level distribution across the image. Therefore, a pre-processing step is needed to correct for the bias field signal before submitting corrupted MRI images as input to the Frangi filter. In order to perform an accurate segmentation, vesselness filters were used such as the Frangi filter into a structured random forrest for classifying voxels into positive (i.e PVS) and negative (background). However, before performing a structural segmentation of a very narrow feature some pre-processing image steps were required, especially bias field correction and brain extraction that allowed to give as input only the region-of interest, eliminating the scalp. There are computer software's that allow brain extraction, bias field correction and alignment such as FSL.

In order to segment perivascular spaces several steps of image processing have to be taken into account. In this study the implementation can be divided in three pipelines: Pre-Frangi, Filtering (implementation of Frangi), and Pos-Frangi.

Firstly, the first step (Pre-Frangi) includes the optimization of images previously acquired, bias field correction and

brain extraction, allowing the selection of regions of interest, serving as input to the filter (figure 2.1).
Secondly, the segmented region of interest is given as input to the Frangi filter along with required parameters, using Matlab. At the end of the current Chapter is also shown all the trials that were used to realize a parameter optimisation are shown, so as to select the best parameter combination for each sequence.
At last, similarly to the first stage, FSL is used to optimize the first created mask, containing the region of interest, eliminating non PVS zones.

2.2.1 FSL for brain segmentation

FSL is a comprehensive library of analysis tools for FMRI, MRI and DTI brain imaging data [43, 44]. FSLs automated segmentation toolbox (FAST) can be used to segment raw images, normally T1,T2 and proton-density images into certain probability for tissue types such as CSF, GM and WM, performing a segmentation and bias field correction. The BET toolbox allows brain extraction where non-brain tissues with highly variable contrast and geometry (i.e. scalp) are eliminated (figure 2.3), leaving all the brain intact [43].The FAST toolbox uses the BET function to remove non-brain. All volumetric results are highly sensitive to errors here.

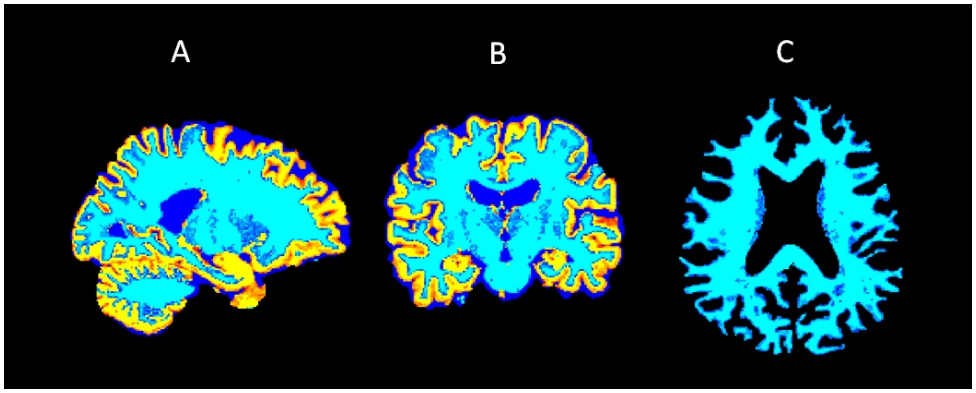

Figure 2.2: Brain probability maps based on gray matter(GM), white matter(WM),and CSF using FSLs automated segmentation toolbox - FAST. A and B (GM in yellow, CSF in blue and WM in light-blue); C - Axial view of the WM mask (light-blue).

Also, the bias field correction is necessary since the MRI RF(radio-frequency field) inhomogeneity causes

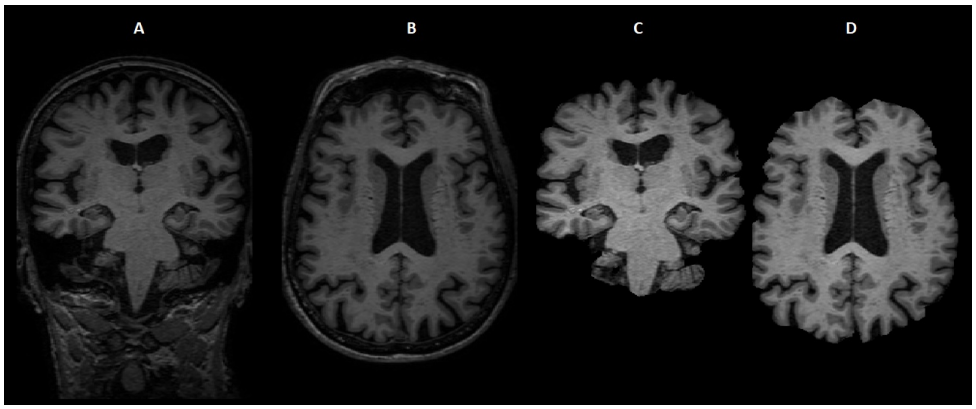

Figure 2.3: Comparison between brain with scalp(A and B - before applying BET function) , and after applying skull stripping (BET: C and D), in a T1W.

intensity variations across space, causing problems for segmentation. The FAST toolbox uses the BET function to remove non-brain. Figure 2.2 shows an example of a resulting probability map for three tissue type, White matter, gray matter and CSF represented in yellow, light-blue and green, respectively.

FMRIB's Linear Image Registration Tool (FLIRT)

Linear registration and motion correction are important components of structural and fuctional brain image analysis, where accuracy and robustness are required. The registration problem is to find the best geometric alignment of two volumetric brain images. After the selection of the desired ROI, and in the context of this work is the white matter (WM), the FLIRT (FMRIB's Linear Image Registration Tool)[45] was used in order to perform an affine registration from T1W space to T2W and T2-Flair (figure 2.4).

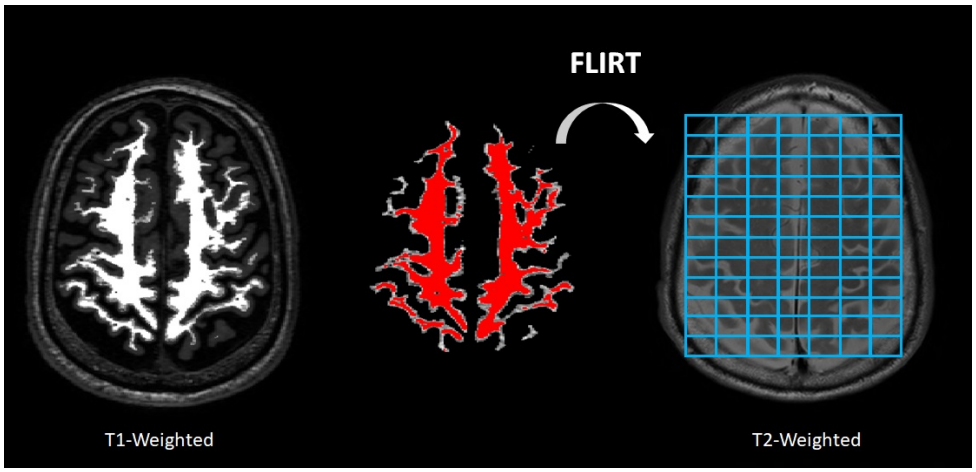

Figure 2.4: Linear registration in a T1W white matter mask, our region of interest (ROI) in red, to T2W, using FLIRT.

The following command lines used to perform an accurate registration was: an input (-in) and a reference (-ref) volume. The calculated affine transformation that registers the input to do the reference which is saved as an affine matrix and a output volume (-out). To align it with the reference volume the transform matrix generated is applied to the input volume. The implementation of FLIRT can be divided in two stages: the first stage requires an input (-in) and a reference volume (-ref). After the implementation of the first stage, an affine matrix of the two volumes aligned is generated. The second stage requires the application of a transformation containing the generated affine matrix, and the output given will be the input given volume aligned in the desired reference space. In addition, FLIRT can also be used to apply a saved transformation to a volume (-applyxfm, -init and -out) or to apply a transform that aligns the NIFTI mm coordinates (-applyxfm, -usesqform and -out, but not -init). For these usages the reference volume must still be specified as this sets the voxel and image dimensions of the resulting volume [45].

After having a reliable segmentation of the mask containing the WM along with PVS the implementation of the filter takes place. As it is shown in figure 2.5, the usage of the frangi requires several input parameters.

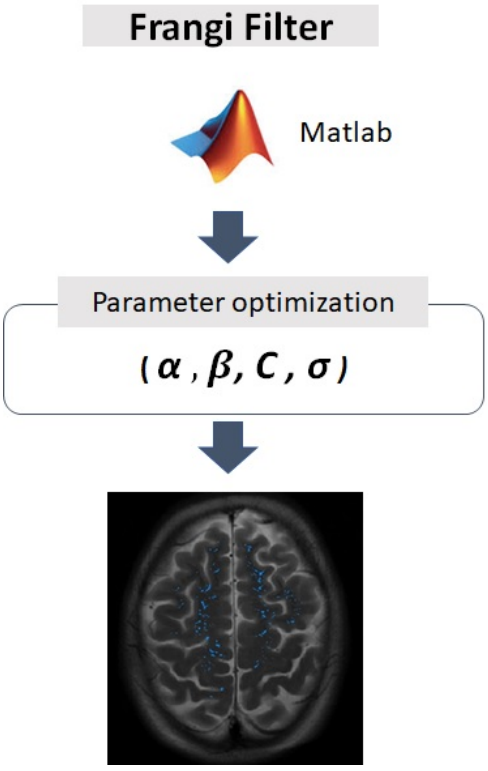

Figure 2.5: Implementation of the Frangi Filter method, using Matlab.

2.3 Enhancement filtering

Most state-of-the-art enhancement filters employ the analysis of 2nd order derivatives of image intensity, which is encoded in a Hessian matrix involving eigenvalues. Several enhancement filters characterize the local structure by analyzing the 2nd order intensity derivatives or Hessian at each point in the image. Also, in these type of analysis, a Gaussian scale space of the image is used to enhance local structures of several sizes [41].

2.4 Frangi Filter

Vessels generally consist of elongated structures that occupy a small area of the total Area being analyzed in the images, and either are lighter or darker comparing with their respective background. Regarding the context of the following work, a vessel enhancement filter was chosen for the extraction of PVS, and it can be described as a filtering process that searches for geometrical structural and common such as tubular or elongated and dot-like features [37, 46].

Thereafter, a common approach, defined by [37], in order to analyze the local behaviour of an image I , is to consider its Taylor Expansion in the neighborhood of a point X_0,

$$I(X_0 + \delta X_0, S) \approx I(X_0, S) + {\delta_{x_0}}^T \nabla_{0,S} + {\delta_{x_0}}^T H_{0,S} \times \delta_{X_0} \tag{2.1}$$

where $\nabla_{0,S}$ is referred as the Gradient vector and $H_{0,S}$ the Hessian matrix of the image computed in X_0 at a scale S.

To calculate these differential operators of I , some concepts of linear space theory are required. Differentiation is defined as a convolution with derivatives of Gaussian's with Lideberg parameter,γ, being useful to compare the response of differential operators at multiple scales.

$$\frac{\partial}{\partial x} I(x,S) = S^{\gamma} I(x) * \frac{\partial}{\partial x} G(x,S) \tag{2.2}$$

where the D-Dimensional Gaussian at a scale S, $G(x,S)$ is defined as

$$G(x,S) = \frac{1}{\sqrt{2\Pi S^2}^D} e^{-\frac{||x||^2}{2S^2}} \tag{2.3}$$

The second order directional is given by the third term in equation (2.1).

The second order derivative of a Gaussian Kernel, $D_{xx}G$, generates a probe kernel that measures the contrast between the inside and outside range ($-S$,S) in the direction of the derivative. Eigenvalue analysis of the Hessian allows the extraction, in the three orthonormal directions of curvature (λ_1,λ_2 and λ_3) in which the local second order structure of the image can be decomposed, as illustrated in figure 2.6. This approach is the one followed in this work.

The Frangi filter has been largely used for enhancing blood vessels in retinal images. This filter can enhance and capture the geometrical shape of a PVS. However, one limitation of this method is that it relies on the image processing step for the ROI masks, and requires high resolution and quasi isotropic structural MRI. Moreover, this

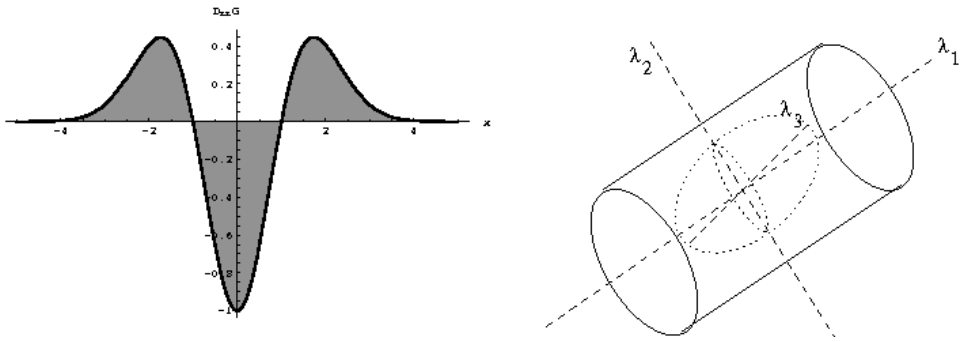

Figure 2.6: In the left, the second order derivative of a Gaussian kernel probes inside/outside contrast of the range $(-1,1)$. In the right, the second order ellipsoid describing the local principal directions of curvature (λ_1,λ_2 and λ_3), adapted from [46].

filter analyses the second order derivatives of an image I, defined in the Hessian matrix [38], $H_s(v)$ as:

$$H_s(v) = \begin{pmatrix} I_{xx} & I_{xy} & I_{xz} \\ I_{yx} & I_{yy} & I_{yz} \\ I_{zx} & I_{zy} & I_{zz} \end{pmatrix} \tag{2.4}$$

to describe the "vesselness" *F(v)* of a voxel *v* at a scale *s* as :

$$F_s(v) = \begin{cases} 0 & \lambda_2 or \lambda_3 \geq 0, \\ (1 - e^{\frac{-R_A^2}{2\alpha^2}}) \cdot e^{\frac{R_B^2}{2\beta^2}} \cdot (1 - e^{\frac{-s^2}{2c^2}}) & otherwise, \end{cases} \tag{2.5}$$

where λ_1,λ_2 and λ_3 are the ordered eigenvalues $(|\lambda_1|) \leq (|\lambda_2|) \leq (|\lambda_3|)$ of the Hessian matrix , $R_A = |\lambda_2|/|\lambda_3|, R_B = |\lambda_1|/(|\lambda_2\ \lambda_3|)^{1/2}, S = (\lambda_1{}^2 + \lambda_2{}^2 + \lambda_3{}^2)^{1/2}$.

This method takes into account two geometric ratios based on the second order ellipsoid.
The first ratio accounts for the deviation from a blob-like structure but cannot distinguish between a line/plate-like pattern.

$$R_B = \frac{\text{volume}/(4\Pi/3)}{(\text{Largest cross-section Area}/\Pi)^{3/2}} = \frac{|\lambda_1|}{(|\lambda_2\lambda_3|)^{1/2}} \tag{2.6}$$

This ratio attains its maximum for a blob-like structure and its zero whenever $\lambda_1 \approx 0$, or λ_1 and λ_2 tend to vanish.

$$R_A = \frac{\text{Largest cross-section Area}/(\Pi)}{(\text{Largest Axis Semi-Length})^2} = \frac{|\lambda_2|}{|\lambda_3|} \tag{2.7}$$

The second ratio refers to the largest area-cross section of the ellipsoid and accounts for the aspect ratio of the two largest second order derivatives. Thus, this ratio is essential to distinguish between plate-like and line-like structures.

α,β and C are the thresholds which control the sensitivity of the filter to the measures R_A, R_B and S.

λ_K will be the eigenvalue with the K-th smallest magnitude $(|\lambda_1| \leq |\lambda_2| \leq |\lambda_3|)$. For example, a pixel belonging to a vessel region will be signaled by λ_1 being small, ideally zero, and λ_2 and λ_3 of a large magnitude. The sign of

Table 2.2: Structure based on Hessian eigenvalue analysis. Eigenvalues are sorted according to magnitude, whereas H = high and L =low magnitude and +/- indicates the sign of the eigenvalue.

		3D	
orientation pattern	λ_1	λ_2	λ_3
Plate-like structure (bright)	L	L	H^-
Plate-like structure (dark)	L	L	H^+
tubular structure (bright)	L	H^-	H^-
tubular structure (dark)	L	H^+	H^+
blob-like structure (bright)	H^-	H^-	H^-
blob-like structure (dark)	H^+	H^+	H^+

eigenvalues are indicators of brightness or darkness.

The eigenvalues are obtained through eigenvalue decomposition of the Hessian matrix, i.e, eig$H(x,s)$ for $\lambda_i, i = 1,...,D$ which can be computed fast for 2x2 and 3x3 Hessian matrices. The respective eigenvectors point out in singular directions (u_1,u_2,u_3). $u1$ indicates the direction along the vessel (minimum intensity variation), u_2 and u_3 form a base for the orthogonal plane.

Thereafter, the local relevant structures in the image can be enhanced by analyzing the signs and magnitudes of the ordered Hessian eigenvalues, with respect to their orientation, shape and foreground vs background brightness.

In T1-Weighted MR images, PVS appear as hipointense comparing with their relative background, so it is expected that λ_1, λ_2 have lower values and λ_3 have a positive sign. In the other hand, PVS that are present in T2-Weighted images, a bright tubular structure is expected: $|\lambda_1| \leq |\lambda_2|, |\lambda_3|$ and $|\lambda_2| \sim |\lambda_3|$, $|\lambda_1| \sim 0$ and λ_2 ,λ_3 ≤ 0. For a dark structure it is expected that $|\lambda_2|$, $|\lambda_3| \geq 0$.
Given a set of scales $S \in [s_{min}, s_{max}]$, the responses are combined as:

$$F(v) = maxF_s(v) \tag{2.8}$$

where s_{min} and s_{max} are the minimum and maximum scales at which relevant structures are expected to be found.

2.4.1 Implementation of the Frangi Filter

The implementation of Frangi filter was based on three pre-existing main functions written by D.Kroon University of Twente (June 2009), provided in Mathworks. These three main functions were implemented in Matlab R2016(b). The main objective was to apply the Frangi Filter, performing a parameter optimization, in the nifti files (T1 and T2) containing WM as our region of interest, previously segmented with brain extraction (BET) and bias field correction (FAST), so that the expected output could be possible to obtain. All the nifti files (presented in .nii format) were converted to .mat format using Nifti toolbox, allowing Matlab to recognize it. Afterwards the first main function (imgaussian) allowed to select which nifti file was wanted to serve as input to be filtered.
Moreover, the second main function used, Hessian3D.m take as input the volume matrix (I) defined by the previous function, and Sigma σ. This function filters the image with an Gaussian Kernel (if Sigma is zero no gaussian filtering) followed by the calculation of second order gradients, which approximates to the second order derivatives of the image. The given outputs are the second order derivatives of the image (Dxx, Dyy, Dzz, Dxy, Dxz and Dyz).
The third main function, Frangi3D.m, uses the eigenvectors calculated in the Hessian3D to compute the likeliness

of an image region to vessels, according to the method described on [37, 46], and take as input the input volume matrix (I), a certain range scale (Sigma - σ) and the thresholds that control the sensitivity of the filter (α , β and C). While running this function, for each sigma scale range a matrix containing the filtered 3D image is generated named I_{out}. Afterwards, NIFTI toolbox was used for the conversion of the generated matrix into .nii format, and then visualization in FSLeyes.

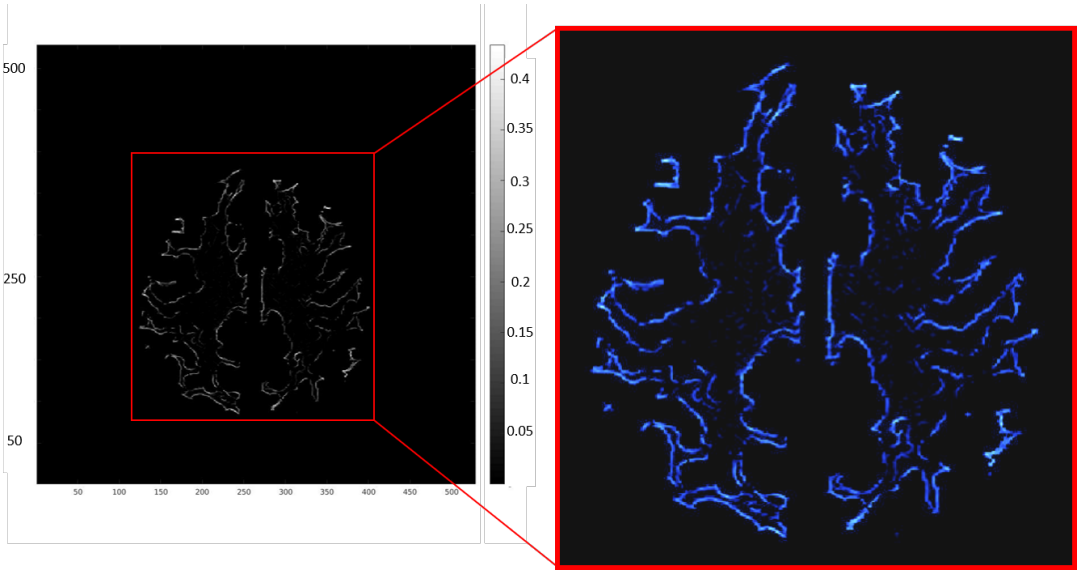

Figure 2.7: Single slice view in Matlab of the matrix I_{out} generated after applying Frangi Filter.

2.4.2 Parameter optimization

In order to obtain a Ground truth for the clinical validation of the output images generated after using the filter, allowing the extraction of PVS, is important to perform a certain parameter optimization so that the main features that are extracted after applying the filter are as close to reality as possible, with the same structure and shape, and also decrease the false positive and negative rate, obtaining a high value of clinical validity and reliability. Furthermore, as it was explained in the previous section, the main parameters that control the sensitivity of the filter are (α, β, and C). The other parameter that takes a huge importance in the extraction of these features is Sigma (σ), that controls the range that a certain feature is expected to be found in a scale of (S_{min}, S_{max}). These parameters can differ from each MRI sequence and resolution of the scanner. Regarding the context of this work, since perivascular spaces are features with a radius no more than 3mm, thus, the value of sigma has to be taken in account. Table 2.3 represents the range used during the optimisation of parameters. In an attempt to find the best sequence for the frangi filter usage, firstly a range containing the minimum and the maximum accepted value for the filter to work was determined, using FSLeyes to perform a qualitative evaluation. Afterwards, in several trials trying to see, and understand which changes occur in the output as the values were changing, and at the same time, verify each parameter behaviour and their impact in the final enhancement mask, it was decided to assign to each parameter, according to their sensitivity, a certain increment. The value of Sigma was selected by trial-error in a several test trials, then it was realized that for the enhancement of these structures, the range of sigmas had to contain low values, in a scale of approximately between 0.6 and 2 voxels. Higher Sigma values lead to the

Table 2.3: Frangi Filter parameters optimisation procedure for both MRI sequences : T1-Weighted and T2-Weighted.

	α	β	C	σ
minimum accepted value	0.05	0.05	10	0.05
maximum accepted value	10	10	900	2
increment	0.01	0.01	10	0.01

enhancement of other structures that do not correspond to perivascular spaces.

Post-Frangi

After the implementation of the Frangi filter, the Post-Frangi procedure starts in order to perform an improvement of the final output mask given by matlab. In most of the cases, the matrix generated by the filter (I_{out}) contains border zones and enhanced regions that do not correspond to PVS. Due to the extraction of the WM mask, using FSL function (*FAST*), in some cases, this segmentation can present small regions that have the same contrast of CSF, and PVS, leading to its enhancement by the filter.

In figure 2.8 is presented the masks that allow an accurate segmentation of PVS.

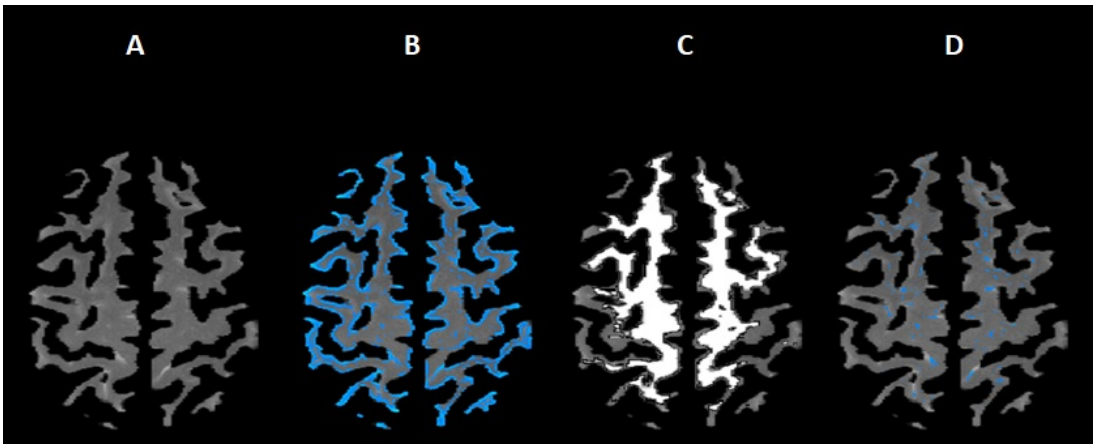

Figure 2.8: Segmentation of PVS on a T2W in FSL. (A) WM mask obtained FSL($fast$). (B) PVS mask (light blue) given by Frangi Filter displaying PVS and border zones.(C) Binarized WM mask (white), assuming a brain probability mapping of 1. (D) PVS extraction (light blue) final mask.

In Figure 2.8, (A) represents the region that is given to the frangi filter in matlab. This mask is also the output given from the FAST function in FSL, representing the intersection of the binary mask with the brain, obtained by BET function, using $fslmaths$.

Here, the brain probability mapping considered for the mask is zero in order to pick up border areas that contain not only WM, and also to ensure that the mask given to the filter contains the whole area corresponding to WM in its entirety (figure 2.8 (B)). Afterwards, given the certain parameters to the filter, the output given by the matlab is saved in nii format, and is represented in light-blue in (B). Furthermore, the current mask (B) contains PVS inside, but at the same time a border surrounding WM is enhanced leading to a inadequate quantification, so a second binary mask is needed. Similarly to obtain (A), $fslmaths$ allows to create a binary mask represented in (C). The white area results from the output of the binarized mask, using a brain probability mapping of 1, to ensure all the

area is WM (figure 2.8 (C)).

Lastly, *fslmaths* is used one more time to intersect mask (C) with (B) resulting in the mask containing only PVS (D). Taking into account the MR sequence that is under test, another FSL function, (*FLIRT*) can be used to perform a linear registration.

A summary of the Post-Frangi procedure is demonstrated in the following scheme, in figure 2.9.

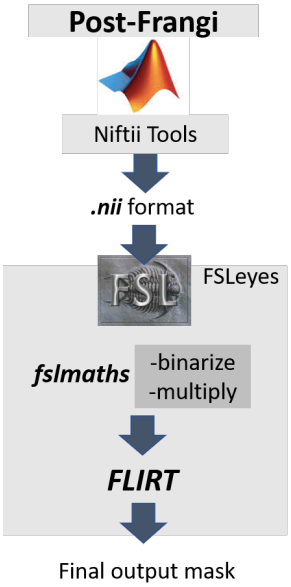

Figure 2.9: Post-Frangi procedure method.

After the Post-Frangi procedure is completed, is important to validate its output. In here, basically searched for enhanced zones that did not rigorously match PVS, and also, check if border zones of the mask were successfully removed.

2.5 Implementation - Part II

2.5.1 Quantification using Brain Atlas

Based on the cerebrovascular diseases, in this thesis, the quantification of PVS was performed in different ways. Firstly, each brain had a corresponding volume of PVS considering the whole white matter region. After the extraction of these structures, demonstrated in the the previous sections, its quantification was performed using a FSL function ($fslstats$), applied only to the mask containing the PVS that were extracted. This distribution allowed to compare the density of PVS by disease. Similarly to these, and also because in literature review a quantification method by brain lobe was not specified or performed, it was interesting to check if there was a significance difference of PVS by brain lobe, and for further analysis, to see if this distribution remains constant for each brain disease. Moreover, in order to perform an accurate brain lobe analysis, the quantification was based on an adult atlas provided by the Imperial College of London, displayed in figure 2.10, containing the mean of 30 subjects in the MNI space, including 95 brain regional probabilistic maps, demographics, handedness and label names (data from A Hammers, R Allom et al. 2003, IS Gousias et al. 2008, I. Faillenot et al. 2017).

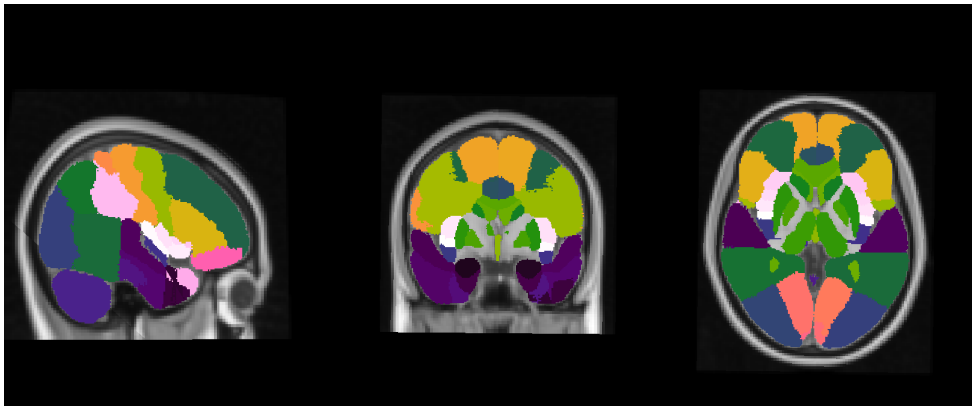

Figure 2.10: Hammers adult atlas provided by Imperial College of London, representing 95 brain regions, represented in MNI152 (T1) space.

This atlas was created in the MNI-space (MNI152,T1, 2mm). In order to use this atlas in the T2-space, $Flirt$ function was necessary as a registration procedure, since the voxel location in the MNI space was different from the voxel location presented in T2 space, giving as input the MNI space image, and as reference the brain containing PVS (T2-Weighted). After performing this step, it is possible to use these brain regions for segmentation. Each color area, representing a specific brain area was established as a label, represented by a certain number (1-95). For a further analysis, accordingly to the principal five brain lobes (frontal, temporal, parietal, motor and somatosensory, and occipital), FSL was used to extract only these desired brain areas. Particularly, $fslmaths$ was implemented in a bash script using several thresholds.

To aggregate an accurate brain region a lower and a upper threshold was established, containing the range that allowed to aggregate each area, fulfilling the requirements to build an entire lobe. After running the script, as summarized in figure 2.11, it was possible to extract PVS in each corresponding brain lobe, using $fslmaths$, based on the intersection of the mask generated by the frangi filter with the created brain lobe mask.

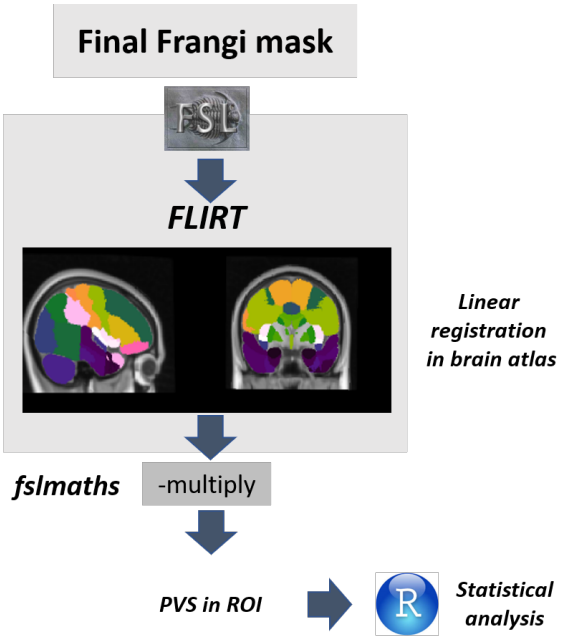

Figure 2.11: Pos-Frangi implementation - Part II scheme.

2.5.2 Visual rating scale using Wardlaw and Patankar user guide

Visual ratings are commonly used by clinicians in order to assign a certain degree of pathology [47]. Also, these ratings can be used when there is a lack of quantitative information regarding the patient. In the context of perivascular spaces, visual ratings can be used with quantitative methods to understand the physiological condition of each patient, as well as their connection with disease type and age.

Several PVS rating scales are either limited in their anatomical location, in the range of EPVS that they describe, or in their method of assessing severity. Additionally, some scales were tested using specific MRI sequences rather than standard structural brain MRI. In this present work, visual ratings were used according with the visual rating scale proposed by Patankar and Potter et al [47, 48]. This visual rating scale was consulted in [47] and was our online user guide to our ratings. According to the online user, PVS are rated 0 (no PVS), 1 (mild: 1-10 PVS), 2 (moderate: 11-20 PVS), 3 (frequent: 21-40 PVS) or 4 (severe: $\geq$ 40 PVS).

Table 2.4: PVS visual rating scores given by the Wardlaw and Patankar scale.

Wardlaw and Patankar visual rating scale	
Severity	Perivascular spaces number
0	0
1	1 - 10
2	11 - 20
3	21 - 40
4	>40

This user guide will enable a cross-comparison between the analysed groups and facilitate the assignment of a severity scale.

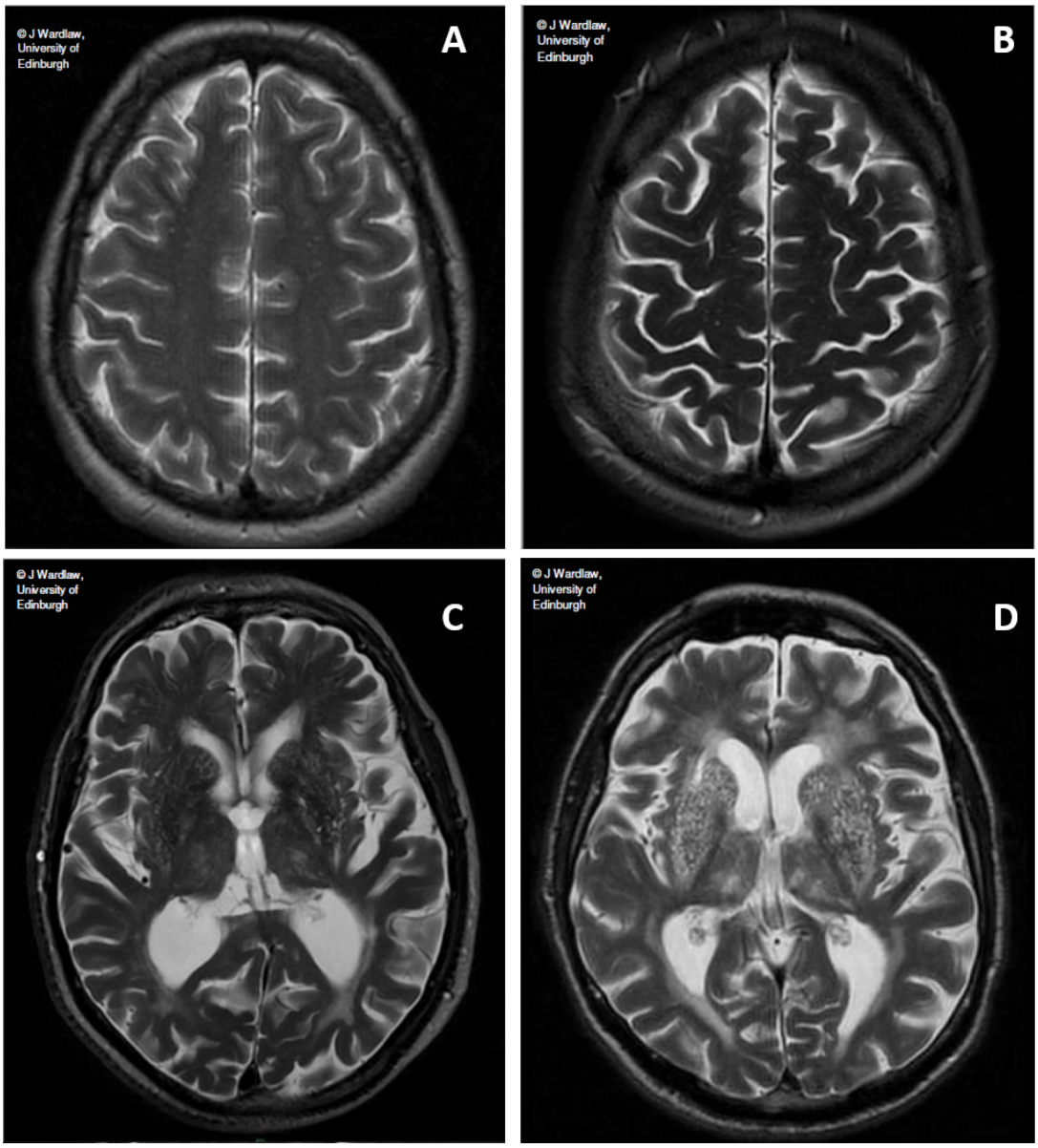

Figure 2.12: Perivascular spaces visual rating scale proposed by Patankar and Potter et al [47, 48].PVS are rated with mild (A) (1-10 PVS), moderate (B) (11-20 PVS), frequent (C) (21-40 PVS), or severe (D) ($\geq$ 40 PVS).

Chapter 3

PVS segmentation

3.1 Parameter optimization in T1-Weighted images

In T1-Weighted MR images, CSF appear as hipointense regions, containing the darker pixels when compared with white-matter (WM). In this MR sequence PVS are easily distinguishable from WM, regarding their intensity. Regarding previous trials, the first parameter to be tested in the T1-Weighted sequence is the sigma (σ). Likewise in the T2-Weighted sequence, several trials were performed in order to obtain the optimal sensitivity matching the desired output mask, using value incrementation, while observing each parameter behaviour and sensitivity obtaining a specific value parameter combination that will allow structure enhancement. The visualization of the output given with different σ scale ranges are illustrated in figures 3.1 and 3.2.

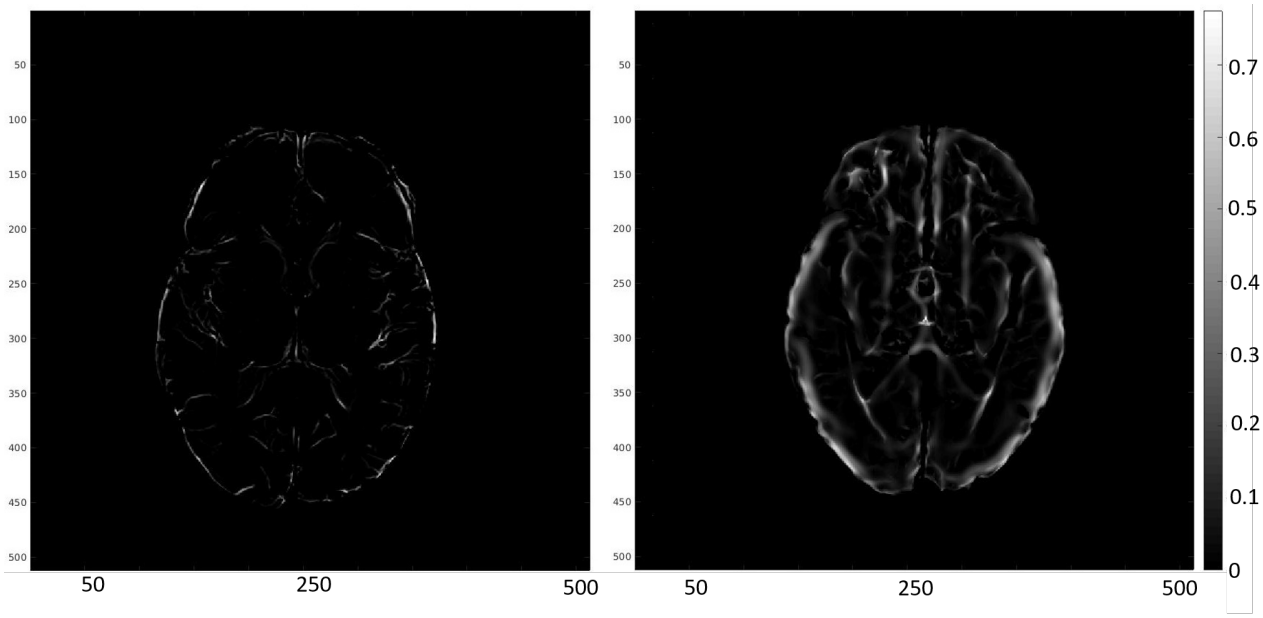

Figure 3.1: Axial view (T1-Weighted) in Matlab of the output matrix generated after implementing the Frangi Filter with different sigma scale ranges, σ = 1.6 (in the left) and σ = 6 (in the right).

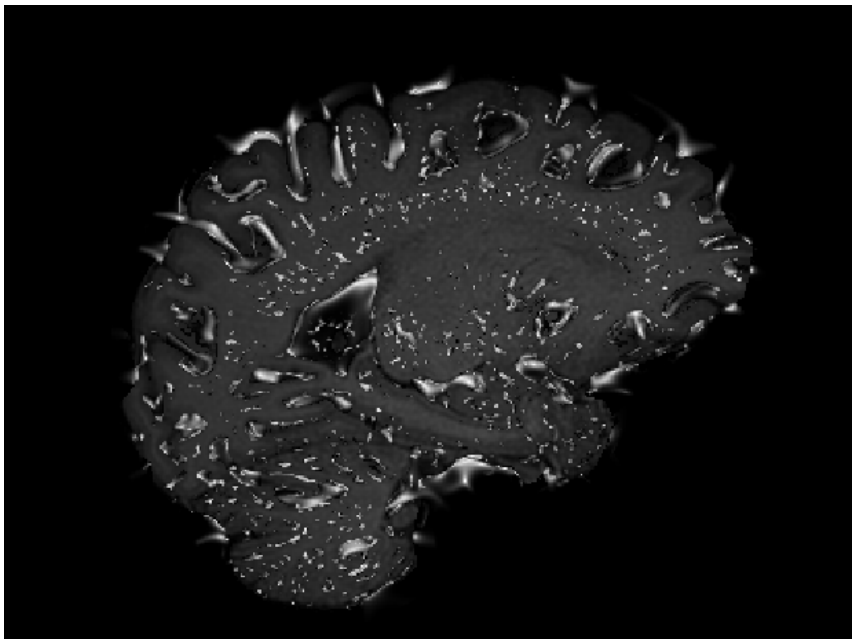

Figure 3.2: Visualization of the output given by the Frangi filter, using $\sigma = 6$ in a T1-Weighted MRI (sagital view), using FSL.

Firstly, during the test-trials a certain scale of sigma was used, i.e, σ = [1 7] with an increment of 1, and it was realized, using a certain range of sigma scale containing high values that most structures generated by the Frangi filter do not resemble perivascular spaces. In addition, it was noted, using (σ = 6) that the filter creates some kind of a layer around the white matter, and in its majority overlaps grey matter. Through the increment it was also realized that for a range of sigma reaching values higher than 6, the output of the matrix generated by matlab, containing the image filtered, will not differ, remaining similar to images that used a σ = 6. Moreover, figure 3.2 demonstrates a higher sensitivity in the enhancement of hipointense regions presented in the brain. The same output was capable to detect regions not easily seen contributing to the enhancement of the majority of PVS. However, the referred output was not used for quantification analysis since other regions that do not correspond to PVS were also mapped. Throughout the trials it was realized that the best Frangi parameters set found are represented in the following images contained in this subsection. The performance of the Frangi filter in T1W had a positive capability in the detection and mapping of PVS only when a significant contrast between CSF and WM was displayed. Figures 3.3 and 3.4 correspond to a segmentation in this modality (T1W). In here, elongated features that are displayed in the most peripheric areas of the brain were more easily mapped since they displayed a greater contrast between CSF-WM.

Table 3.1: Some trials performed, using different parameters of the Frangi filter, in T1-Weighted MR images with the purpose of finding the best sequence. Parameters in test are marked with $\star$.

Sensitivity parameters range	**Frangi sigma scale** $\sigma \in [s_{min}, s_{max}]$	**MR sequence**	**Output analysis**
α *= [0.01-0.05] , β = 0.1 , C = 300	σ = 0.06	T1-Weighted	Voxels corresponding to PVS were successfully delineated. Voxels regarding other hipointense regions were mapped, resulting in false positives.
α* = 0.1 , β = 0.1 , C = 300	σ = 0.06	T1-Weighted	PVS morphology was successfully delineated. No false positives were displayed. Only voxels regarding PVS were marked.
α* = 10 , β = 0.1 , C = 300	σ = 0.06	T1-Weighted	Majority of enhanced regions overlapped PVS, however, false positives is clearly displayed.
α*= 100 , β = 0.1 , C = 400	σ = 0.06	T1-Weighted	Filter sensitivity increased, enhancing any voxel that displayed a slightly hipointense contrast compared with background. Impossible to distinguish PVS.
α = 0.1 , β* = 0.01 , C = 400	σ = 0.06	T1-Weighted	PVS morphology was successfully delineated. No false positives were displayed. Only voxels regarding PVS were marked.
α = 0.1 , β *= 10 , C = 400	σ = 0.06	T1-Weighted	PVS morphology was successfully delineated. No false positives were displayed. Only voxels regarding PVS were marked.
α = 0.1 , β* = 100 , C = 400	σ = 0.06	T1-Weighted	Most of perivascular spaces were successfully enhanced, however, border zones regarding regions that do not correspond to PVS start to be delineated and extracted.
α = 0.1 , β = 0.1 , C* = 10	σ = 0.06	T1-Weighted	Resulting output showed a lot of false positives. The filter was not capable to delineate any PVS.
α = 0.1 , β = 0.1 , C* = 0.01	σ = 0.06	T1-Weighted	Resulting output showed a lot of false positives. The filter was not capable to delineate any PVS.
α = 0.1 , β = 0.1 , C* = [250-400]	σ = 0.06	T1-Weighted	PVS morphology was successfully delineated. No false positives were displayed. Only voxels regarding PVS were marked.

Furthermore, PVS that were displayed closely to the ventricles were not so easily seen due to the lack of contrast displayed. Even in this cases, the filter was capable to map and detect these structures displayed with a poor contrast. the range containing α must increase, allowing the filter to extend/increase the range of sensitivity that a certain feature is expected to be found. Therefore, for the filter to be capable to detect and delineate those non-easily seen PVS, the range containing had to increase, allowing the filter to extend the range of sensitivity that a certain feature is expected to be found. Increasing the value of this parameter allowed the filter to capture and delineate a higher number of structures in the same ROI, however, if the same parameter increased to much, WM voxels regarding WM that do not resemble as PVS started to be enhanced, generating false positives in the output mask.

It was noticed that the performance of the Frangi segmentation and mapping in the T1W was higher in coronal acquisitions, enhancing PVS in the expected voxels. In addition, figures 3.3, 3.4 and 3.5 correspond to obtained segmentation in coronal T1W MR images. In these data-sets, the majority of enhanced structures were dot like features. When comparing with the non filtered image, PVS that are displayed with dot-like and elongated features were positively mapped in the corresponding hypointense voxels. Therefore, presented results suggest that the filter can delineate with some precision detailed and clear hypointense regions.

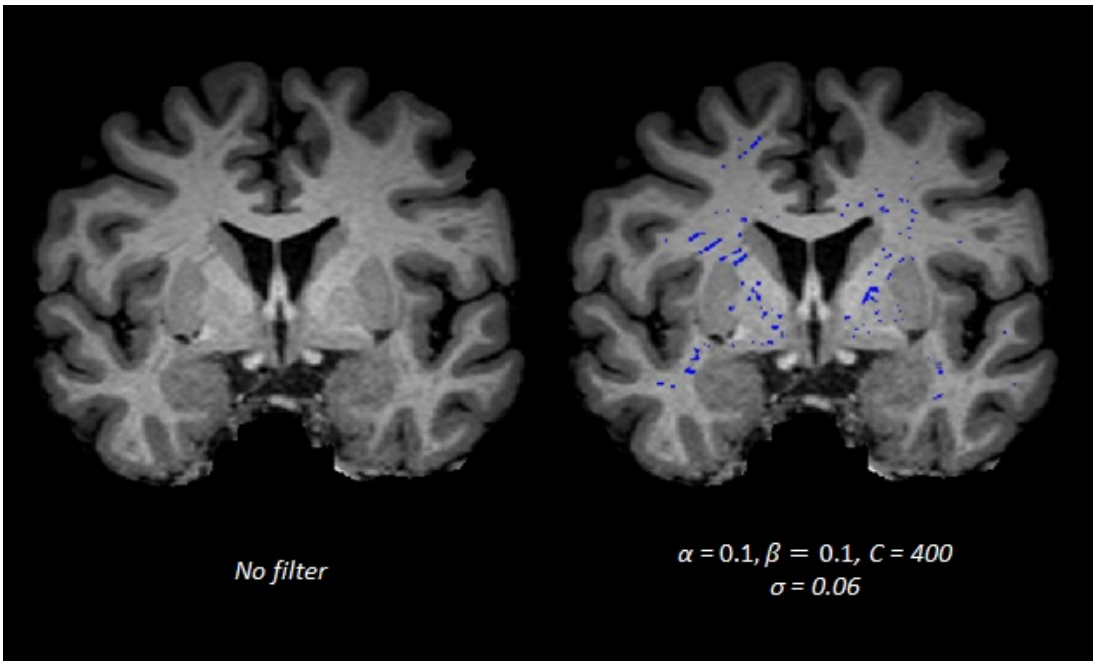

Figure 3.3: Example of the final PVS segmentation in a coronal T1-Weighted MRI, using Frangi filter. Respective segmentation is represented in blue.

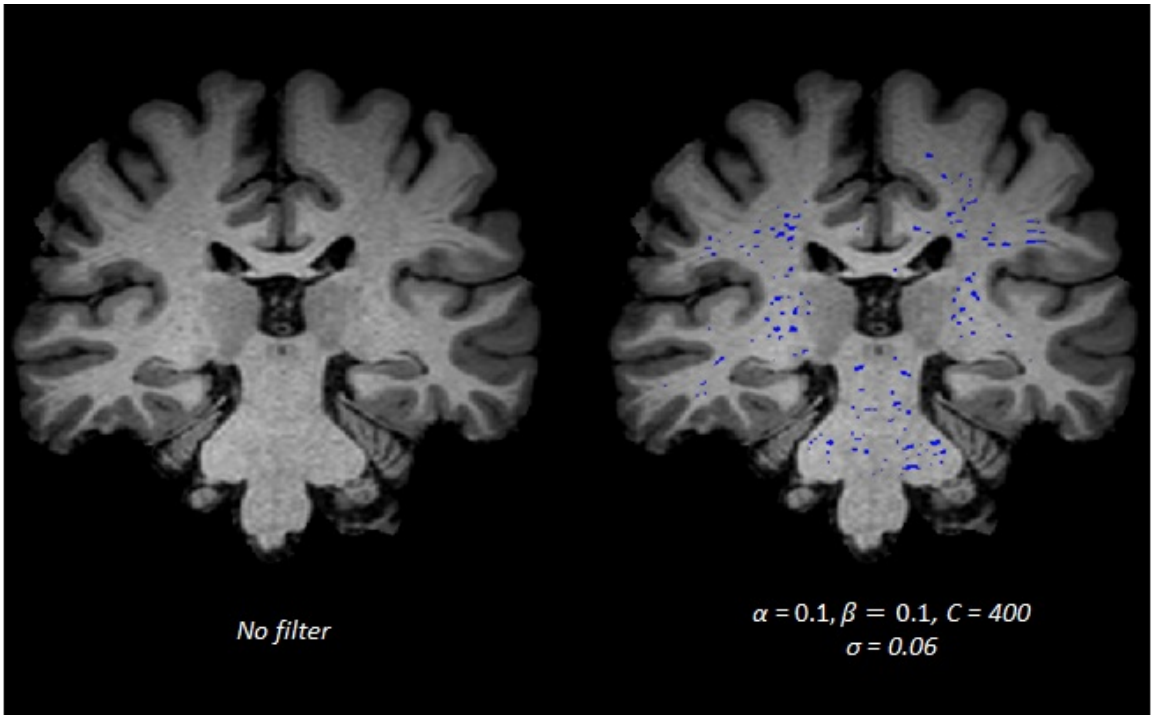

Figure 3.4: Example of the final PVS segmentation in a coronal T1-Weighted MRI, using Frangi filter. Respective segmentation is represented in blue.

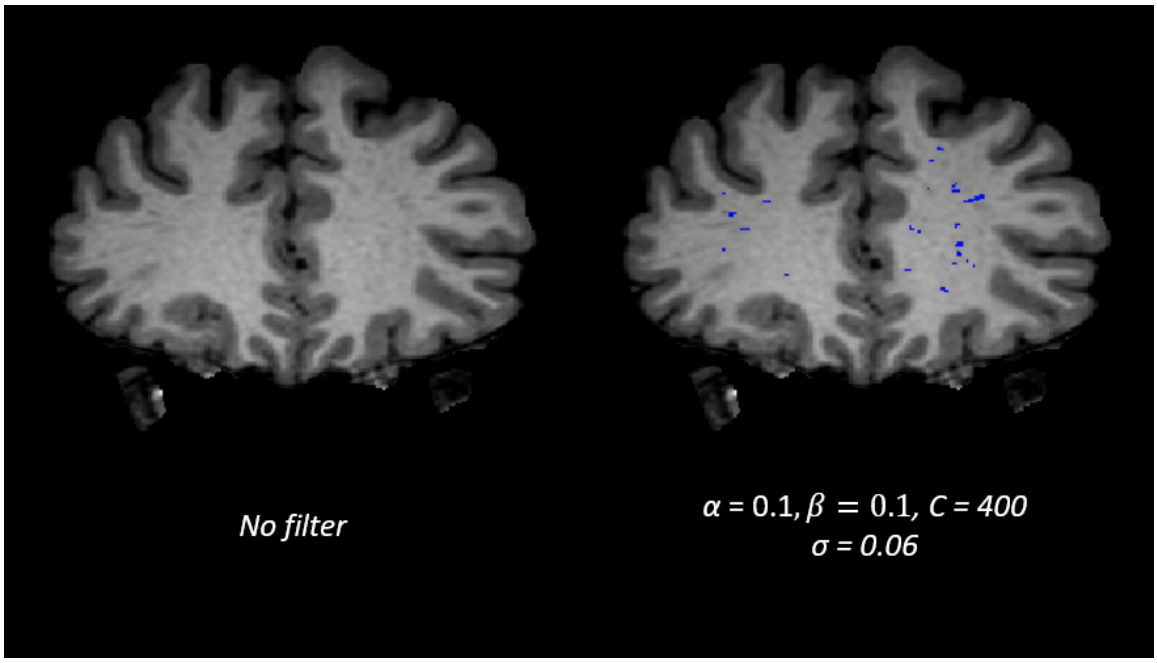

Figure 3.5: Example of the final PVS segmentation in a coronal T1-Weighted MRI, using Frangi filter. Respective segmentation is represented in blue.

Furthermore, in figure 3.3 elongated features were more easily mapped and captured compared with other features. This can be explained due to the fact that elongated features occupy large areas, being more easier for the filter to recognize and differentiate hypointensities from the background, and consequently, lead to a more efficient mapping and delineation of the cavity.

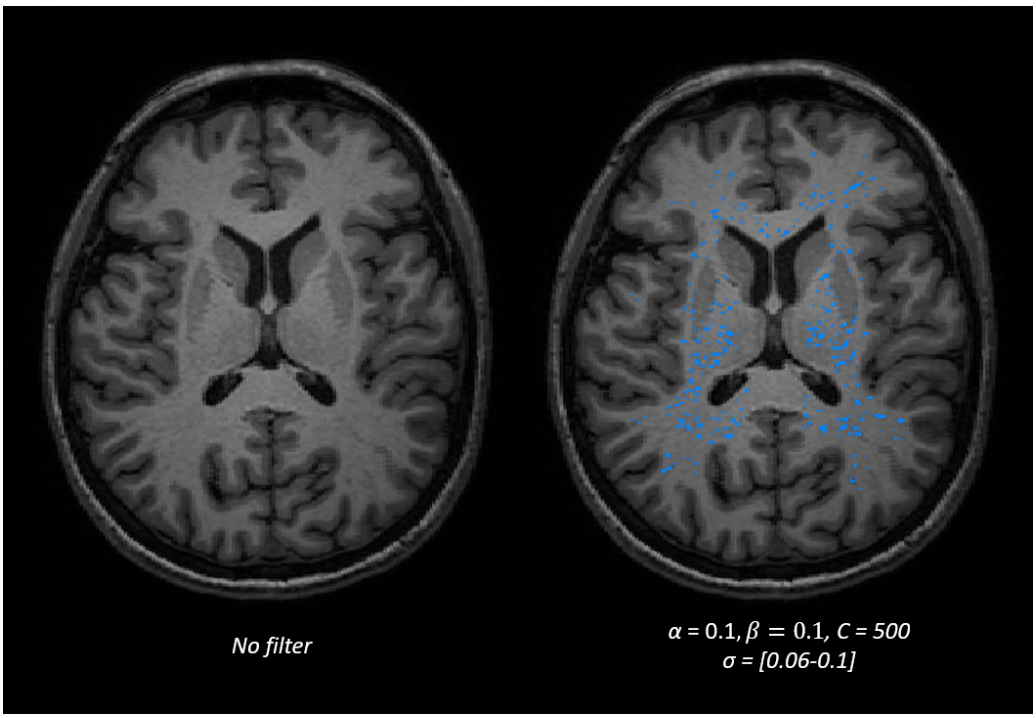

Figure 3.6: Example of the final PVS segmentation in a axial T1-Weighted MRI, using Frangi filter. Respective segmentation is represented in blue.

3.2 Parameter optimization in T2-Weighted images

Trials performed in the following MR images (T2W) were executed in order to obtain an optimal sensitivity matching the desired output mask using the same method (value incrementation) while observing each parameter‘s effect.

T2-Weighted images present a good contrast between CSF and WM, when comparing with the remaining sequences, which may enable better results concerning the segmentation of PVS. Regarding previous tests, the first parameter to be tested in the T2-Weighted sequence is sigma (σ). As shown, this parameter controls the scale that a certain feature and structure is expected to be found, and as consequence, it must be the first parameter to be tested, allowing an accurate enhancement of the desired structures.

For application to this MR acquisition, sigma (σ) revealed a great sensitivity. The optimal value for this parameter was contained in a range between [0.06 - 0.1]. Outside this range the output does not behave as it was expected (figure 3.7) when a higher sigma is used, the output begins to form a single volume, being unable to determine any PVS. On the other hand, if a value for σ below 0.05 is used, the Frangi output will not be capable to enhance any PVS. Figure 3.7 shows the results for the same slice using a value for σ inside (a) and over the admitted range (b), using matlab, during the implementation of the frangi filter. Due to these results, the chosen value for sigma (σ) in order to find the best values for the remaining parameters was $\sigma = 0.06$.

Afterwards, each of the remaining parameters of the frangi were tested according to their sensitivity. Table 3.2 summarizes some of the trials that were conducted in order to test which set of parameters are most suitable for the enhancement of PVS.

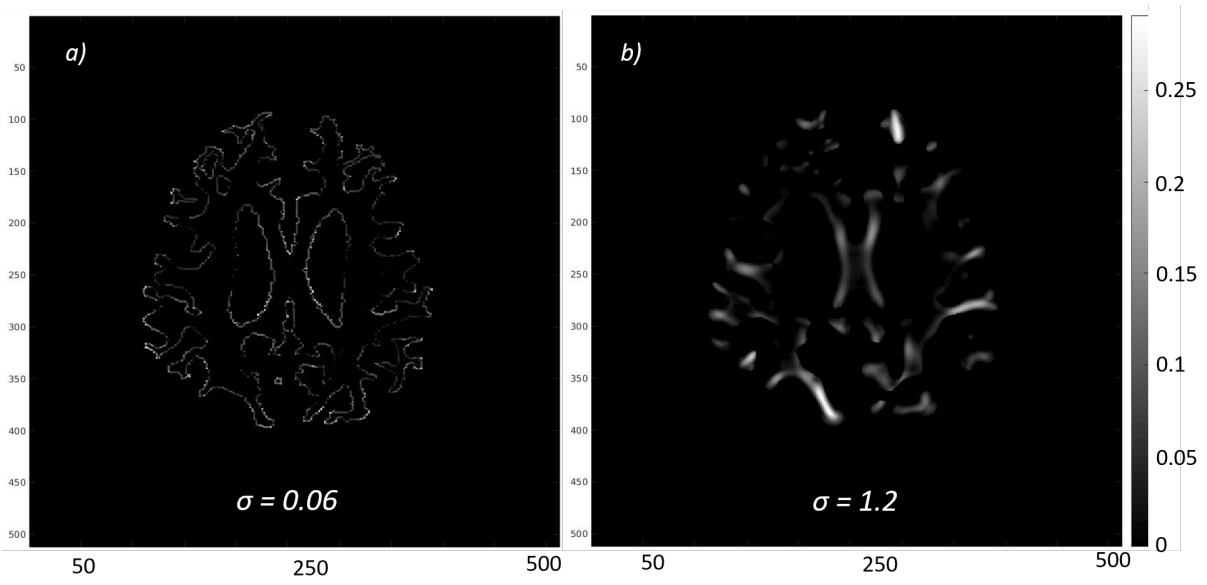

Figure 3.7: Same slice, in matlab, of a T2-Weighted MR image containing PVS using different sigma values. In (a) a sigma ($\sigma = 0.06$) is used, and in (b) a ($\sigma > 1$) is used.

Through the trials it was noted that a small increment in α leads to a large impact in the enhancement of the structures by the filter (figure 3.8). In the same axial slice, several α values were tested. The value that results in a more reliable output is $\alpha = 0.05$, enhancing only hyperintense regions that correspond to a perivascular space (figure 3.8 (a) represented in blue). However, if an higher value is attributed to this parameter, the filter will start to

Table 3.2: Some trials performed, using different parameters of the Frangi filter, in T2-Weighted MR images with the purpose of finding the best sequence. Parameters under test are flagged with a ($\star$).

Sensitivity parameters range	**Frangi sigma scale** $\sigma \in [s_{min}, s_{max}]$	**MR sequence**	**Output analysis**
α *= 0.01 , β = 0.1 , C = 300	σ = 0.06	T2-Weighted	PVS were positively mapped, however, some features were discontinued. No false positives displayed.
α* = [0.05-0.1] , β = 0.1 , C = 300	σ = 0.06	T2-Weighted	PVS morphology was well delineated. Filter was capable to detect elongated and dot-like features, recognizing non-easily seen PVS. No false positives were displayed.
α* = 10 , β = 0.1 , C = 300	σ = 0.06	T2-Weighted	Sensitivity increased leading to the enhancement of any slightly hiperintense region compared with the background. False positives displayed.
α*= 100 , β = 0.1 , C = 400	σ = 0.06	T2-Weighted	Increased false positives were displayed, overlapping the segmentation of PVS.
α = 0.05 , β* = 0.01 , C = 400	σ = 0.06	T2-Weighted	PVS morphology was successfully delineated. No false positives were displayed.
α = 0.05 , β *= 10 , C = 400	σ = 0.06	T2-Weighted	PVS morphology was successfully delineated. No false positives were displayed.
α = 0.05 , β* = 100 , C = 400	σ = 0.06	T2-Weighted	Most of PVS were successfully enhanced, however, border zones regarding regions that do not correspond to PVS start to be delineated and extracted.
α = 0.05 , β = 0.1 , C* = 0.01	σ = 0.06	T2-Weighted	Increased false positives were displayed. The filter was not capable to delineate any PVS.
α = 0.05 , β = 0.1 , C* = 10	σ = 0.06	T2-Weighted	Increased false positives were displayed. The filter was not capable to delineate any PVS.
α = 0.05 , β = 0.1 , C* = [250-500]	σ = 0.06	T2-Weighted	PVS morphology was well delineated. Filter was capable to detect elongated and dot-like features, recognizing non-easily seen PVS. No false positives were displayed.

delineate structures that do not correspond to PVS, resulting in false positives (figure 3.8 (a) represented in orange). In a comparison for the same slice, it is clearly seen that the slice containing the higher value for α possesses an higher number of segmented structures. As a consequence, is shown that the value $\alpha = 0.05$ allows practically an optimal segmentation of PVS, enhancing only hyperintense regions that correspond to a PVS, excluding false positives from the segmented output. However, if this value increases, several micro hyperintense regions that do not resemble a PVS will also start to be enhanced, resulting in false positives. This behaviour was consistent for other MR images for the same values.

Other parameter that revealed having a great impact on the results when its values were increased was C. Even so, this parameter only requires a minimum value to result in an acceptable output. For values lower than 50, the segmented mask showed a lot of noise, enhancing regions that do not correspond to PVS. In this example, $C = 0.01$, the final output represents a cluster of points forming almost a tridimensional volume, impossible to distinguish and enhance only PVS. Through the trials the admitted values for C, in order to obtain a reliable segmentation had to be higher than 50.

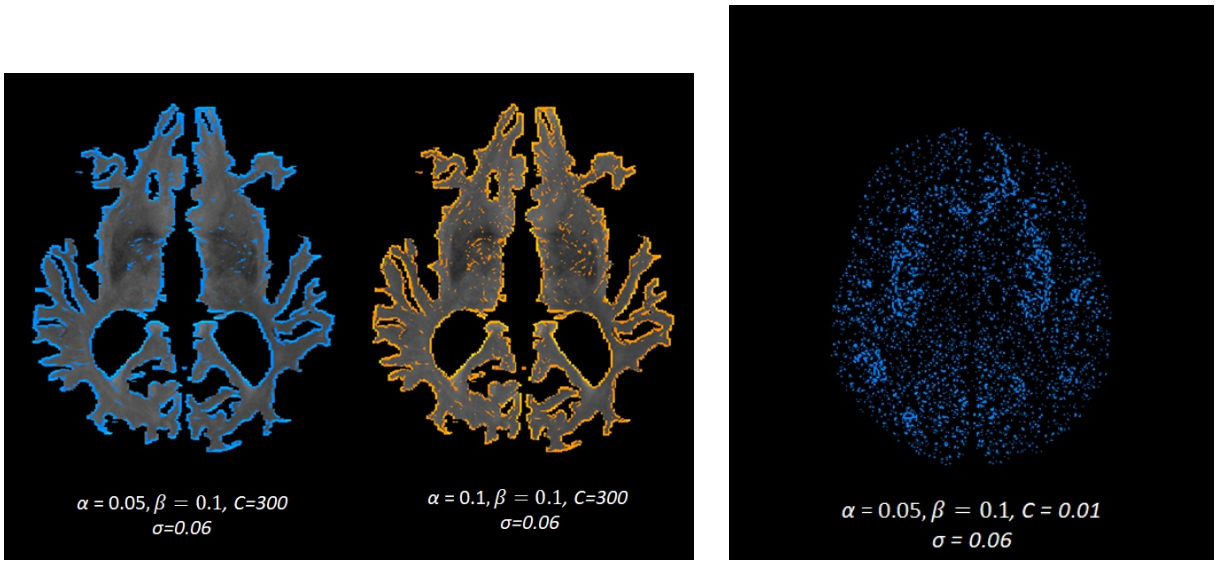

(a) T2-Weighted axial view.

(b) T2-Weighted axial view.

Figure 3.8: Visualisation in FSLeyes of the Frangi filter output mask using diferent parameters.

Figure 3.9 shows the best set of parameters obtained by applying the Frangi filter ($\alpha = 0.05, \beta = 0.1, C = [300-500], \sigma = 0.06$). In the representative axial slice of the WM, each hyperintense structure assigned to a PVS was positively marked in light-blue, even those that appear with a lower intensity and which were hard to be detected through visual inspection. This set of values contributed to a reliable segmentation, mapping with precision PVS. As evaluated through visual inspection in many of slices, PVS delineation appear to be very symmetrical in both hemispheres.

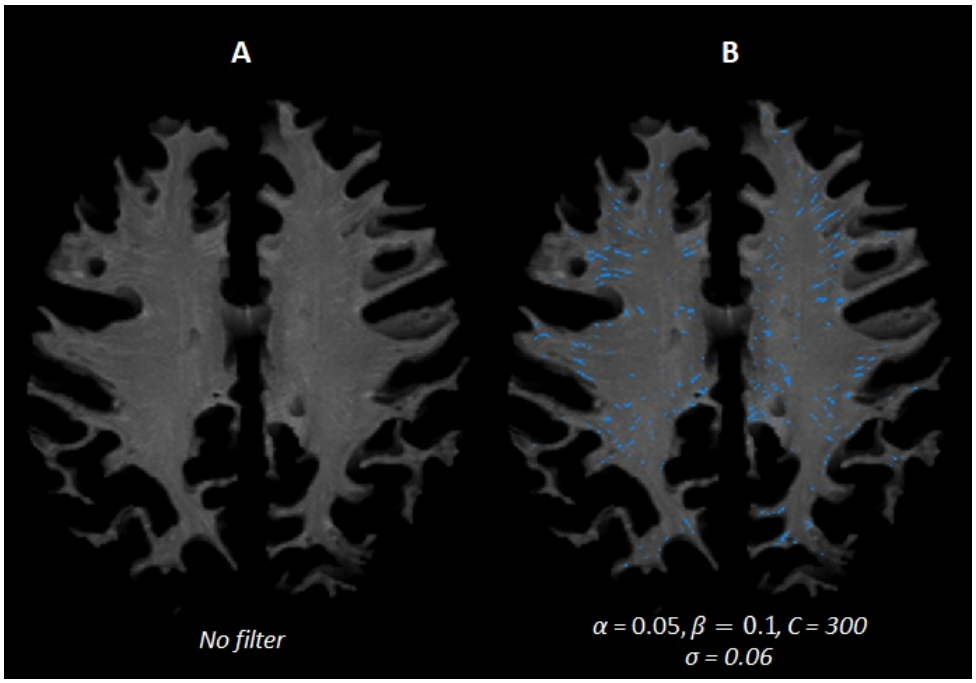

Figure 3.9: Segmentation of PVS of a T2-Weighted image.

PVS visible in the (T2-Weighted) White-matter mask axial slice presenting small high-signal areas were obtained using the mentioned parameter set (figure 3.9), and the respective output revealed that PVS appear linear

when parallel and dot-like when perpendicular to the imaging plane. Moreover, in the same figure, an increase number of PVS was found, presenting almost the same pattern, defined as small, sharply and elongated features following the orientation of perforating arterioles, running perpendicular to the brain surface. Furthermore, PVS were clearly distinguishable from lacunes. The Frangi filter could extract and perform a reliable delineation of the features since the segmentation (in light-blue) occupies exactly the correct space while looking at the non-filtered WM mask. Areas where small hyperintensities arise, the filter is able to detect PVS, if using the mentioned parameter set ($\alpha = 0.05, \beta = 0.1, C = 300, \sigma = 0.06$).

Consistent with these results, another example, presented in figure 3.10 strengthens observation that the performance of the filter applied to this modality provides promising results. In this figure, PVS were hard to be detected through visual inspection, even so, the filter could successfully delineate the majority of PVS, enhancing its tubular shape and size. In the same image, PVS near the most periphery brain areas seem to display a more elongated shape, while comparing to those marked in the rest of the slice.

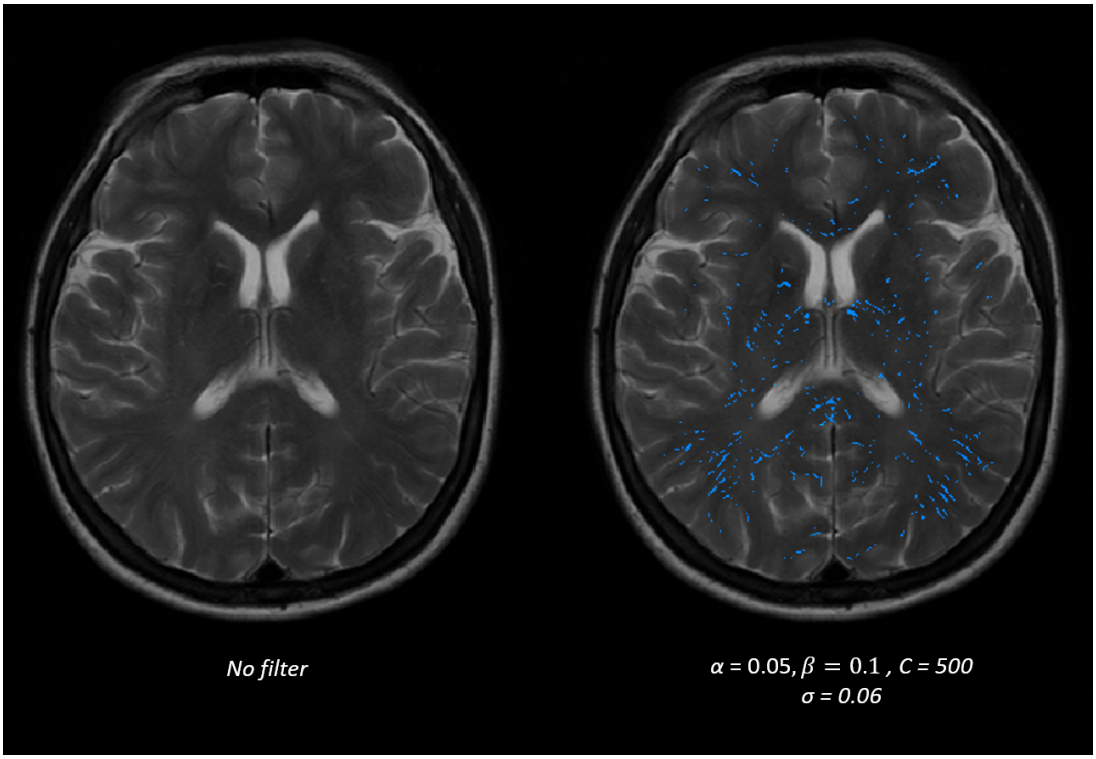

Figure 3.10: Segmentation of perivascular spaces procedure on a T2-Weighted.

From the presented figures, it is plausible to affirm that PVS in multiple slices follow a similar pattern, appearing round in the center regions of the axial slices with elongated features in the most periphery and posterior regions. The filter also clearly allowed to distinguish PVS from large WM lesions such as lacunes and other WMH based on its shape (above 3 mm spheroid shape), spatial distribution and orientation, avoiding these areas. These results suggest that, further improvement in T2-Weighted image resolution may result in the detection of more PVS, and assist in an automatic process analysis. Furthermore, this method provides an accurate segmentation, also contributes to the analysis of PVS orientation, spatial distribution and density. Masks obtained by the Frangi filter could be used in combination with other measurements and medical data to provide a better diagnosis and to understand the role of PVS in neurological disease. One limitation noted in this method relies in the processing

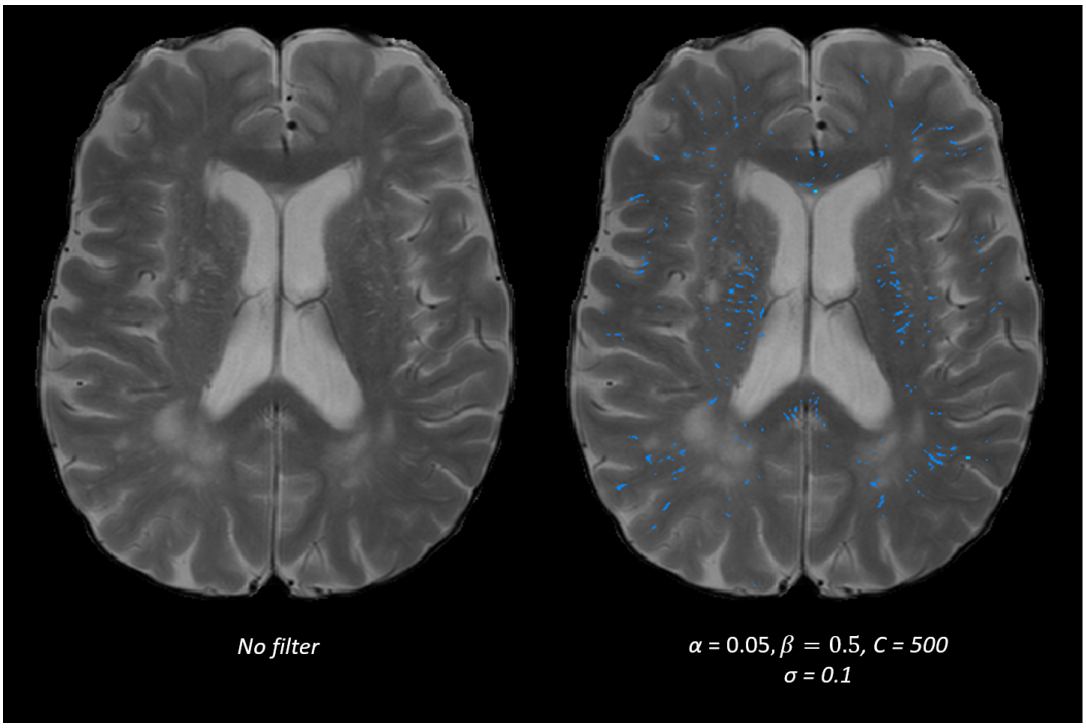

Figure 3.11: Segmentation of perivascular spaces procedure of a T2-Weighted. PVS obtained using Frangi filter are mapped in blue.

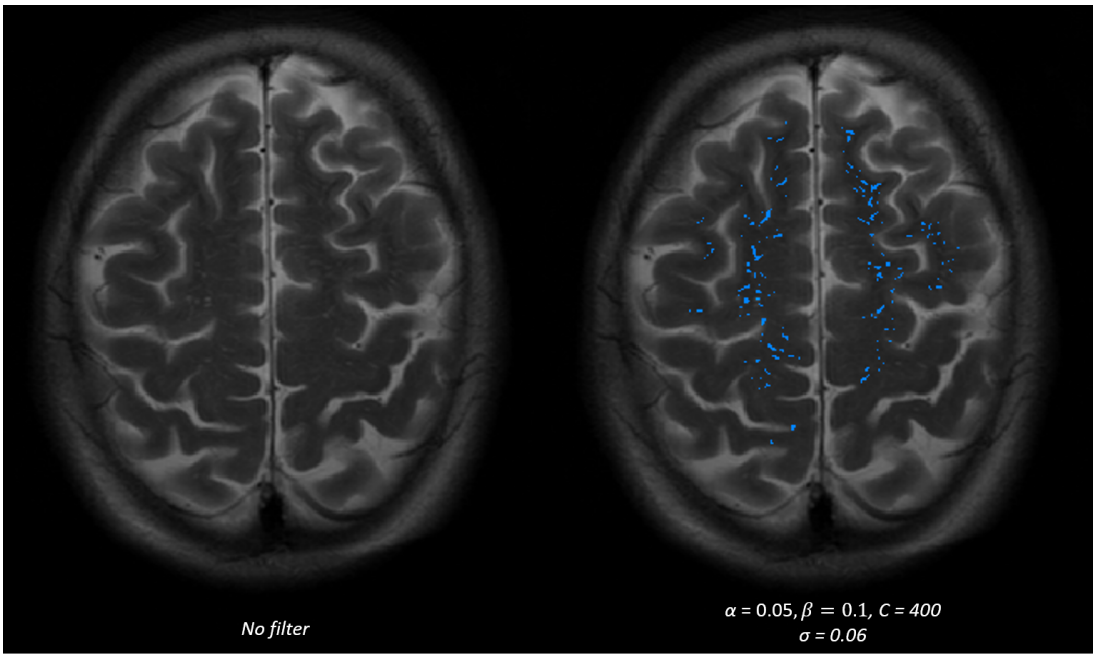

Figure 3.12: Segmentation of PVS procedure of a T2-Weighted. PVS obtained using Frangi filter are mapped in blue.

of the region of interest (ROI) that is given as input to the filter which should to a map of the WM. If the output given by $FSL-FAST$ function contains any border zones of giry, that appear with the same intensity of CSF, these regions can be enhanced, giving rise to false positives.

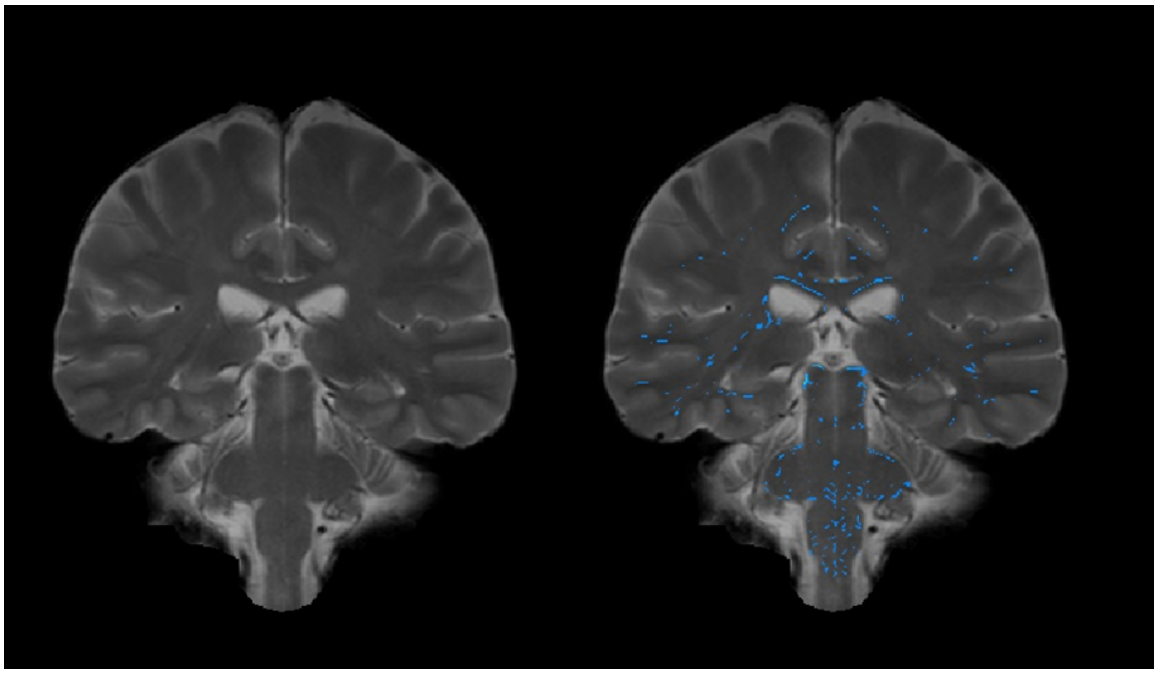

Figure 3.13: T2-Weighted coronal MRI showing the non-filter brain, presenting perivascular spaces (at left), and their respective segmentation in centrum semiovale and brainstem (marked in light blue) using the frangi filter ($\alpha = 0.05, \beta = 0.1, C = 300, \sigma = 0.06$). PVS appear to be small, round and oval-like, arising with more density in the brainstem.

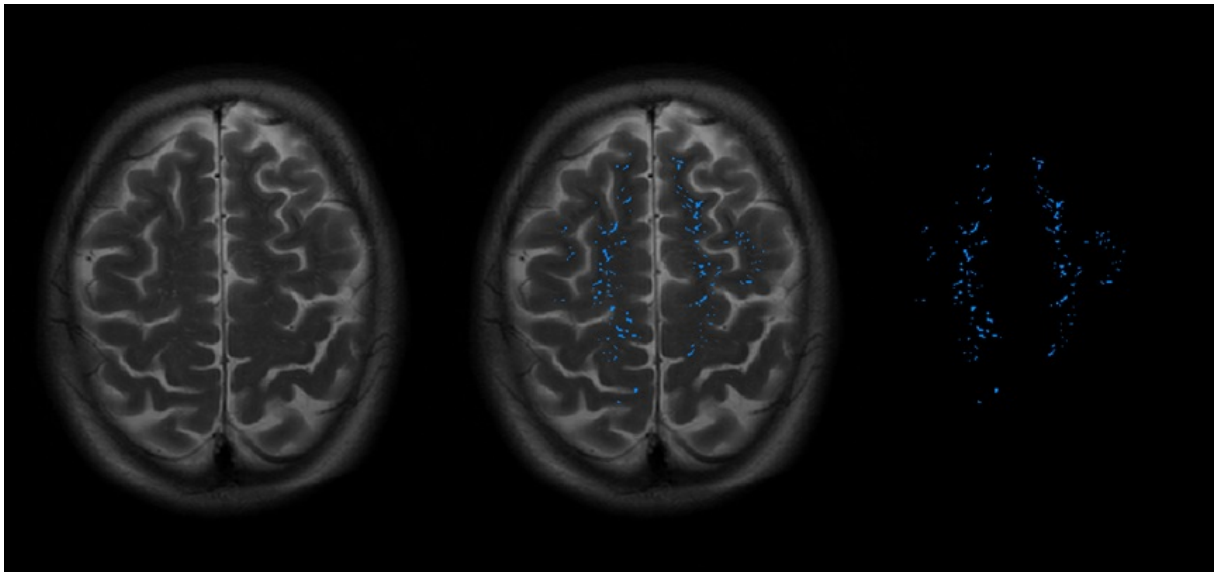

Figure 3.14: T2W MR sequence showing the enhancement of perivascular spaces. PVS obtained using Frangi filter are mapped in blue.

3.3 Segmentation in T2-FLAIR

The same procedure was repeated for the Fluid attenuated inversion recovery (FLAIR) images. The FLAIR sequence is useful in the detection of subtle changes at the periphery of the hemisphere and in the periventricular region close to CSF. Brain tissue appears more similar to the T2-Weighted images with grey matter brighter than white matter, while the CSF is dark instead of bright since this sequence removes signal from the cerebrospinal fluid (CSF) from the resulting images. To null the signal from fluid, the inversion time (TI) of the FLAIR pulse sequence is adjusted such that at the equilibrium there is no net transverse magnetisation of fluid.

The application of the Frangi Filter to this type of images could not detect any PVS. Also, in the visual ratings using FSLeyes it was extremely difficult to distinguish PVS, that appear as hipointense regions due to low intensity and so more difficult to distinguish CSF from the WM (background). This MR sequence can not be used for segmentation since the enhancement of regions from the filter do not match PVS.

Nevertheless, this sequence can have an important role in Validation since it can detect areas containing WMH (White matter hyperintensities), that appear as large hyperintensities in these images. In the following figure 3.18, a mask containing WM was submitted to the Frangi filter with the purpose to enhance PVS that appear dark in this type of images, presenting the same signal as CSF.

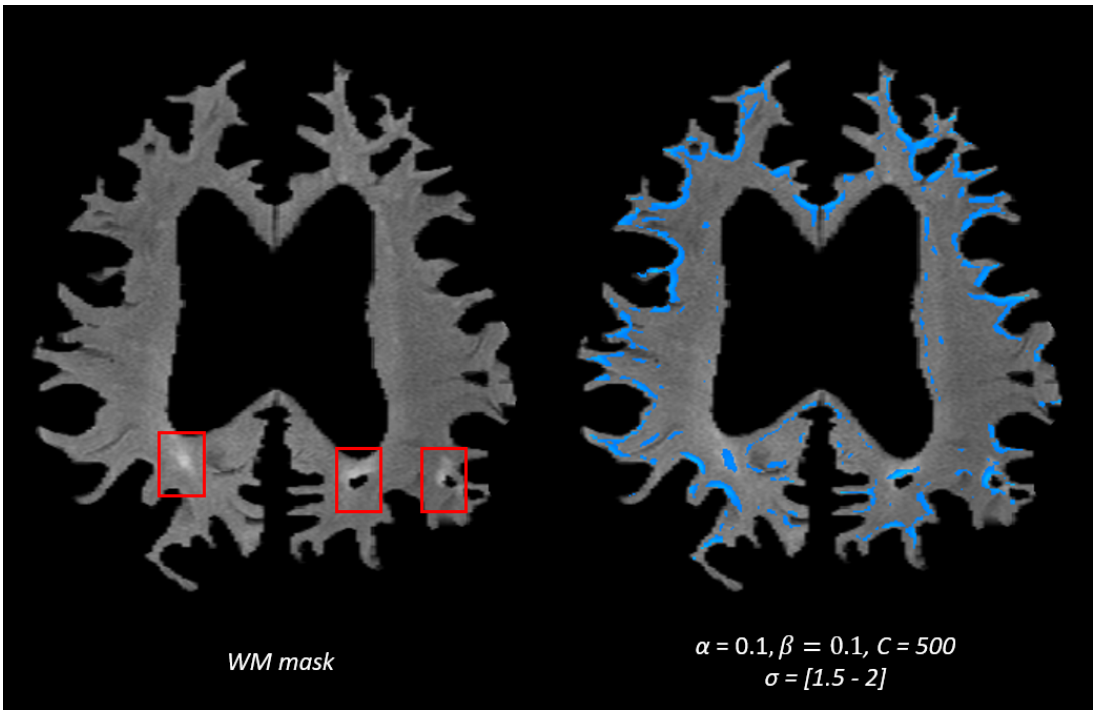

Figure 3.15: Segmentation of perivascular spaces procedure of a T2-Weighted image using matlab and FSL.

Results indicate that the Frangi filter showed a capability to map and delineate hyperintense areas regarding white-matter lesions (WML), thus, the given output in this sequence could be useful if combined with T1W and T2W masks, eliminating remaining WMH areas in the PVS mask.

3.4 T1-Weighted vs T2-Weighted images - Segmentation analysis

Regarding the analysis performed throughout the trials, it was found that the segmentation displayed in T2W is more similar to what is expected, getting closer to the ground-truth. The comparison of a segmentation using optimized parameter set in both MR sequences (figure 3.18) indicates that T2-Weighted MR images provided a higher CSF-WM contrast to the filter compared with T1W, allowing the filter to recognize more easily the shape and orientation of vessel-like features.

The optimised parameter set included ($\alpha = 0.1, \beta = 0.2, C = 400, \sigma = 0.06$) and ($\alpha = 0.05, \beta = 0.1, C = 500, \sigma = 0.06$) for the T1W and T2W, respectively.

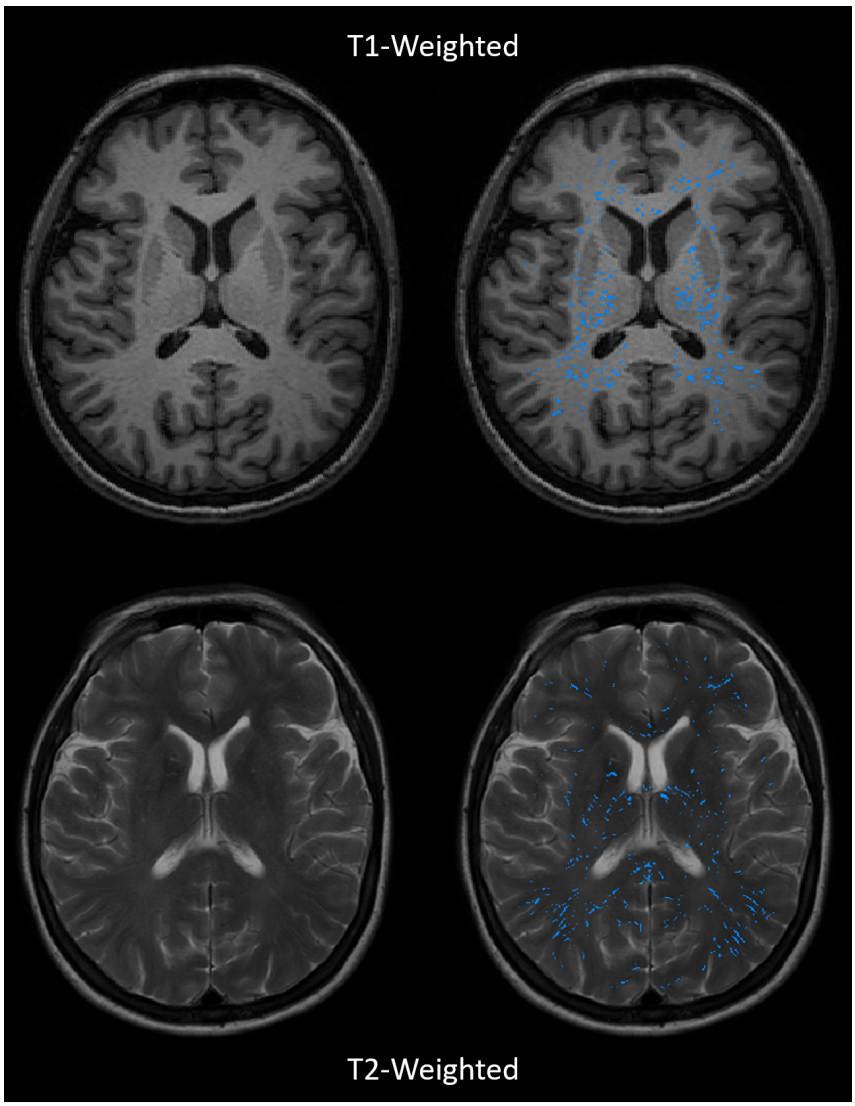

Figure 3.16: Brain axial slices presenting PVS. From left to right: T1W brain with no filter applied, T1W brain with Frangi filter, T2W without filter, and T2W filtered. PVS are marked in light-blue.

In the same figure, when comparing the two given outputs, it was noticed that in the most periphery brain areas PVS presented in its majority elongated shapes. However, in areas near the ventricles PVS started to display more dot-like features. These features are more easily captured in the T2W segmentation when compared with the T1W. Also, PVS that were difficult to detect in T1W were successfully captured in T2W allowing a more reliable

mapping.

The results may indicate that the sensitivity in T2W enabled to capture and delineate a higher number of structures, as well as the enhancement of expected vessel-like features. For the T1W to be capable to detect PVS, elongated features in the periphery, as demonstrated in the T2W, α had to be higher, allowing the sensitivity between the CSF and background (WM) increase. However, it was noticed in these cases the enhancement of false positives. Consequently, the modality of choice for PVS mapping analysis in this work was the T2W.

3.5 Verification and Validation

The main goal of this section is to validate if obtained images using the Frangi filter correspond to the expected PVS segmentation. In addition, the main purpose is to verify if this method allows a reliable PVS mapping and extraction on MR images, understanding the behaviour and accuracy displayed in T1W and T2W. In the context of this work, a positive mapping can be defined as the usability that the filter has to delineate and mark only voxels corresponding to contrast displayed by CSF, in T2W MR images the contrast of PVS corresponds to the brightest pixels, as in T1W MR images the contrast enhanced by PVS correspond to darker pixels when comparing with the background (WM).

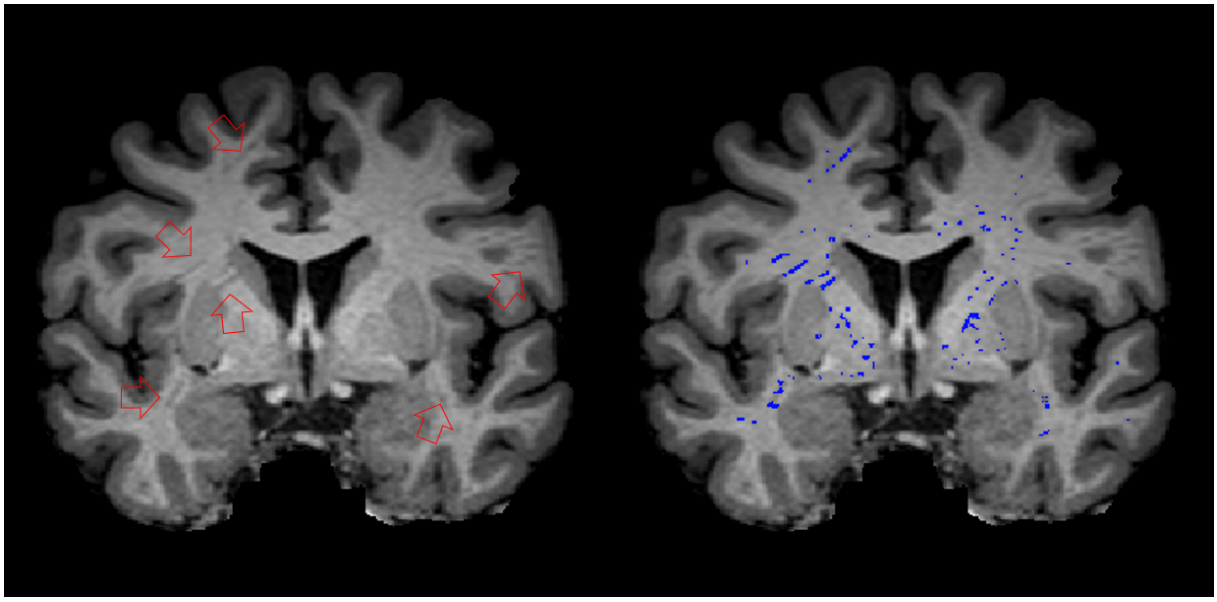

Figure 3.17: Implementation of Frangi Filter in a coronal T2-Weighted MR image. After implement the skull-stripping (BET) with no filter applied (In the left) and the extraction pvs generated by the filter, marked in light-blue (in the right). Red arrows are pointing to PVS displayed in WM.

However, motion artifacts and WM lesions may display the same contrast as CSF, mostly in T2W MR images appearing as hyperintense regions. In order to perform a reliable segmentation it is important that the filter is capable to avoid voxels regarding these artifacts and lesions. On the other hand, PVS can arise in the the boundaries of WM lesions, overlapping the hiperintensity area. Therefore, in these cases, the filter must be capable to perform a correct mapping. This verification will strengthen results obtained in further PVS quantification.

Figures 3.17 and 3.18 demonstrate the segmentation of perivascular spaces in different patients, obtained in a coronal T1W and T2W MRI, respectively. Both images contain red arrows that are pointing to PVS, displayed

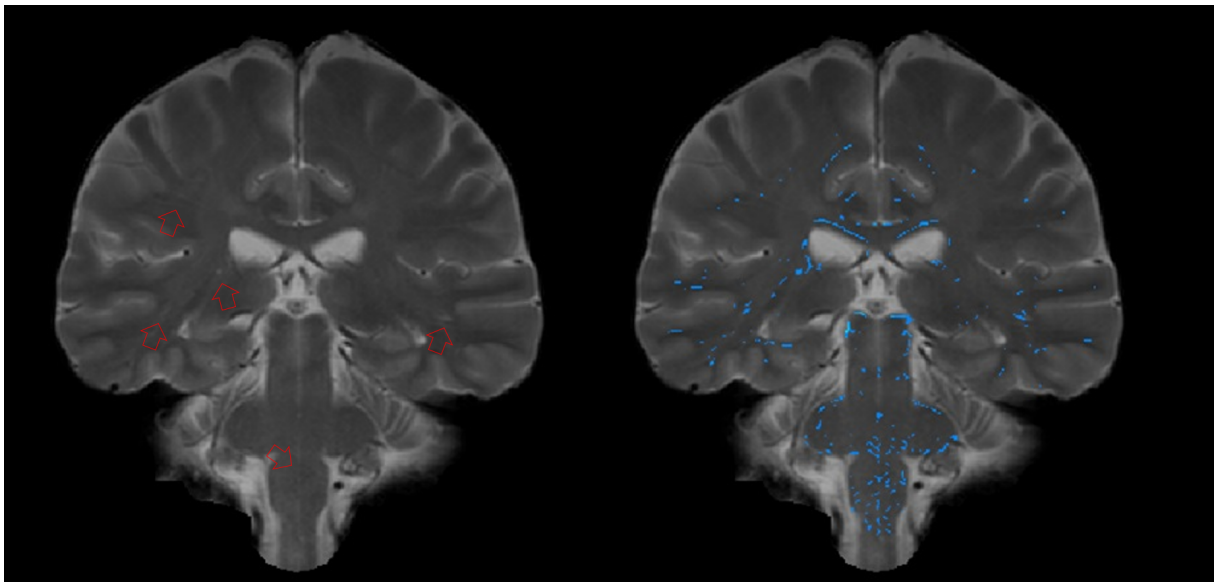

Figure 3.18: Implementation of the Frangi Filter in a coronal T2-Weighted MR image. The non filtered brain image contain the red arrows that are pointing to PVS in WM, and the PVS extraction generated by the filter, marked in light-blue.

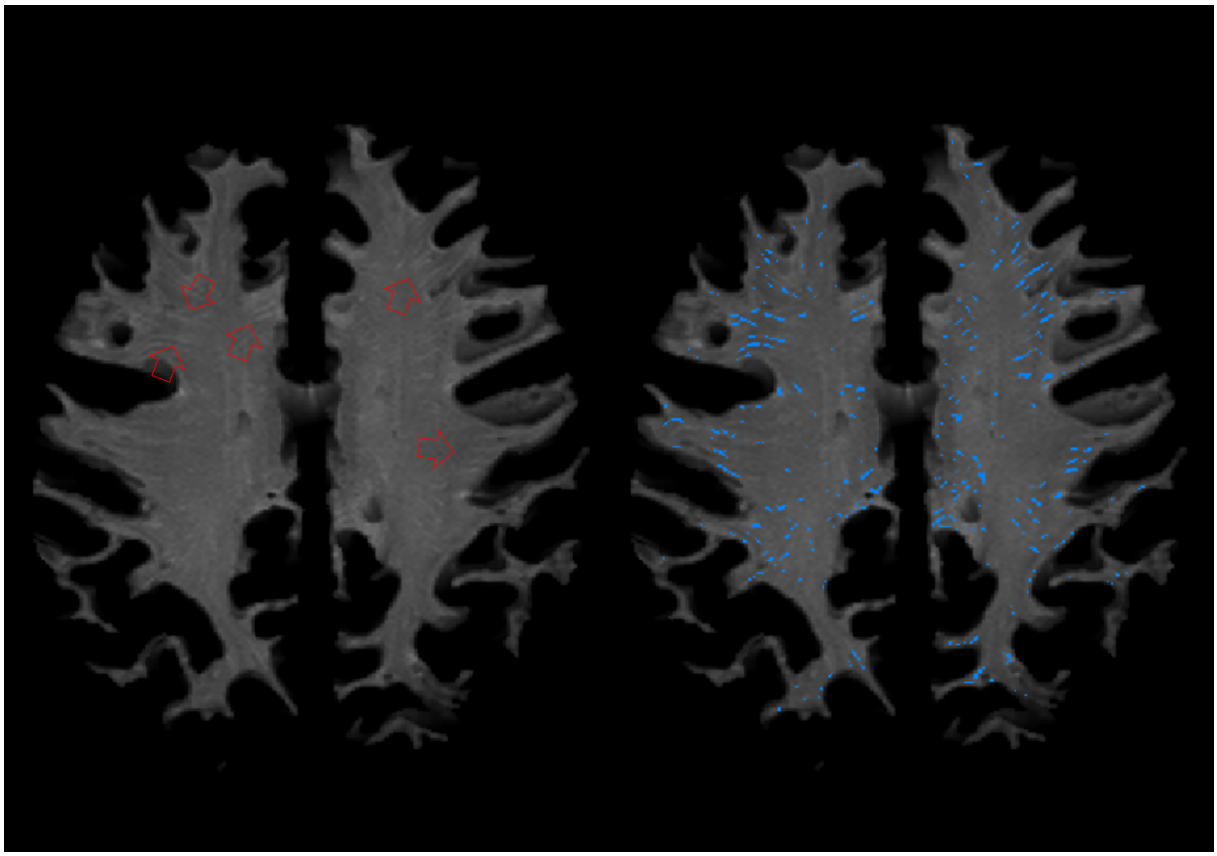

Figure 3.19: Implementation of the Frangi Filter in a axial T2-Weighted WM mask. The non filtered WM mask contains the red arrows that are pointing to PVS, as the PVS generated by the filter are marked in light-blue.

with CSF contrast. The segmentation represented in the T1W was capable to map and delineate almost the totality of visible PVS. PVS that presented elongated features were easily captured by the filter (marked in blue), however, a minority number of hypointense structures located in the most peripheric regions of the brain were not mapped.

In figure 3.18 a great density of hyperintensities in the brainstem that were not so easily seen were successfully captured by the filter. The segmentation illustrated in Figure 3.19 demonstrates the reliability of the filter in capturing structures that are not easily visible, delineating each PVS, enhancing the correct orientation and shape. These results reinforce the mapping capability in T2W.

White matter hiperintensities and Motion distortion artifacts

Movement artifacts in MRI degrade image quality and may lead to misinterpretation. Motion artifacts can be identified as ghosting or blurring, leading to an unreliable analysis. In some cases PVS can arise in the boundaries of WM lesions, overlapping the hyperintensity area, so the filter must detect these structures in these cases. In this subsection, some examples of the output given by the filter when it is presented in cases like the ones reported.

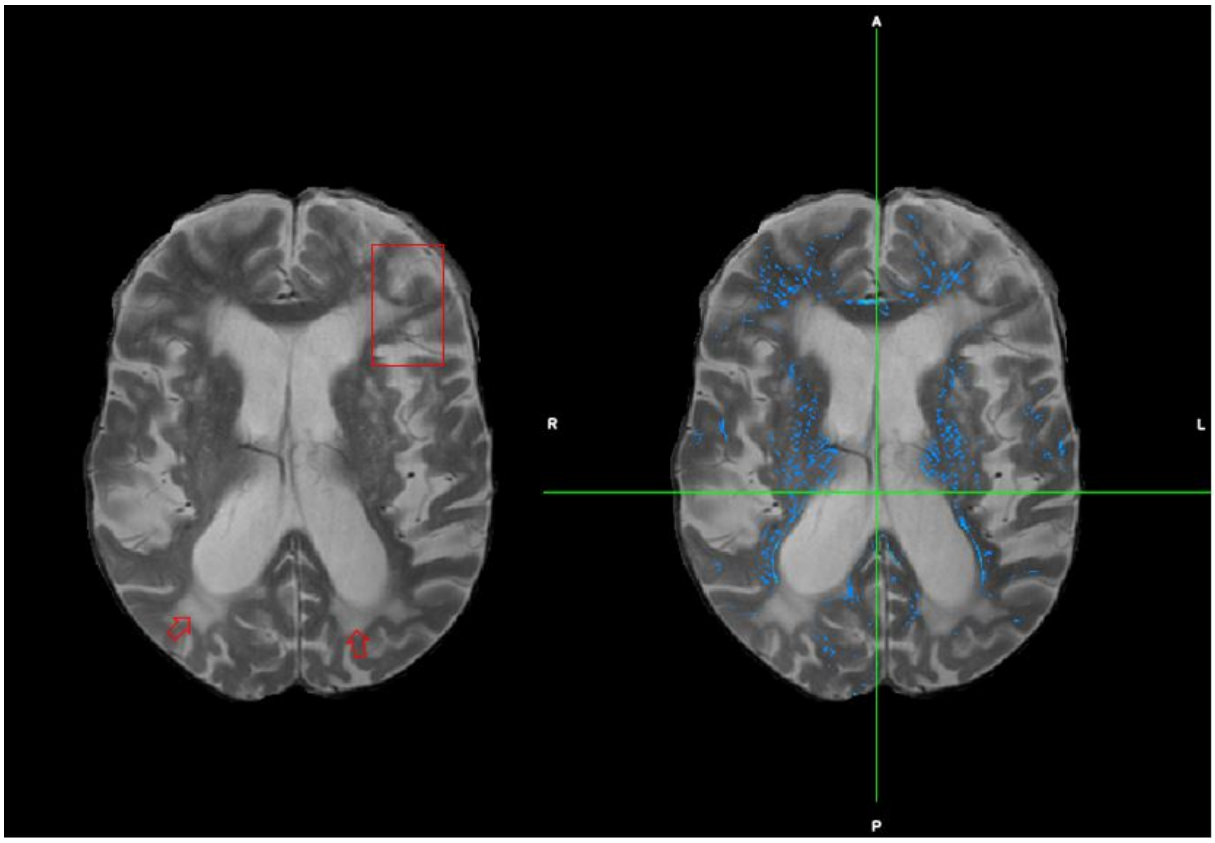

Figure 3.20: Enhancement of PVS in a axial T2W presenting white matter lesion. The red arrows indicate some white matter hyper intensity areas, and some visible PVS appear inside the red square. PVS are marked in light-blue.

During the first stage of image processing, when a brain presenting severe white matter lesion, the mask created using FSL function, FAST, in some cases can be compromised. Since these lesions have the same intensity as CSF, during image processing, in order to create a mask for the respective WM, GM and CSF, the software used can ignore some of the areas that contain severe lesion, and some parts of the white matter can be misunderstood as CSF, vanishing in the final mask, generated by FSL. The mask that is given as input to the filter has to be very optimised, so that any area containing a PVS is presented to the filter, and not misunderstood as CSF. The following examples describe a segmentation trial in a brain presenting severe white matter lesion. Particularly, in figure 3.20 a severe white matter lesion is presented, as well as motion artifacts.

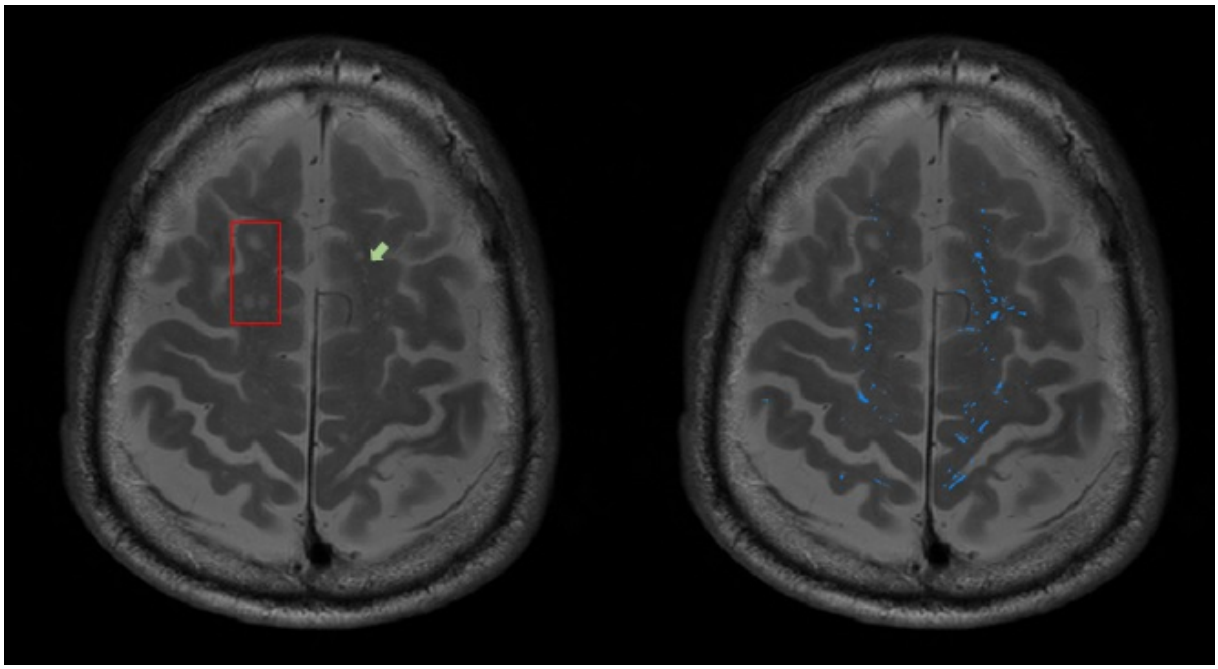

Figure 3.21: T2W MR sequence showing the enhancement of perivascular spaces in a patient diagnosed with Multiple System Atrophy (MSA) (in the right). The output given by Frangi filter (in blue) did not enhance lacune areas (marked inside the red square).

The areas containing severe white matter lesion are marked with red arrows, and the red square contains a zone affected by motion. In here, the final output mask avoided WMH and motion distortion areas.

A good example of reliability of the output given by Frangi is presented in figure 3.21, where the enhancement of PVS occurs, avoiding areas with other WM lesions as lacunes, shown inside the red square. Moreover, the green arrow is pointing to perivascular spaces that arise in WM. The Frangi output performed a correct segmentation, although, in some areas in the neighbourhood of grey matter (GM) with CSF, the filter detected some areas that may not correspond to a PVS. This problem needs to be accounted, and may concern to a problem during processing of the WM mask, used as input in the Frangi filter. If the mask created by FSL using FAST function, after binaring, contains regions of CSF that appear as hyperintense, the filter will probably enhance these regions misleading to an incorrect and unreliable segmentation. In case of the filter marked a lacune this would lead to a wrong quantification of PVS. In the same figure (3.21), inside the the red square, lacunes (extremely enlarged PVS) are displayed.

Another contribution to the reliability on the output given by Frangi filter is shown in figure 3.22, where the enhancement of PVS occurs avoidoided areas with increased WMH (represented inside of the red squares). Segmented PVS in the boundaries of WHM were delineated.

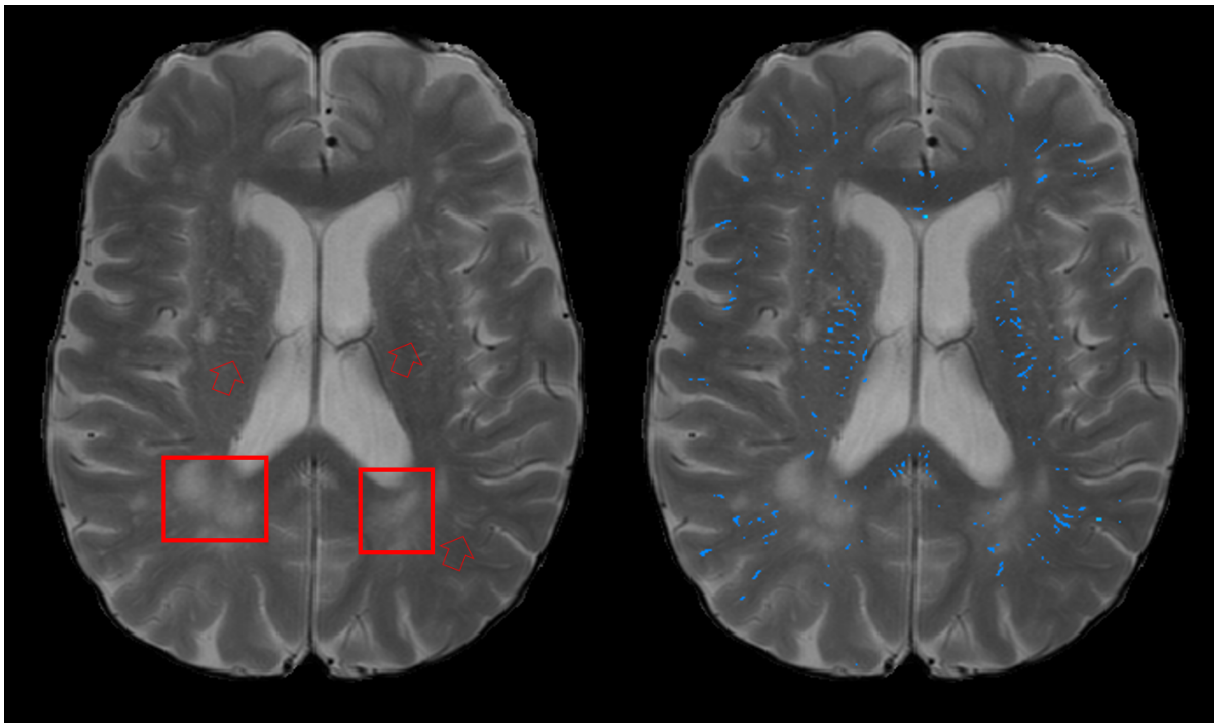

Figure 3.22: T2W MR sequence showing the enhancement of PVS in a patient diagnosed with Multiple System Atrophy (MSA).

Chapter 4

Statistical analysis

4.1 Quantification resulting from the PVS segmentation

After performing the quantification of PVS in all subjects according to their disease, it is necessary to use statistical analysis in order to check for statistical significance between diseases for the measured variables. In this work, statistical significance was defined for a p-value below 0.05 (Confidence interval of 95%).

In order to choose an adequate test for our measures, more specifically, a parametric or non-parametric test, several assumptions need to be verified.

The main assumptions for a parametric test are normality, linearity, homoscedasticity, and independency [49, 50]. Before opting between a parametric or non-parametric test, all the assumptions referred above have to be tested.

The first assumption of a parametric test is normality [49]. Normality requires that the scores in the population follow a certain distribution: the normal distribution ($Population(P) \sim N(\mu, \sigma^2)$). When the sample is small, usually the rule of thumb used is that for samples lower than 30 subjects or values, the normality assumption cannot be made. For samples lower than 30 it is advisable to use a normality test (Kolmogorov Smirnov), in which the null hypothesis is $H0 : Population(P) \sim N(\mu, \sigma^2)$, and $H1 : Population(P)$ does not follow a $N(\mu, \sigma^2)$. For smaller samples, e.g, lower than 10 it is not necessary to check for normality, because the test will lead to failure.

The second assumption of a parametric test is homoscedasticity, where equal population variances per group, and equal population variances for every value are required. Furthermore, the null hypothesis is $H0 : \sigma_a^2 = \sigma_b^2$, where the equality of variances between the group a and b are tested. To test homoscedasticity a $F - test$ is used, although, if more then two groups ($k > 2$) are presented, a different test is used (levene test).

While running these 2 tests separately, if the null hypothesis is not rejected, than a parametric test can be used for further statistical analysis.

4.1.1 Statistical analysis regarding Perivascular spaces volume by disease

The obtained test-statistical and p-values for the normality and homoscedasticity tests using Kolmogorov-Smirnov and classical Levene test (based on the absolute deviations from the mean), respectively, are displayed in table 4.1 . This analysis showed a significant value in the normality test ($p < 0.05$). On the other hand, no significant values were found in the deviations from the mean (homoscedasticity test). These results give us a better understanding regarding the obtained distributions, as well as the type of statistical test that should be used along the work. Therefore, all tests should be non-parametric. Also, all statistical analysis results were performed using R-Studio.

The following analysis will focus on the obtained distribution of normalized PVS volumes in each brain lobe, across different groups of patients, where the normalization in each analyzed subject consisted in dividing the segmented PVS volume by the volume of white matter (WM). More specifically, the purpose of the following tests is to check for significant differences for the normalized PVS volumes in each brain lobe, considering different patient conditions.

Table 4.1: Kolmogorov-Smirnov test and Classical Levene‘s test.

	Test-statistic value	**p-value**
One Sample Kolmogorov-Smirnov test	$D = 0.50036$	2.098e - 14*
data: all patient groups.		
Classical Levene‘s test based on the absolute deviations from the mean	$w = 2.4065$	0.07683
data: all patient groups.		

PVS distribution in Patients diagnosed with MSA

Results regarding the distribution of normalized PVS volumes in patients diagnosed with MSA are displayed in table 4.2. A Kruskal-Wallis test using as factors frontal lobe (FL), occipital lobe (OL), temporal lobe (TL) and parietal lobe (PL) demonstrated significant differences between lobes.

Table 4.2: Kruskal-Wallis rank sum test between the normalized volumes of perivascular spaces distributed by brain lobe in patients diagnosed with MSA.

Kruskal-Wallis rank sum test	**Test-statistic**	**df(n-1)**	**p-value**
Data: perivascular spaces normalized volumes in MSA.	$\chi^2 = 13.387$	3	0.00387

The same distribution can be seen in figure 4.1 (boxplot). Figures 4.1 illustrate the distributions of the normalized volumes in different lobes. PVS volumes presented a narrow distribution in the parietal and temporal lobes, on the other hand, the obtained PVS distribution in FL was more wide by comparing with the other brain lobes. Moreover, lower medians can be observed for the occipital, parietal and temporal lobes compared to the frontal lobe.

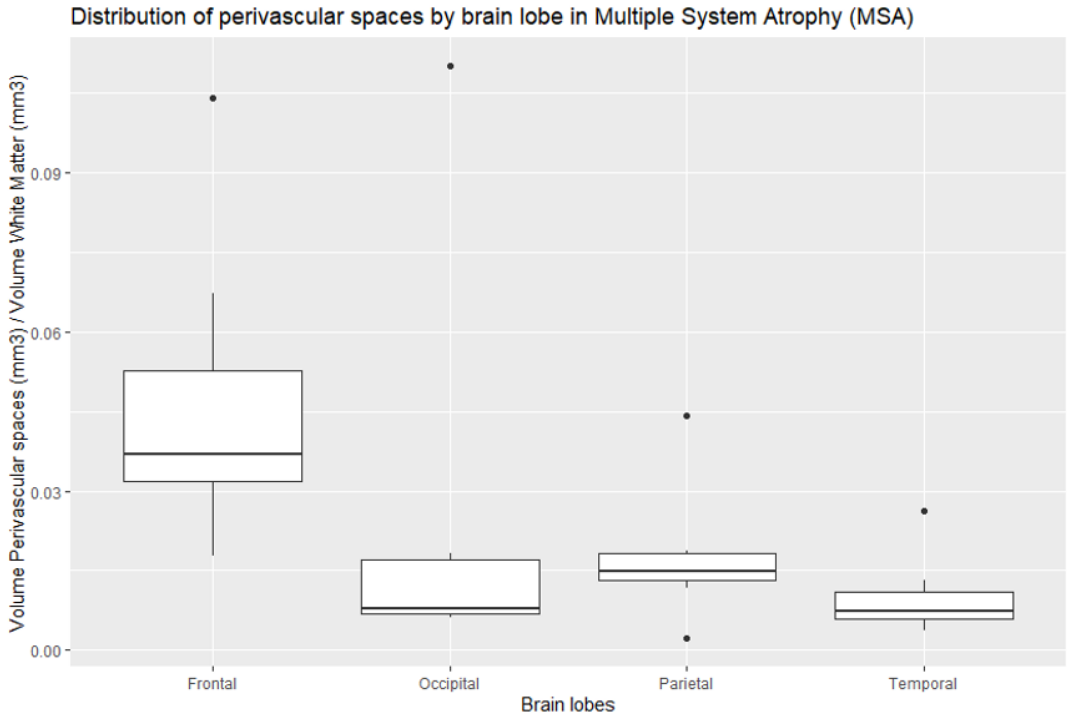

Figure 4.1: The central mark indicates the median; the upper and lower edges of the box correspond to the 25th and 75th percentiles, respectively; the upper and lower extremes represent the maximum and minimum values, respectively; and the dots correspond to the outliers.

Results consistent with figure 4.1 are displayed in table 4.3. In here, multiple comparisons were performed in order to understand the significant difference found. Differences found in multiple comparison test using Tukey HSD along each brain lobe are concordant with the results observed in figure 4.1. Post-hoc comparisons shown in table 4.3 evidence that the obtained normalized PVS volume means in frontal lobe were higher while comparing with the ones in the temporal lobe, resulting in a close to significance-level (p = 0.05351).

In the other hand, no significant differences were found between the remaining lobes.

Table 4.3: Obtained values from the *TukeyHSD* Multiple comparisions regarding the distribution of perivascular spaces normalized volume means by brain lobe, in patients diagnosed with MSA, using a 95% confidence level.

brain lobes	occipital-frontal	parietal-frontal	temporal-frontal	parietal-occipital	temporal-occipital	temporal-parietal
p-value	0.36813	0.16210	0.05351*	0.95624	0.70998	0.94219

PVS distribution in Patients diagnosed with PSP

Boxplots regarding the distribution of normalized PVS volumes in PSP patients can bee seen in figure 4.2. The volumes in the frontal and occipital lobe presented very similar medians compared with the parietal and temporal lobes. In addition, obtained values regarding the volume of PVS in the frontal lobe showed less variability amongst the remaining brain lobes. Moreover, decreased values were found in the temporal lobe, making the respective distribution visually distinguishable from the remaining regions.

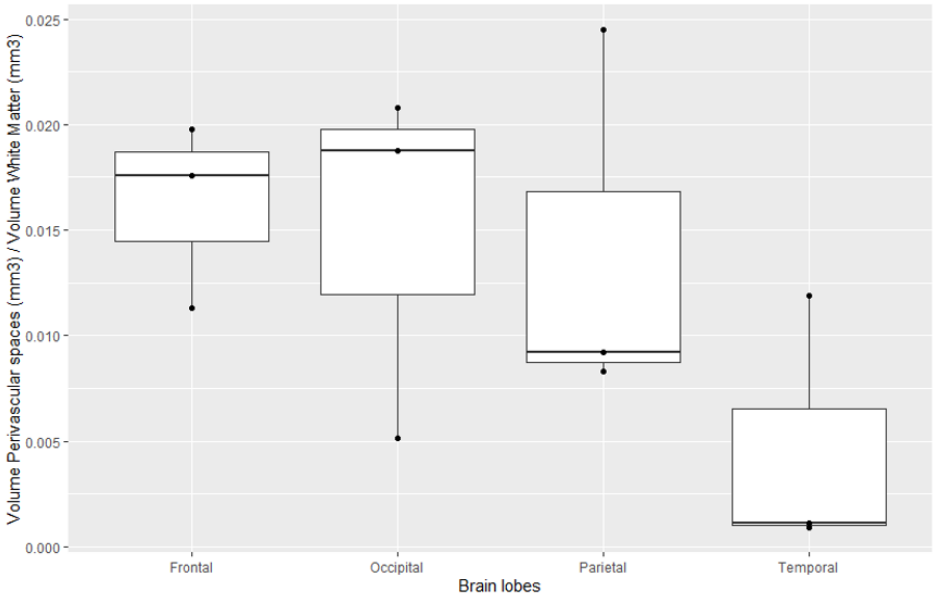

Figure 4.2: Distribution of perivascular spaces by brain lobe in PSP patients. The central mark indicates the median; the upper and lower edges of the box correspond to the 25th and 75th percentiles, respectively; the upper and lower extremes represent the maximum and minimum values, respectively; and the dots correspond to the outliers.

Despite the apparent differences across the medians, no statistically significant differences were found between the groups (p = 0.129) given a 95% confidence level, neither their interaction, given by post hoc comparisons, showed in tables 4.4 and 4.5. However, differences between the parietal and frontal (p = 0.06), and the temporal and occipital (p = 0.097) lobe may show a tendency towards significance, in a 90% confidence interval.

Table 4.4: Kruskal-Wallis rank sum test between the normalized volumes of perivascular spaces distributed by brain lobe in patients diagnosed with PSP.

Kruskal-Wallis rank sum test	**Test-statistic**	**df(n-1)**	**p-value**
Data: perivascular spaces normalized volumes in PSP.	$\chi^2 = 5.6667$	3	0.129

Table 4.5: Obtained values from the *TukeyHSD* Multiple comparisions regarding the distribution of perivascular spaces normalized volume means by brain lobe, in patients diagnosed with PSP, using a 95% confidence level.

brain lobes	occipital-frontal	parietal-frontal	temporal-frontal	parietal-occipital	temporal-occipital	temporal-parietal
p-value	0.99401	0.63332	0.06846	0.77096	0.09756	0.35611

Results of the analysis of PVS distribution in patients diagnosed with Fabry disease

Similar to the previous analysis, figure 4.3 illustrates the distribution of PVS in both FD patients. Among the obtained data, the lobes where a higher value was found regarding the metric analyzed were the frontal and Parietal lobes. On the other hand, the temporal lobe revealed a lower density of normalized PVS between the remaining lobes.

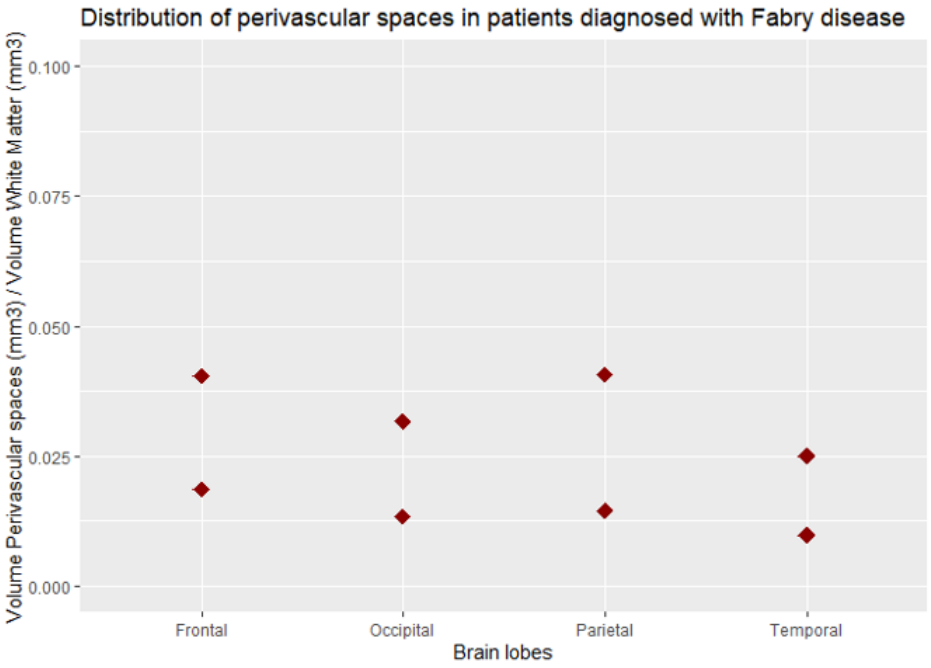

Figure 4.3: Distribution of normalized PVS across different brain lobes. Each red dot represents a normalized volume for a given patient in the respective regions of interest (brain lobes).

Comparison of PVS normalized volumes distribution by patient group

After analyzing each group individually, figure 4.4 illustrates the distribution of the same analyzed metric across different regions of interest (different brain lobes) to determine whether there are significant differences in this same region of interest between the different groups. The analysed groups displayed are the controls (HLT), Multiple System Atrophy (MSA) and Progressive Supranuclear Palsy (PSP).

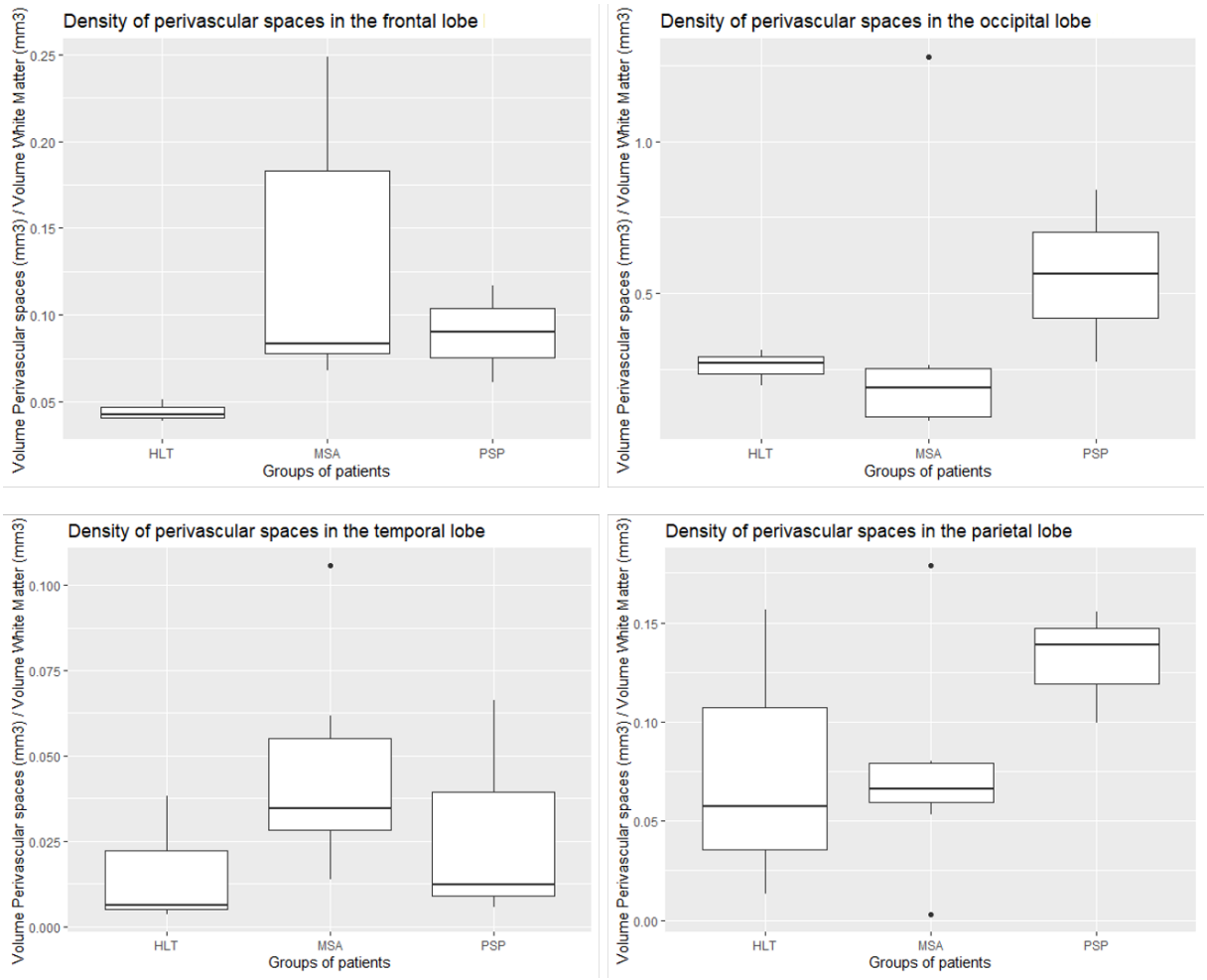

Figure 4.4: The central mark indicates the median; the upper and lower edges of the box correspond to the 25th and 75th percentiles, respectively; the upper and lower extremes represent the maximum and minimum values, respectively; and the dots correspond to the outliers.

The groups where a greater difference was observed concerning the medians of the analyzed metric were patients diagnosed with MSA and PSP, mainly observed on the occipital and parietal lobes.

On the other hand, the lobe where a lowest variability was found in the obtained metric across the analysed groups was the temporal lobe. In this brain region, visual trends displayed in the boxplots can be confirmed by analyzing the value given by TukeyHSD multiple comparisons test. In table 4.6, the p-values regarding the multiple comparisions between different groups are displayed. The difference between groups concerning the distribution of normalized PVS volume was found to be less significative in the temporal and occipital lobes (higher p-values).

Difference between groups obtained in the frontal lobe were considered more significative , while comparing with the remaining brain lobes.

In order to see if any significative value was achieved, a multiple comparisons test was performed. According with the Kruskal Wallis multiple comparisons test, the distribution concerning the analyzed metric was found to be less significative, in the parietal and temporal brain lobes.

Table 4.6: Obtained values from the *TukeyHSD* Multiple comparisions regarding the distribution of perivascular spaces normalized volume means by brain lobe using a 95% confidence level.

	MSA-HLT	**PSP-HLT**	**PSP-MSA**			
	Multiple comparision TukeyHSD p-value			***kruskal-wallis*** χ^2	$df(n-1)$	***p-value (kruskal-wallis test)***
frontal lobe	0.1211887	0.6200567	0.5579179	6.6248	2	0.03643
occipital lobe	0.9680215	0.5758043	0.6077585	4.3391	2	0.1142
temporal lobe	0.3477222	0.8723731	0.6698178	2.7441	2	0.2536
parietal lobe	0.9997415	0.4463290	0.3250871	2.3171	2	0.3139

Comparison groups regarding perivascular spaces normalized volumes

Similarly to the previous metric, the following analysis considered all obtained values in the brain lobes, according with each group type. The distribution for the four groups of the median values across the ROIs (brain lobes) can be consulted in figure 4.5.

Lowest variability and reduced values can be observed for the Healthy group (HLT) compared to the PSP and FD.

In terms of boxplot distribution, the medians corresponding to the MSA and HLT group look very similar while comparing with the remaining groups. Also, a decreased number of outliers can be observed for patients diagnosed with MSA amongst the remaining groups.

No statistically significant group differences were found for either of the groups (p = 0.2293), displayed in table 4.7.

Moreover, post hoc comparisons given by Tukey HSD amongst the ROIs (brain lobes) did not reveal statistically significant, neither significant interactions between the groups (table 4.8).

Table 4.7: Analysis of variance statistical test regarding normalized PVS volumes presented in all groups.

	df (n-1)	***Sum Sq***	***Mean Sq***	**F-value**	**p-value**
groups	3	0.00201	0.00067	1.4819	0.2293

Table 4.8: Obtained values from the *TukeyHSD* multiple comparisions regarding the distribution of normalized PVS volume means in all analysed groups, using a 95% confidence level.

Patient groups	HLT - FD	MSA - FD	PSP - FD	MSA - HLT	PSP - HLT	PSP - MSA
p-value	0.61801	0.99913	0.93702	0.34183	0.19549	0.89734

Comparison regarding normalized PVS volumes between healthy and pathological groups

Since no significance was found between the previously analyzed values between the four groups, potentially due to their small size, a new test was attempted by grouping all patients, more specifically, a group including MSA,

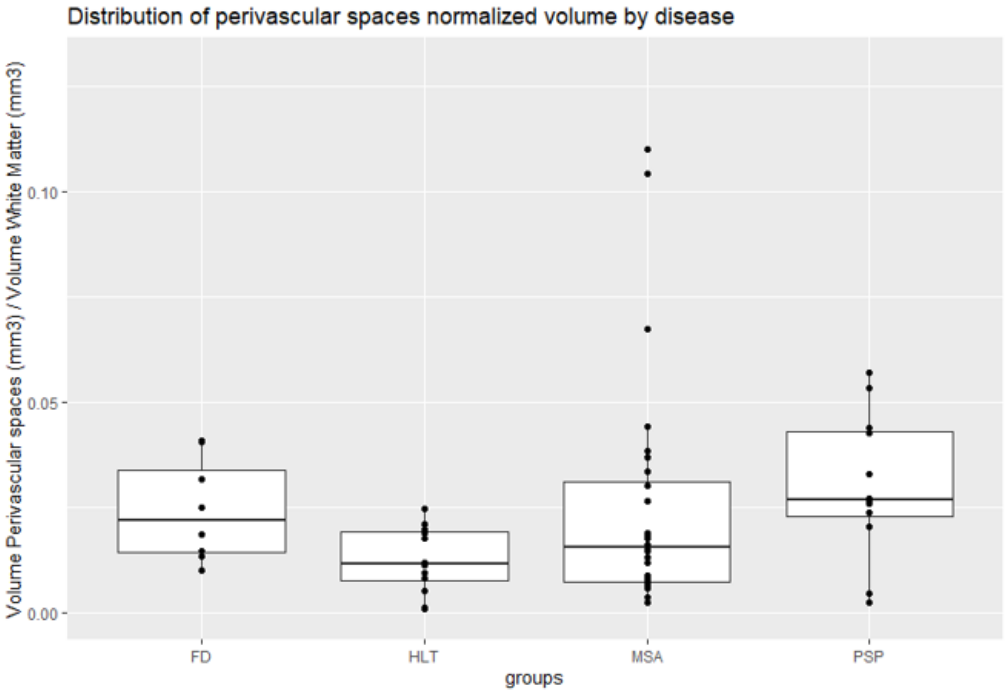

Figure 4.5: The central mark indicates the median; the upper and lower edges of the box correspond to the 25th and 75th percentiles, respectively; the upper and lower extremes represent the maximum and minimum values, respectively; and the dots correspond to the outliers.

PSP and Fabry‘s disease, and compare them with controls.

Thus, in this trial, the first group used concerned control subjects (HLT), and the second group concerned all patients. Consequently, a data frame was created displaying all obtained values regarding these two groups.

Figure 4.6 illustrates the comparison of the analyzed metrics between controls subjects and patients. Healthy subjects displayed a lower variability regarding the analyzed metric compared with pathological subjects. In addition, a small number corresponding to the Pathology group reached increased volumes of normalized PVS when compared with the other group.

Similar to previous tests, in order to determine the existence of significance amongst the groups and their interaction, the Mann-Whitney Rank Sum test was used, and the results can be consulted in table 4.9.

Table 4.9: Mann-Whitney test between healthy and pathological patients. Pathological patients include patients diagnosed with MSA, PSP and FD.

Wilcoxon Rank SumTest (Mann-Whitney)	**W**	**df (n-1)**	**p-value**
Data: healthy (HLT) and pathological patients (MSA,PSP,FD)	400	1	0.0382*

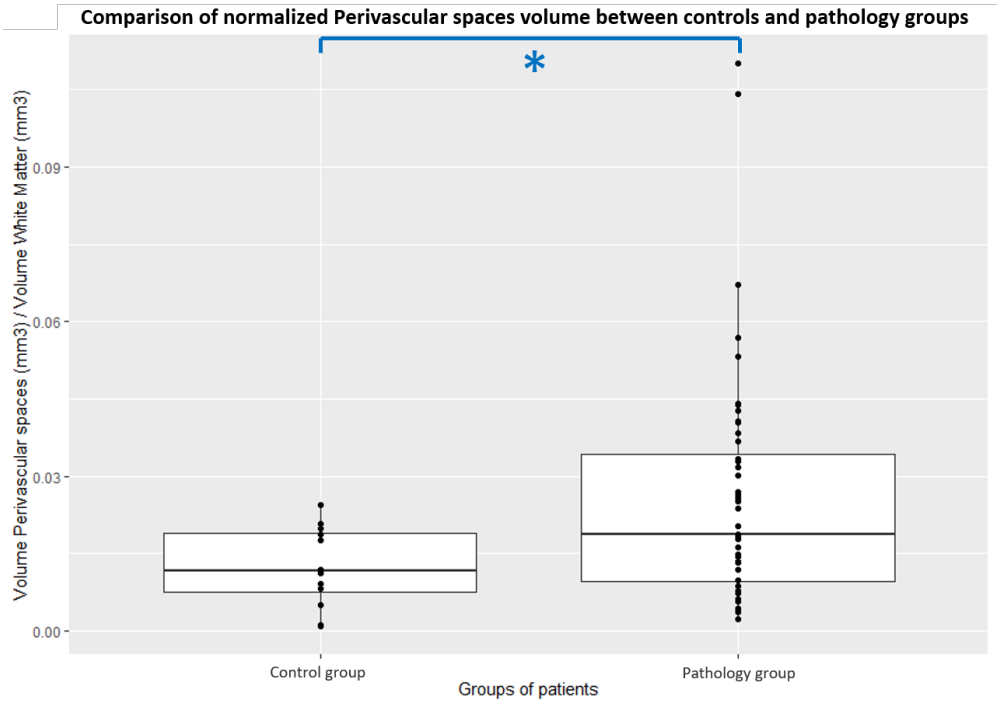

Figure 4.6: The central mark indicates the median; the upper and lower edges of the box correspond to the 25th and 75th percentiles, respectively; the upper and lower extremes represent the maximum and minimum values, respectively; and the dots correspond to the outliers.

Based on p value, at a confidence interval of 95%, a significant difference was found between the analyzed groups ($p = 0.0382$) leading to the rejection of the null hypothesis (H0: equality between medians).

Visual ratings based on the Wardlaw and Patankar proposed scale

Qualitative measurements were performed across the data in order to understand if the severity scores were related with quantitative measurements. In addition, in the context of PVS, the comparison between these visual ratings with quantitative results provided by the segmentation using the Frangi filter would allow to a better understanding of the impact that the enlargement and distribution of these structures present in each patient‘s physiological condition.

In this work, qualitative measurements were performed based on the proposed scale by Wardlaw and Patankar et al. Some examples resulting from the attribution regarding the respective scoring are displayed in figure 4.7. According to these guidelines, a certain value of severity was assigned to each patient.

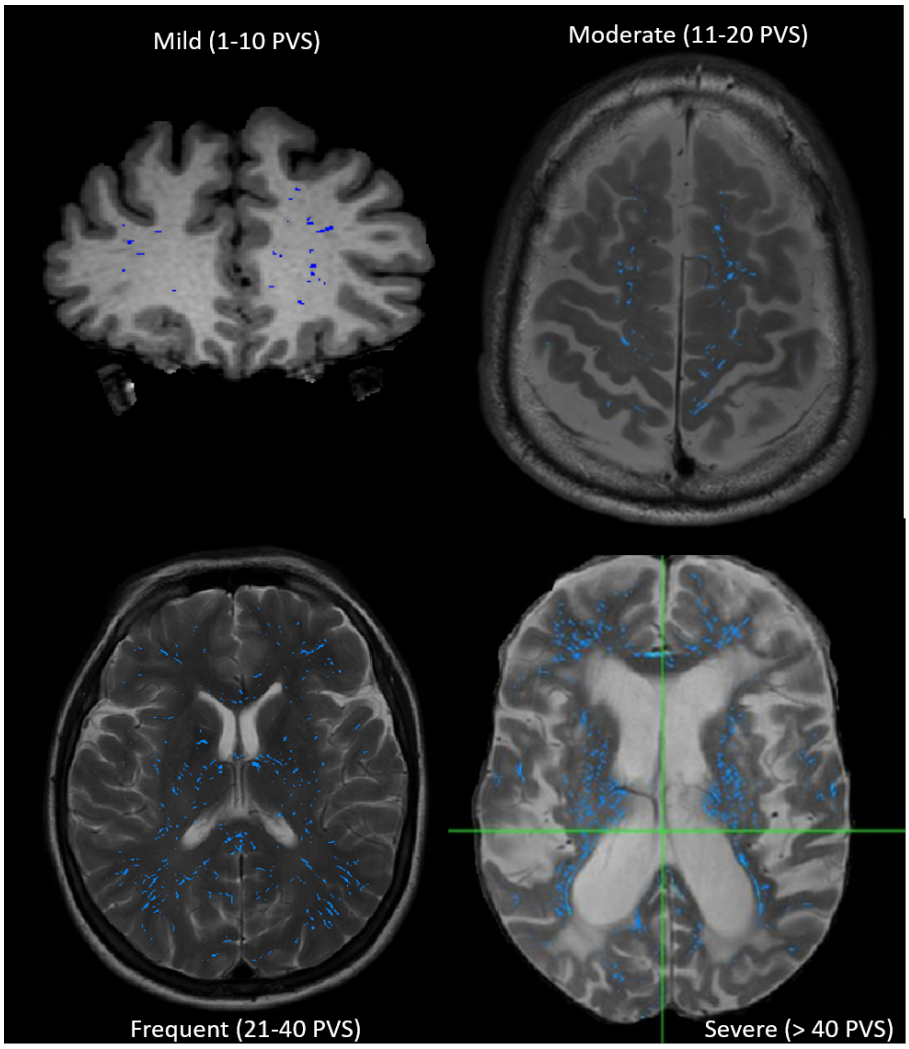

Figure 4.7: Visual scoring according to the Wardlaw and Patankar scale [47] after applying the Frangi segmentation.

Figure 4.8 summarizes the visual rating scores given to all patients.

The results showed that patients diagnosed with MSA displayed more variable severity rating scores, whereas in the majority of the cases scale Frequent (3) and Severe (4) scores were assigned. In addition, the patient for whome the minimum score of severity was observed belonged to the same group.

Furthermore, similarly to MSA, patients diagnosed with PSP also obtained higher visual rating scores, being the majority of cases assigned to the frequent level (3).

Moreover, both FD patients presented the same score level.

In order to see if PVS visual rating scores have a clear connection within obtained PVS computational total volume, obtained by the segmentation using Frangi filter, the following associations between these two metrics can be consulted in figure 4.8.

Obtained PVS computational total volumes and PVS visual rating scores were compared, using a Linear model. In here, the corresponding volume of each patient was assigned to a certain visual rating score (1-4) and they can be consulted in figure 4.8. In addition, the linear model represents a continuous quantitative response variable (PVS normalized volumes) and an explanatory variable, which corresponds to a categorical variable with four levels

(visual rating scores). The results obtained in this study can consulted in tables 4.10 and 4.11.

The intercept given by the linear model corresponds to the average response of the reference class for a patient with mild PVS score, as the remaining betas explain how much each of the remaining classes differ from the reference class.

Table 4.10: Linear model regarding the visual rating scores obtained.

Visual ratings given by Wardlaw and Patankar scales	Estimate	Std. Error	t value	$Pr(>\|t\|)$
(Intercept)	0.06195	0.04737	1.308	0.2176
moderate (11-20 pvs)	-0.01626	0.05470	-0.297	0.7719
frequent (21-40 pvs)	0.03578	0.05024	0.712	0.4912
Severe (>40 pvs)	0.12207	0.05470	2.232	**0.0474***

Table 4.11: Linear moder regarding Wardlaw and Patankar visual rating scores obtained.

Multiple R - Squared	**Adjusted R - Squared**	**F - statistic**	**p - value**
0.5602	0.4403	4.671	**0.02437***

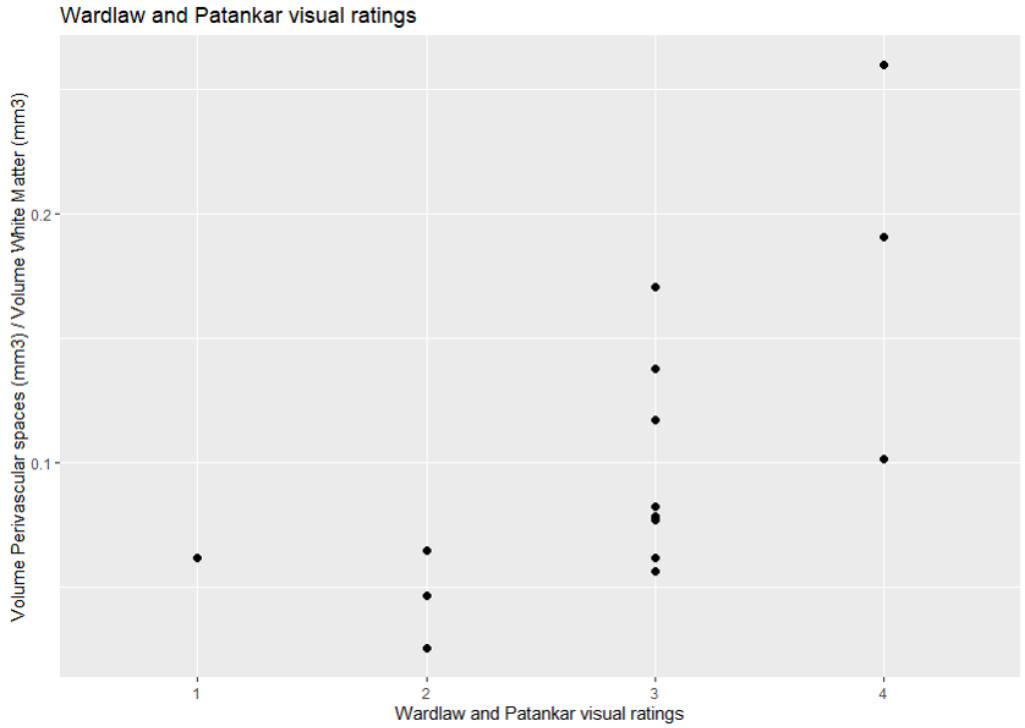

Figure 4.8: Visual rating scores obtained in all patients regarding the proposed scale by Wardlaw and Patankar et al.

In other words, the purpose of these trials is to verify once more the performance of the filter and strengthen clinical validation.

PVS total volume increased significantly with PVS count, [coefficient of linear regression: 0.0619, p-value = 0.0243*]. These results indicate that PVS visual rating scores may have a positive association with PVS volume, therefore, this method indicates that a patient who is assigned a more severe rating is more likely to have a higher volume of PVS.

Chapter 5

Discussion

PVS and cerebrovascular disease

PVS allow interstitial solutes to be cleared from the brain, resulting in an important part of the brain circulation and drainage system. However, dysfunction of PVS pathways can occur if there is deposition of substances causing stagnation of fluid. Therefore, this stagnation may result in an enlarged PVS due to the accumulation of fluid. Finding a method that provides further information regarding quantitative analysis of a patient (regarding the severity and presence of these cavities) would allow a better understanding and characterization of PVS severity in aged people and its associations with dementia, stroke and vascular diseases.

The major goal of this thesis was the segmentation of these structures and further quantification. In addition, this work focused the analysis in groups of patients diagnosed with MSA, PSP and FD.

PVS segmentation

The process of PVS counting can be laborious and error-prone, so efforts to improve its efficiency and accuracy are extremely important. Finding a segmentation method for these cavities will avoid clinicians manually each structure and double-counting, will allow a better characterization in terms of spatial distribution, orientation and volume, perform a fast screening in each patient resulting in an easy and more reliable qualitative analysis, and above of all, will allow physicians to save time. PVS manually marking can be very time consuming, thus, a segmentation method will be useful to perform a fast screening in several patients at the same time. Moreover, this method will make possible to track quantitative measurements and disease progression in each patient.

Several techniques including markov models, random forest segmentation, algorithm automatic detection and threshold methods have been proposed in order to enhance these structures. The method applied in this work concerns the use of the 3D Frangi vesselness filter.

Frangi filter performance

As shown in chapter 4, the Frangi filter allowed a correct identification and extraction of PVS capturing the 3D geometrical shape, showing it can act as a promising tool and give clinical support in both qualitative and quantitative measurements.

In other words, given certain parameters, the Frangi Filter allowed a detection of PVS that were hardly identifiable, mostly in T1-Weighted MR images. PVS that could barely be spotted visually, were identified (as is shown in the figures).

During the filtering process a greater speed and precision was noticed regarding the calculation of the matrices containing the corresponding eigenvalues and eigenvectors of each image, avoiding problems of error overload memory when using matlab. Although, in some MR images that displayed a higher number in slices, specially in some T1-Weighted MR images, the calculation of the referred matrices lead to the shutdown of the system, making matlab unable to calculate the referred matrices, and consequently, the output mask containing the PVS was not generated.

Trials regarding parameter optimization were performed with the purpose to find the optimal sensitivity in the generated output provided by the Frangi filter, making the segmentations closer to what is expected from visual inspection and to be used as a reliable clinical tool. Therefore, different values were assigned to each parameter $(\alpha, \beta, C, \sigma)$ to understand their behaviour among the trials, and improve the PVS mapping.

Since PVS quantification is performed by a neuroradiologist, an image with high PVS-tissue contrast is ideal. This difference in contrast was an important contributor to the filter performance.

T2-Weighted MR images offered a higher contrast of PVS-CSF (or PVS - White-matter) compared with T1-Weighted MR images. Furthermore, PVS that are difficult to detect in T1W were successfully displayed in T2W MR images allowing a more reliable mapping (figure T1 vs T2).

Consequently, the modality of choice for PVS mapping analysis in this work was the T2W. Only in one patient T1W segmentation was used (fig 3.17).

Parameter optimisation in T1, T2 and T2-FLAIR

Throughout the trials it was found that the parameters that revealed a greater sensitivity were alpha(α) , C and Sigma(σ).

Sigma (σ) controls the scale for which a certain feature is expected to be found. It revealed to be the most sensitive parameter found, therefore, it was the first parameter tested. The behaviour and sensitivity showed by σ was very similar in both sequences(T1W and T2W). The admissible found value for σ included a range between [0.06 - 0.1], a value outside this range lead to a poor mapping (figure 4.9). Moreover, a small increment in alpha (α) lead to a large impact in the the PVS morphology captured by the filter. Using an $\alpha = 0.05$ allowed to minimise false positives displayed in the output mask, enhancing in its majority only voxels corresponding to PVS. Also, it was noticed that α controls the sensitivity that a structure (hiperintense or hipointense) is enhanced comparing with the respective background. Consequently, in the context of a this study, where PVS are extracted based in contrast(CSF-WM) and morphology, these parameters are extremely important in PVS mapping.

Furthermore, C only required a threshold value for the filter to allow the PVS mapping. Figure 4.10 (b) represents a case where a value lower than 50 is used, consequently the segmented mask displayed false positives, not corresponding to PVS. The minimum admissible value found for C was 200.

Therefore, the best parameter obtained for the T2W MR sequence was ($\alpha = 0.05, \beta = 0.1, C = [300-500], \sigma = 0.06$), and the respective segmentation is illustrated in figures 3.19 and 3.21.

Using this parameter set allowed the filter to avoid areas not belonging to PVS. Particularly, areas containing

severe white matter lesion were not segmented by the filter (figures 4.30 and 4.31). In these areas, PVS that were displayed in the neighbourhood of the respective WMH were positively mapped. Figure 4.32 illustrates the avoidance by the filter in voxels regarding other WMH like lacunes. Moreover, the filter allowed to avoid areas caused by motion artifacts (figure 4.31).

A comparison given the filter regarding both sequences, illustrated in figure 4.20 and 4.21, indicate that the performance of the Frangi filter was higher in the T2W, being capable to detect a higher number of PVS, as well as a more reliable morphology according to what was expected by looking at the non filtered image, specially PVS that display elongated features are more easily enhanced in the T2W. A plausible explanation for this is the PVS-WM contrast, higher in the T2W modality, compared with the T1W. The same pipelines used in these modalities (T1W and T2W) were replicated for the T2-Flair, where a poor performance in the mapping of PVS was noted. A plausible explanation is the poor contrast between CSF and WM, blocking the filter to detect any structure. However, as opposed to the segmentation performed in the T1W and T2W, the output given by the Frangi filter in this modality showed a capability to mark and detect areas containing WM lesions, thus, segmentation in the T2-Flair can be important since it is possible to subtract the respective output mask by the T2W segmentation, and as a consequence, an improvement in the T2W mask can be performed, eliminating non desired areas. The lack of CFS-WM contrast displayed in the T2-Flair MR images, making the filter unable to recognize any contrast changes between PVS (hipointense) and WM. Therefore, the filter could only detect contrast changes in areas displaying a significant contrast difference compared with the respective background, such as WMH. As a consequence, no PVS found were mapped using this modality, and areas regarding WM lesions, that appear as hiperintense were mapped.

PVS quantification

The purpose of PVS quantification was to check for significant differences along the distribution of normalized PVS volumes regarding brain lobe and patient group. Throughout the statistical analysis it was found that means regarding the MSA patients (figure 5.1) in the frontal lobe were significantly higher when compared with the temporal lobe (p = 0.05351). Statistical results regarding brain lobes comparison showed a potential significance among the patient groups. Values obtained in the frontal lobe were considered more significant (p = 0.03643) when comparing with the remaining brain lobes. However, multiple comparisons test (table 5.7) revealed no significant differences between patient groups, while comparing with the remaining brain lobes.

Moreover, a lower variability and reduced values illustrated in figure 5.5 were observed for the control group (HLT), when compared with the PSP and FD patients. Despite visual differences across the group medians no significant differences were found across the groups (p>0.05). This fact can be explained by the reduced sample size. However, when all patients were grouped together, more specifically,a group including MSA, PSP and Fabry‘s disease, and compared them with controls, the Mann-Whitney test showed a statistically significant difference between the groups (p = 0.0382) leading to the rejection of the null hypothesis. This result may indicate that the PVS volumes increase with certain cerebral pathological conditions, thus, PVS distribution and volume may have a possible connection with cerebrovascular diseases.

Quantitative measurements will better characterize the severity of PVS in ageing people and their associations with dementia, stroke and vascular diseases.

Wardlaw and Patankar visual rating scores

Results obtained regarding PVS visual rating scores showed a clear connection within PVS computational total volume given by application of the Frangi filter. The following associations between these two metrics can be consulted in figure 4.8. A total Obtained PVS computational total volumes and PVS visual rating scores were compared, using a Linear model. In here, the corresponding volume of each patient was assigned to a certain visual rating score (1-4) and they can be consulted in figure 4.8. In addition, the linear model represents a continuous quantitative response variable (PVS normalized volumes) and an explanatory variable, which corresponds to a categorical variable with four levels (visual rating scores)

The intercept given by the linear model corresponds to the average response of the reference class for a patient with mild PVS score, as the remaining betas explain how much each of the remaining classes differ from the reference class. In other words, the purpose of this trials was to verify once more the performance of the filter, strengthen clinical validation. PVS total volume increased significantly with PVS count, [coefficient of linear regression: 0.0619, p-value = 0.0243*]. These results indicate that PVS visual rating scores may have a positive association with PVS volume, therefore, this method indicates that a patient who is assigned a more severe rating is more likely to have a higher volume of PVS.

Chapter 6

Conclusions

PVS allow interstitial solutes to be cleared from the brain contributing to the brain homeostasis. Dysfunction of these structures can occur if there is a deposition of substances causing stagnation of CSF, leading to the dilation of these cavity forming an enlarged PVS, visible in MRI.

This work focused the segmentation and further quantification of PVS in the brain. Manual delineation of tubular structures such as PVS in a three-dimentional image can be very time consuming, and clinicians have to check multiple views to obtain a very accurate delineation.

Therefore, the first main goal proposed in this work was to optimize a method capable to detect and map PVS morphology and features displayed in MR images. This achievement would empower and make clinicians able to perform a better characterization in terms of spatial distribution, orientation and volume, monitoring each patient‘s condition. After accomplishing the first goal, the second main objective proposed was the PVS quantification based on a brain atlas, for further quantification in the major brain lobes. This analysis would enable multiple comparisons along these ROIs and check for statistical significance between patient groups.

In order to be able to implement the defined objectives, this work includes three different pipelines, that can be summarized as Pre-Frangi, Enhancement filtering, and Post-Frangi.

Pre-Frangi included the optimization of images previously acquired, without any kind of processing, allowing the selection of regions of interest, more precisely White-matter, serving as an input to the filter. FSL was used to fulfill the needs regarding the creation of the ROI.

Afterwards, using Matlab R2016(b) as software, the Frangi filter was used for PVS mapping. Given certain values to α, β, C and σ, the filter could capture the majority and geometrical shape of PVS displayed in WM. Concluded the filtering stage, the Post-Frangi procedure allowed to improve and empower the resulting mask given by matlab. The matrix generated by the filter I_{out} contains border zones and enhanced regions that do not correspond to PVS. These border zones needed to be removed. Consequently, a WM mask with a brain probability mapping = 1 was created using $fslmaths$, removing all border zones, ensuring that only PVS inside WM were extracted.

A final assessment in this work focused on the statistical analysis regarding multiple comparisons across the analyzed metrics between patient groups. All tests presented in Chapter 5 concerns the statistical analysis found regarding PVS distributions across the patient groups. R-Studio was used as a statistical tool for our measures.

Moreover, for validation, it was investigated whether the PVS volumes were related with visual rating scores. These ratings can be used with quantitative methods to understand the physiological condition of each patient, as well as its progression.

Enhancement filtering

In this work, the Frangi filter was successfully implemented and applied to our data sets, accomplishing the first defined goal. Throughout the trials, the parameters used in the Frangi filtering process were set to allow a correct identification and mapping. Results presented in Chapter 4 reinforce that PVS were positively mapped, with more precision in T2W MR images. Moreover, using the best parameters found, the filter‘s sensitivity increases, being capable to extract PVS 3D geometrical shape, showing that it can act as a clinical support tool in qualitative and quantitative measurements. Filter performance was not equal in both sequences, and a plausible explanation is differences in CSF-WM contrast. T2W segmentation showed a more reliable PVS mapping and morphology, being capable to detect PVS in the boundaries of WM. On the contrary, T1W segmentation revealed a less sensitive PVS detection, presenting false positives in the output mask. A comparison given the filter regarding both sequences(T1W,T2W and T2-Flair) indicate that the performance of the Frangi filter was higher in the T2W image, making it the most suitable for PVS mapping, being capable to detect a higher number of PVS.

Filter validation

Results shown in chapter 4, more precisely, figures 4.30 to 4.32 illustrate that the filter can avoid voxels regarding areas displaying WMH. Despite WMH presenting the same contrast as PVS, the filter could avoid areas that belong to WMH, such as severe WM lesions and lacunes. It is also demonstrated that the filter was capable to extract elongated and dot like features of PVS that were not easily seen when comparing with the non filtered image.

PVS quantification

Quantification analysis were performed using FSL, accomplishing the second defined goal.
Regarding the performed statistical analysis, the defined metric concerned the volume of PVS divided by the corresponding WM volume. Post hoc comparisons given by Tukey HSD showed a tendency for statistical significance between brain lobes regarding the normalized PVS volumes in MSA group. The distribution of this metric was higher in the frontal lobe when compared with the temporal lobe ($p = 0.05351$). Reduced medians were observed for the occipital, parietal and temporal lobes. On the other hand, post hoc comparisons in the FD and PSP groups revealed no significant differences across the brain lobes in the analyzed metric ($p = 0.6823$) and ($p = 0.129$), respectively. In brain lobe analysis, regarding the analyzed metric, a tendency towards statistical significance in the frontal lobe was seen. In the contrary, the same distribution was found to be less significative, in the parietal lobe and temporal brain lobes. Moreover, a lower variability and reduced values were observed for the control group (HLT) compared to the remaining groups. However, post hoc comparisons given by Tukey HSD amongst the ROIs (brain lobes) did not reveal statistically significant, neither significant interactions between the groups ($P = 0.2293$). However, statistical significance was found when all patients were clustered, more specifically, a group including MSA, PSP and Fabry were compared with control patients ($p = 0.0382$). This results strengthens

visual differences observed in the figure 5.6, where differences across the medians corresponding to the healthy and pathological groups were considered statistically significant. This result may indicate that the PVS volumes increase with certain cerebral pathological conditions.

Wardlaw and Patankar visual rating scale

The results of this experiment suggest a fair reliability regarding the output of the segmentation method, given by the PVS computational total volume and count vs validated PVS rating scores, through visual inspection.

The purpose of these trials were to verify once more the performance of the filter, strengthen clinical validation. In this work, PVS total volume increased significantly with PVS count (coefficient of linear regression: 0.0619, p-value = 0.0243*), therefore, based on a 95% confidence interval, these results strengthen that PVS visual rating scores may have a positive association with PVS volume.

Final statement

The Frangi filter, given certain parameters, showed a positive performance in PVS mapping. The segmentation of these structures will enable the analysis of PVS spatial and volumetric distributions with other markers of SVD, such as acute lacunar infarcts, WMH, lacunes, and microbleeds. Moreover, obtained results indicate that this PVS quantification method is promising for assessing PVS count and volume from conventional clinical MR scans, and could complement by giving neuroradiologists clinical support in visual rating scores.

Currently, PVS count is performed visually rather than using an automatic threshold-based way, therefore, this method could complement subjective visual rating scales by achieving a precise quantification.

Furthermore, future studies could use this method in longitudinal studies where PVS burden can be assessed in relation with other measures to study possible changes in cerebral blood brain barrier permeability, perfusion and cerebrovascular reactivity.

Limitations and Future Work

The present study presented some limitations that could be addressed in future studies. Firstly, one of the main limitations was the lack of contrast between CSF-WM, specially presented in T1W MR images. This limitation lead to the decrease in sensitivity regarding the Frangi filter output mask. A possible approach should focus on the MR acquisition with a more powerful magnetic field strength. Increasing the magnetic field would provide to the filter a higher sensitivity detection, better conditions to differentiate and improve CSF-WM contrast, leading to the decrease of false positive rate in this modality (T1W). However, the use of MRI scanners with a higher magnetic field strength may not be easily accessible, and on the other hand it would lead to greater memory oveload during the eigenvalue and eigenvalue matrix calculations in matlab, probably causing a shutdown in the system. Therefore, an approach to overcome the referred issued, so as to get a more supported validation should include samples previously marked by clinicians and neuroradiologists. This process can be very laborious and time consuming but would help to eliminate false positives, decreasing possible errors in the output mask and perform a continuous improvement in the parameter ranges, used for the Frangi filter. Moreover, marked images can be used with the output masks given by the filter. This method is commonly used as a measure of overlapping two sets of images A and B, allowing the comparison and similarity between these two samples. Furthermore, the values resulting from the calculation of Dice coefficient will allow to adjust the Frangi parameters used for PVS mapping.

Future studies should focus the quantification of PVS using other regions of interest (ROI) in brain atlas, more precisely, in the brainstem and basal ganglia. It would be very interesting to perform volume comparisons for results found with quantification in these regions.

Another limitation in this study concerns the small sample size regarding some patient groups, more specifically FD and PSP. Statistical significance was not found between patient groups probably due to the lack of statistical power. Future work should include larger samples, which could also prove important to confirm the results hereby obtained regarding the statistical differences obtained between control and pathological groups. The use of a larger sample would further enhance the utility of PVS quantification as monitoring tool for the analyzed metrics providing a relatively straightforward confirmation regarding PVS distribution in disease progression, by investigating PVS volume differences across age.

Bibliography

[1] T. Truelsen, S. Begg, and C. Mathers. The global burden of cerebrovascular disease. *Geneva: World Health Organisation*, 2000.

[2] V. L. Feigin, B. Norrving, and G. A. Mensah. Global burden of stroke. *Circulation research*, 120(3):439–448, 2017.

[3] G. Banerjee, D. Wilson, H. R. Jäger, and D. J. Werring. Novel imaging techniques in cerebral small vessel diseases and vascular cognitive impairment. *Biochimica et Biophysica Acta (BBA)-Molecular Basis of Disease*, 1862(5):926–938, 2016.

[4] F. N. Doubal, A. M. MacLullich, K. J. Ferguson, M. S. Dennis, and J. M. Wardlaw. Enlarged perivascular spaces on mri are a feature of cerebral small vessel disease. *Stroke*, 41(3):450–454, 2010.

[5] X. Zong, S. H. Park, D. Shen, and W. Lin. Visualization of perivascular spaces in the human brain at 7 t: sequence optimization and morphology characterization. *NeuroImage*, 125:895–902, 2016.

[6] C. M. Eng, D. P. Germain, M. Banikazemi, D. G. Warnock, C. Wanner, R. J. Hopkin, J. Bultas, P. Lee, K. Sims, S. E. Brodie, et al. Fabry disease: guidelines for the evaluation and management of multi-organ system involvement. *Genetics in Medicine*, 8(9):539, 2006.

[7] L. Ballerini, R. Lovreglio, M. d. C. V. Hernández, J. Ramirez, B. J. MacIntosh, S. E. Black, and J. M. Wardlaw. Perivascular spaces segmentation in brain mri using optimal 3d filtering. *Scientific reports*, 8(1): 2132, 2018.

[8] R. E. Feldman, J. W. Rutland, M. C. Fields, L. V. Marcuse, P. S. Pawha, B. N. Delman, and P. Balchandani. Quantification of perivascular spaces at 7 t: A potential mri biomarker for epilepsy. *Seizure*, 54:11–18, 2018.

[9] J. Wuerfel, M. Haertle, H. Waiczies, E. Tysiak, I. Bechmann, K. D. Wernecke, F. Zipp, and F. Paul. Perivascular spaces—mri marker of inflammatory activity in the brain? *Brain*, 131(9):2332–2340, 2008.

[10] R. Rouhl, R. Van Oostenbrugge, I. Knottnerus, J. Staals, and J. Lodder. Virchow-robin spaces relate to cerebral small vessel disease severity. *Journal of neurology*, 255(5):692–696, 2008.

[11] A. MacLullich, J. Wardlaw, K. Ferguson, J. Starr, J. Seckl, and I. Deary. Enlarged perivascular spaces are associated with cognitive function in healthy elderly men. *Journal of Neurology, Neurosurgery & Psychiatry*, 75(11):1519–1523, 2004.

[12] I. Kilsdonk, M. Steenwijk, P. Pouwels, J. Zwanenburg, F. Visser, P. Luijten, J. Geurts, F. Barkhof, and M. Wattjes. Perivascular spaces in ms patients at 7 tesla mri: A marker of neurodegeneration? *Multiple Sclerosis Journal*, 21(2):155–162, 2015.

[13] A. Fellgiebel, M. Müller, M. Mazanek, K. Baron, M. Beck, and P. Stoeter. White matter lesion severity in male and female patients with fabry disease. *Neurology*, 65(4):600–602, 2005.

[14] S. Groeschel, W. K. Chong, R. Surtees, and F. Hanefeld. Virchow-robin spaces on magnetic resonance images: normative data, their dilatation, and a review of the literature. *Neuroradiology*, 48(10):745–754, 2006.

[15] J. Ramirez, C. Berezuk, A. A. McNeely, C. J. Scott, F. Gao, and S. E. Black. Visible virchow-robin spaces on magnetic resonance imaging of alzheimer's disease patients and normal elderly from the sunnybrook dementia study. *Journal of Alzheimer's Disease*, 43(2):415–424, 2015.

[16] H. Mestre, S. Kostrikov, R. I. Mehta, and M. Nedergaard. Perivascular spaces, glymphatic dysfunction, and small vessel disease. *Clinical science*, 131(17):2257–2274, 2017.

[17] D. F. Moore, C. R. Kaneski, H. Askari, and R. Schiffmann. The cerebral vasculopathy of fabry disease. *Journal of the neurological sciences*, 257(1-2):258–263, 2007.

[18] L. Ginsberg, R. Manara, A. R. Valentine, B. Kendall, and A. P. Burlina. Magnetic resonance imaging changes in fabry disease. *Acta Paediatrica*, 95:57–62, 2006.

[19] K. Crutchfield, N. Patronas, J. Dambrosia, K. Frei, T. Banerjee, N. Barton, and R. Schiffmann. Quantitative analysis of cerebral vasculopathy in patients with fabry disease. *Neurology*, 50(6):1746–1749, 1998.

[20] J. T. Clarke. Narrative review: Fabry disease. *Annals of internal medicine*, 146(6):425–433, 2007.

[21] R. C. Reisin, C. Romero, C. Marchesoni, G. Nápoli, I. Kisinovsky, G. Cáceres, and G. Sevlever. Brain mri findings in patients with fabry disease. *Journal of the neurological sciences*, 305(1-2):41–44, 2011.

[22] J.-i. Takanashi, A. J. Barkovich, W. P. Dillon, E. H. Sherr, K. A. Hart, and S. Packman. T1 hyperintensity in the pulvinar: key imaging feature for diagnosis of fabry disease. *American journal of neuroradiology*, 24(5): 916–921, 2003.

[23] S. S. Rao, L. A. Hofmann, A. Shakil, et al. Parkinson's disease: diagnosis and treatment. *Am Fam Physician*, 74(12):2046–54, 2006.

[24] A. U. Khan, M. Akram, M. Daniyal, and R. Zainab. Awareness and current knowledge of parkinson's disease: a neurodegenerative disorder. *International Journal of Neuroscience*, 129(1):55–93, 2019.

[25] M. Lew. Overview of parkinson's disease. *Pharmacotherapy: The Journal of Human Pharmacology and Drug Therapy*, 27(12P2):155S–160S, 2007.

[26] M. S. Lee, C. H. Lyoo, and T. S. Chung. Parkinsonism and dementia associated with giant virchow-robin spaces. *Journal of movement disorders*, 8(2):106–107, 2015.

[27] Z. Ahmed, Y. Asi, A. Sailer, A. Lees, H. Houlden, T. Revesz, and J. Holton. The neuropathology, pathophysiology and genetics of multiple system atrophy. *Neuropathology and applied neurobiology*, 38(1):4–24, 2012.

[28] S. Koga and D. W. Dickson. Recent advances in neuropathology, biomarkers and therapeutic approach of multiple system atrophy. *Journal of Neurology, Neurosurgery & Psychiatry*, 89(2):175–184, 2018.

[29] M. Federoff, L. V. Schottlaender, H. Houlden, and A. Singleton. Multiple system atrophy: the application of genetics in understanding etiology. *Clinical Autonomic Research*, 25(1):19–36, 2015.

[30] H. Ling. Clinical approach to progressive supranuclear palsy. *Journal of movement disorders*, 9(1):3, 2016.

[31] A. Kowalska, Z. Jamrozik, and H. Kwieciński. Progressive supranuclear palsy–parkinsonian disorder with tau pathology. *Folia neuropathologica*, 42(2):119–123, 2004.

[32] D. R. Williams and A. J. Lees. Progressive supranuclear palsy: clinicopathological concepts and diagnostic challenges. *The Lancet Neurology*, 8(3):270–279, 2009.

[33] R. G. Henderson. Nuclear magnetic resonance imaging: A review1. *Journal of the Royal Society of Medicine*, 76(3):206–212, 1983.

[34] V. P. Grover, J. M. Tognarelli, M. M. Crossey, I. J. Cox, S. D. Taylor-Robinson, and M. J. McPhail. Magnetic resonance imaging: principles and techniques: lessons for clinicians. *Journal of clinical and experimental hepatology*, 5(3):246–255, 2015.

[35] Y. Uchiyama, T. Kunieda, T. Asano, H. Kato, T. Hara, M. Kanematsu, T. Iwama, H. Hoshi, Y. Kinosada, and H. Fujita. Computer-aided diagnosis scheme for classification of lacunar infarcts and enlarged virchow-robin spaces in brain mr images. In *2008 30th Annual International Conference of the IEEE Engineering in Medicine and Biology Society*, pages 3908–3911. IEEE, 2008.

[36] J. Zhang, Y. Gao, S. H. Park, X. Zong, W. Lin, and D. Shen. Segmentation of perivascular spaces using vascular features and structured random forest from 7t mr image. In *International Workshop on Machine Learning in Medical Imaging*, pages 61–68. Springer, 2016.

[37] A. F. Frangi, W. J. Niessen, K. L. Vincken, and M. A. Viergever. Multiscale vessel enhancement filtering. In *International conference on medical image computing and computer-assisted intervention*, pages 130–137. Springer, 1998.

[38] X. Descombes, F. Kruggel, G. Wollny, and H. J. Gertz. An object-based approach for detecting small brain lesions: application to virchow-robin spaces. *IEEE transactions on medical imaging*, 23(2):246–255, 2004.

[39] R. Yokoyama, X. Zhang, Y. Uchiyama, H. Fujita, T. Hara, X. Zhou, M. Kanematsu, T. Asano, H. Kondo, S. Goshima, et al. Development of an automated method for the detection of chronic lacunar infarct regions in brain mr images. *IEICE transactions on information and systems*, 90(6):943–954, 2007.

[40] J. Ramirez, E. Gibson, A. Quddus, N. J. Lobaugh, A. Feinstein, B. Levine, C. Scott, N. Levy-Cooperman, F. Gao, and S. E. Black. Lesion explorer: a comprehensive segmentation and parcellation package to obtain

regional volumetrics for subcortical hyperintensities and intracranial tissue. *Neuroimage*, 54(2):963–973, 2011.

[41] L. Ballerini, R. Lovreglio, M. d. C. Valdés Hernández, J. Ramirez, B. J. MacIntosh, S. E. Black, and J. M. Wardlaw. Perivascular spaces segmentation in brain mri using optimal 3d filtering. *Scientific Reports*, 8(1), Feb 2018.

[42] L. Ballerini, R. Lovreglio, M. d. C. V. Hernández, V. Gonzalez-Castro, S. M. Maniega, E. Pellegrini, M. E. Bastin, I. J. Deary, and J. M. Wardlaw. Application of the ordered logit model to optimising frangi filter parameters for segmentation of perivascular spaces. *Procedia Computer Science*, 90:61–67, 2016.

[43] M. Jenkinson, C. F. Beckmann, T. E. Behrens, M. W. Woolrich, and S. M. Smith. Fsl. *Neuroimage*, 62(2): 782–790, 2012.

[44] M. W. Woolrich, S. Jbabdi, B. Patenaude, M. Chappell, S. Makni, T. Behrens, C. Beckmann, M. Jenkinson, and S. M. Smith. Bayesian analysis of neuroimaging data in fsl. *Neuroimage*, 45(1):S173–S186, 2009.

[45] S. Smith, P. R. Bannister, C. Beckmann, M. Brady, S. Clare, D. Flitney, P. Hansen, M. Jenkinson, D. Leibovici, B. Ripley, et al. Fsl: New tools for functional and structural brain image analysis. *NeuroImage*, 13 (6):249, 2001.

[46] A. F. Frangi, W. J. Niessen, P. J. Nederkoorn, J. Bakker, W. P. T. M. Mali, and M. A. Viergever. Quantitative analysis of vascular morphology from 3d mr angiograms: in vitro and in vivo results. *Magnetic Resonance in Medicine: An Official Journal of the International Society for Magnetic Resonance in Medicine*, 45(2): 311–322, 2001.

[47] G. M. Potter, F. M. Chappell, Z. Morris, and J. M. Wardlaw. Cerebral perivascular spaces visible on magnetic resonance imaging: development of a qualitative rating scale and its observer reliability. *Cerebrovascular diseases*, 39(3-4):224–231, 2015.

[48] G. M. Potter, F. N. Doubal, C. A. Jackson, F. M. Chappell, C. L. Sudlow, M. S. Dennis, and J. M. Wardlaw. Enlarged perivascular spaces and cerebral small vessel disease. *International journal of stroke*, 10(3):376–381, 2015.

[49] H. Finch. Comparison of the performance of nonparametric and parametric manova test statistics when assumptions are violated. *Methodology*, 1(1):27–38, 2005.

[50] M. Jamshidian and S. Jalal. Tests of homoscedasticity, normality, and missing completely at random for incomplete multivariate data. *Psychometrika*, 75(4):649–674, 2010.